The Dissertation Committee for Joshua Dale Bryant Certifies that this is the approved version of the following dissertation:

Characterization of MTHFD2L Expression and Alternative Splicing and Loss of MTHFD1L Activity in Murine Embryos and Adults

Committee:

Dean R. Appling, Supervisor

Michael Drew

Richard Finnell

David Hoffman

Edward Mills

Stefano Tiziani

Characterization of MTHFD2L Expression and Alternative Splicing and Loss of MTHFD1L Activity in Murine Embryos and Adults

by

Joshua Dale Bryant, B.S.

Dissertation

Presented to the Faculty of the Graduate School of

The University of Texas at Austin

in Partial Fulfillment

of the Requirements

for the Degree of

Doctor of Philosophy

The University of Texas at Austin

May 2017

Dedication

I would like to dedicate this work to my parents, who have always been incredibly supportive of me and are the best people that I know.

Acknowledgements

Characterization of MTHFD2L Expression and Alternative Splicing and Loss of

MTHFD1L Activity in Murine Embryos and Adults

Joshua Dale Bryant, Ph.D.

The University of Texas at Austin, 2017

Supervisor: Dean R. Appling

In Eukaryotes, folate-dependent one-carbon (1C) metabolism is a highly compartmentalized process in which mitochondria play a central role. Defects in folate metabolism are associated with diseases such as cancer, Alzheimer's disease, and neural tube defects (NTDs). 1C units are attached to tetrahydrofolate (THF) and carried in various oxidation states between folate-dependent enzymes. There is an exchange of 1C units across the mitochondrial membrane, with 1C donors such as serine and glycine being oxidized to formate in the mitochondria, which is then released into the cytoplasm. 1C units in the cytoplasm can be used for the synthesis of purines, thymidylate, and methionine for the methyl cycle. The core of the pathway in both compartments is catalyzed by the methylene-tetrahydrofolate (MTHFD) gene family. These enzymes catalyze the reversible interconversion between CH_2-THF, CH^+-THF, CHO-THF, and formate. The cytoplasmic protein MTHFD1 is trifunctional and carries the CH_2-THF dehydrogenase, CH^+-THF cyclohydrolase, and 10-CHO-THF synthetase activities necessary to carry out these interconversions. In the mitochondria, two bifunctional isozymes, MTHFD2 and MTHFD2L, carry the dehydrogenase/cyclohydrolase (D/C) activities. The monofunctional enzyme MTHFD1L is responsible for the synthetase

activity. MTHFD2 is only expressed in embryos and transformed cells, and the enzyme responsible for the D/C activity in adults was unknown until the recent discovery of MTHFD2L. In this work, characterization of the expression of MTHFD2L in mouse embryos and adults is described. Expression of MTHFD2L in embryos was found to be switched on between embryonic days 8.5-10.5, and remains high throughout development. MTHFD2L is also widely expressed in adults, with highest expression in brain and lung. A splice variant of MTHFD2L lacking exon 8 was found to be abundant in embryos but was not catalytically active *in vitro* or *in vivo*. MTHFD1L is an essential protein, and SNPs in MTHFD1L are associated with increased risk for Alzheimer's disease and NTDs in humans. Loss of MTHFD1L activity in adult mice with and without a folate deficient diet was investigated. Indications of sex-dependent behavioral anomalies were found, with evidence for genotype-dependent hyperactivity in male mice and diet-dependent anxiety in female mice, but further investigation of these findings is warranted. Finally, metabolic defects associated with NTDs and growth restriction in MTHFD1L-null (*Mthfd1l$^{z/z}$*) embryos were identified. Glycolysis, the TCA cycle, and the metabolism of methionine, purines, and multiple amino acids were found to be disrupted in *Mthfd1l$^{z/z}$* embryos. These altered metabolic pathways suggest potential future therapies for preventing NTDs in humans.

Table of Contents

List of Tables

List of Figures

Chapter 1: Introduction

1.1 FOLATE-DEPENDENT ONE-CARBON METABOLISM

1.1.1 Cellular Folates

1.1.1.1 Folate Structure

"Folates" are a collective group of molecules including folic acid and its reduced derivatives which can carry one-carbon (1C) units in one of several oxidation states. Folates are composed of a pteridine ring that is covalently linked at carbon 6 to para-aminobenzoic acid (PABA) with a poly-γ-glutamate tail (Figure 1.1). Tetrahydrofolate (THF), as shown in Figure 1, is the active form of folate in mammalian cells. Dietary folic acid must first be reduced to THF before it can participate in 1C transfer reactions. This reduction is carried out in two steps by the enzyme dihydrofolate reductase (DHFR). Using NADPH as an electron donor, DHFR first reduces folic acid to 7,8-dihydrofolate (DHF), then further reduces DHF to 5,6,7,8-tetrahydrofolate. Within cells, THF typically has a poly-γ-glutamate tail consisting of 5-7 glutamate residues. Synthesis of the poly-γ-glutamate tail is catalyzed by folylpolyglutamate synthetase (FPGS), which attaches glutamate residues with an amino-γ-carboxyl bond (Shane, 1989). The glutamate tail is essential for retention of folates within a cell (McBurney and Whitmore, 1974; Taylor and Hanna, 1977). The exact length of the tail can vary depending on the organism and the intracellular compartment. In Chinese hamster ovary (CHO) cells, the heptaglutamate form tends to predominate in the mitochondria, while the hexaglutamate form is more common in the cytoplasm (Lin et al., 1993). On the other hand, rat liver cells were found to have a higher proportion of the pentaglutamate in the mitochondria and hexaglutamate in the cytoplasm (Carl et al., 1995).
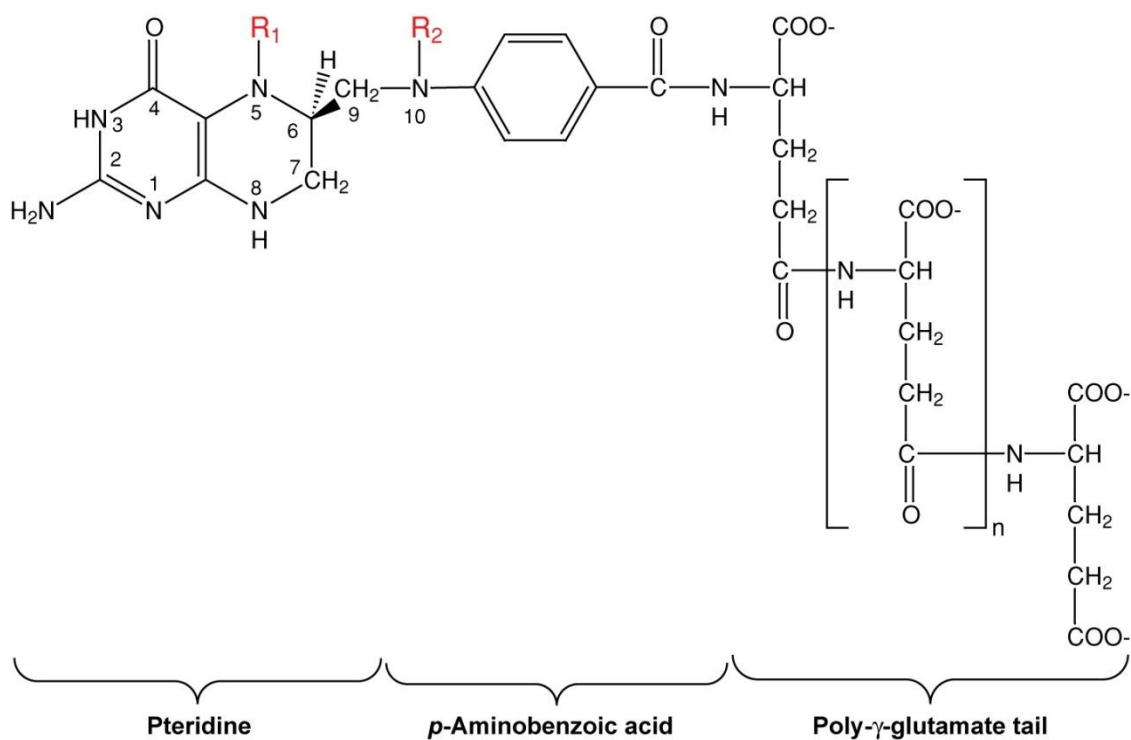
Figure 1.1   Structure of tetrahydrofolate. THF is composed of a pteridine ring, a PABA

moiety, and a poly-γ-glutamate tail. Activated one-carbon units, represented

by R1 and R2, can be carried at N5, N10, or bridging N5 and N10 in various

oxidation states (Figure reproduced from (Tibbetts and Appling, 2010)).

THF can carry 1C units at either N5 on the pteridine ring, N10 on the PABA moiety (R1 and R2 respectively in Figure 1), or as a single carbon bonded between N5 and N10. The most common forms of folate include 5-methyl-THF (CH$_3$-THF), 5,10-methylene-THF (CH$_2$-THF), 5,10-methenyl-THF (CH$^+$-THF), 10-formyl-THF (10-CHO-THF), and 5-formyl-THF (5-CHO-THF). The exact distribution of these cofactors is dependent on the subcellular compartment in which they are found. In rat liver mitochondria, the 10-CHO-THF and THF forms predominate, making up 33.1% and 48.1% of the folate pool, respectively. The folate pool in the cytoplasm is composed primarily of THF (27%), 5-CH$_3$-THF (45%), and 10-CHO-THF (19%) (Horne et al., 1989).

1.1.1.2 Folate transport

The transport of folate into cells is carried out by three main classes of transporters: the reduced folate carrier (RFC), folate receptor proteins (Folr), and the proton coupled folate transporter (PCFT). RFC is the major folate transporter that delivers folates to most tissues and is ubiquitously expressed in mice and humans (Liu et al., 2005; Whetstine et al., 2002). RFC has a very low affinity for folic acid, transporting only reduced folates, and its activity is highly pH dependent (Huang et al., 1997). RFC is maximally active at pH 7.4, and its activity drops off sharply as pH decreases (Zhao et al., 2004). Transport of folates by RFC proceeds by a bidirectional anion antiport mechanism (Goldman, 1971; Henderson and Zevely, 1983; Yang et al., 1984). Nullizygous deletion of RFC is embryonic lethal in mice. Folate supplementation will allow survival of embryos until birth, but pups do not survive for more than two weeks (Zhao et al., 2001).

3

The folate receptor protein (also known as folate binding protein, Folbp) class of transporters are glycolipid linked proteins on the extracellular side of the plasma membrane that import folate unidirectionally into the cell by an endocytotic process (Sabharanjak and Mayor, 2004). There are three homologues of Folr expressed in mammalian cells. Folr1 is expressed both during development and in adults (Elwood, 1989; Kennedy et al., 2003). Folr2 is expressed only in cancer cells and during development, primarily in the placenta (Ross et al., 1999). Folr3 is expressed only in hematopoetic cells (Shen et al., 1994). While deletion of Folr2 has no phenotype (Piedrahita et al., 1999), Folr1 is required for embryonic development. Mice lacking Folr1 do not survive past embryonic day (E) 10 (Piedrahita et al., 1999). Maternal folate supplementation with low doses of folate allows the embryos to survive longer with a variety of defects. Higher doses of folate allow some embryos to survive until birth, but survivors have consistently low serum folate (Spiegelstein et al., 2004).

Mouse PCFT is highly expressed in the duodenum and proximal jejunum (Qiu et al., 2007) and is the primary transporter involved in intestinal absorption of dietary folates (reviewed in (Zhao et al., 2011)). PCFT is a proton coupled symporter and is most active at low pH (Chattopadhyay et al., 2007; Qiu et al., 2006). PCFT can transport a variety of folate species, having the highest affinity for folic acid, 5-CH$_3$-THF, and 5-CHO-THF. Defects in PCFT are associated with hereditary folate malabsorption (Qiu et al., 2006). Although deletion of PCFT in mice is not lethal, mice lacking PCFT show systemic folate deficiency that is characterized by accumulation of immature erythroblasts in the bone marrow and spleen, increased apoptosis in intermediate erythroblasts, and decreased release of reticulocytes from the bone marrow and spleen (Salojin et al., 2011).

4

Transport of folates into the mitochondria from the cytoplasm is accomplished by the mitochondrial folate transporter (MFT). MFT was first identified in the *glyB* line of CHO cells, which is auxotrophic for glycine and has no measurable mitochondrial folates (Titus and Moran, 2000). When glyB CHO cells were transfected with the wild-type hamster MFT cDNA the glycine auxotrophy was rescued and the cells were able to accumulate mitochondrial folates (McCarthy et al., 2004). Although the exact form of folate imported by MFT *in vivo* is currently unknown, isolated mitochondria from rat liver appear to preferentially uptake the reduced folates $5\text{-}CH_3\text{-}THF$ and $5\text{-}CHO\text{-}THF$ and have low affinity for folic acid (Horne et al., 1992). Between $5\text{-}CH_3\text{-}THF$ and $5\text{-}CHO\text{-}THF$, $5\text{-}CHO\text{-}THF$ is more likely to be the physiologically relevant substrate. The only known enzyme to utilize $5\text{-}CH_3\text{-}THF$ is methionine synthase, but it has only been found to localize to the cytoplasm (Rassin and Gaull, 1975). On the other hand, $CH^+\text{-}THF$ synthetase can catalyze the conversion of $5\text{-}CHO\text{-}THF$ to $CH^+\text{-}THF$ and has been reported to localize to the mitochondria (Bertrand et al., 1995; Huang and Schirch, 1995).

1.1.2 Compartmentalization of One-Carbon Metabolism

1.1.2.1 Overview of Folate-dependent One-Carbon Cycle

In Eukaryotes, folate-dependent one-carbon (1C) metabolism is a highly compartmentalized process in which mitochondria play a central role (reviewed in (Tibbetts and Appling, 2010)). There is an exchange of 1C units across the mitochondrial membrane that generally proceeds in a clockwise direction as seen in Figure 1.2, with 1C donors such as serine and glycine being oxidized to formate in the mitochondria which is then released into the cytoplasm. The core of the pathway in both compartments is catalyzed by the methylene-tetrahydrofolate (MTHFD) gene family (reactions 1-3 and 1m-3m). A single trifunctional enzyme, MTHFD1, is responsible for the cytoplasmic
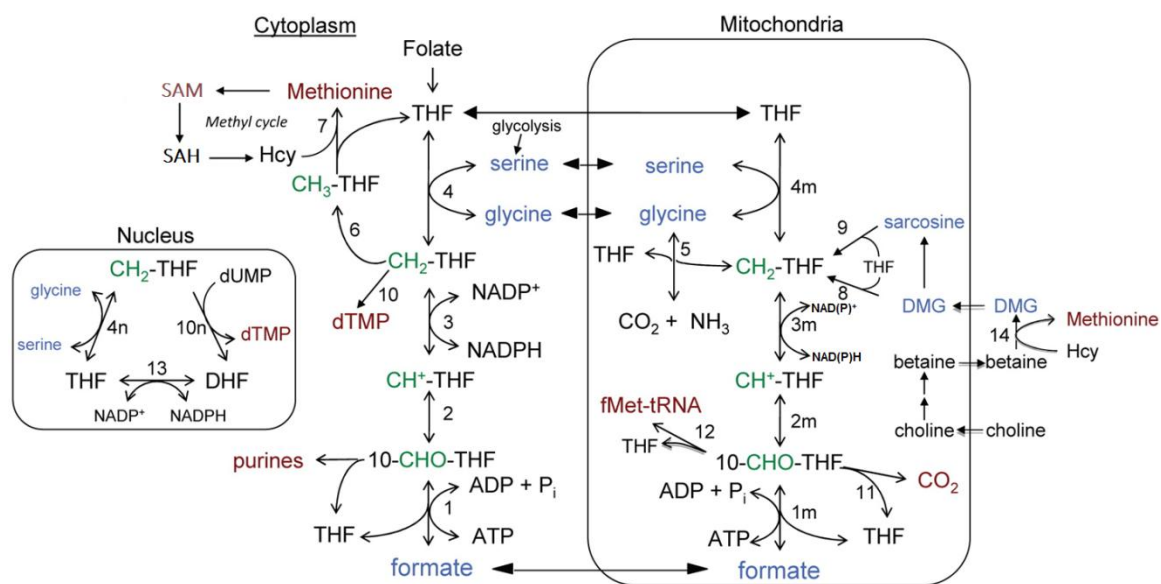
Figure 1.2   Compartmentalization of folate-dependent 1C metabolism. End products of 1C metabolism are in red. 1C donors are in blue. Activated 1C units carried by THF are in green. Reactions are catalyzed by the following: 1, 2, and 3, MTHFD1; 1m, MTHFD1L; 2m and 3m, MTHFD2 or MTHFD2L; 4, 4n, and 4m, SHMT; 5, GCS; 6, CH_2-THF reductase; 7, methionine synthase; 8, dimethylglycine (DMG) dehydrogenase; 9, sarcosine dehydrogenase; 10 and 10n, thymidylate synthase; 11, 10-CHO-THF dehydrogenase (only the mitochondrial activity of this enzyme is shown, but it has been reported in both compartments in mammals); 12, methionyl-tRNA formyltransferase; 13, dihydrofolate (DHF) reductase; 14, betaine-homocysteine methyltransferase. SAH, *S*-adenosylhomocysteine; SAM, *S*-adenosylmethionine; Hcy, homocysteine. Figure adapted from (Tibbetts and Appling, 2010).

10-formyl-tetrahydrofolate (10-CHO-THF) synthetase, 5,10-methenyl-THF (CH^+-THF) cyclohydrolase, and 5,10-methylene (CH_2-THF) dehydrogenase activities (reactions 1-3). Mitochondrially derived formate in the cytoplasm can be attached to THF by the synthetase activity of the MTHFD1. The 10-CHO-THF that is formed can either be used for de novo purine synthesis or reduced to CH_2-THF via the cyclohydrolase and dehydrogenase activities of MTHFD1. This CH_2-THF is available for thymidylate synthesis (reaction 10) or can be further reduced to 5-methyl-THF for use in the methyl cycle (reactions 6 and 7).

The mitochondrial 1C pathway begins with the formation of 5,10-methylene-tetrahydrofolate (CH_2-THF). While serine is the primary 1C donor (reaction 4m) (Davis et al., 2004; Pike et al., 2010), glycine (reaction 5), dimethyglycine (reaction 8), and sarcosine (reaction 9) can also serve as 1C donors for the formation of CH_2-THF. Mitochondrial CH_2-THF dehydrogenase and CH^+-THF cyclohydrolase activities are catalyzed by the bifunctional enzymes MTHFD2 and MTHFD2L (reactions 3m and 2m). The final step, the formation of formate from 10-CHO-THF, is catalyzed by the monofunctional enzyme MTHFD1L (reaction 1m).

The four members of the MTHFD gene family share a similar sequence and domain structure. Both MTHFD1 and MTHFD1L have two structural domains: a large CHO-synthetase domain and a smaller CH_2-THF dehydrogenase/ CH^+-THF cyclohydrolase domain. While both domains of MTHFD1 are catalytically active, only the synthetase domain of MTHFD1L is active (Christensen and Mackenzie, 2008; Walkup and Appling, 2005). MTHFD2 and MTHFD2L both lack the synthetase domain and are composed only of the smaller dehydrogenase/cyclohydrolase domain (Bolusani et al., 2011; Mejia et al., 1986). Unlike MTHFD1, the mitochondrial proteins MTHFD1L,

7

MTHFD2, and MTHFD2L contain an N-terminal mitochondrial targeting sequence (Bolusani et al., 2011; Mejia and MacKenzie, 1988; Prasannan et al., 2003).

1.1.2.2 Mitochondrial One-Carbon Metabolism

The 1C pathway in the mitochondria begins with the formation of CH_2-THF from one of several 1C donors including serine, glycine, dimethylgycine, and sarcosine. Serine is the major 1C donor in mammals (Davis et al., 2004; Pike et al., 2010). The formation of CH_2-THF from serine is catalyzed by the mitochondrial serine hydroxymethyltransferase (SHMT2, reaction 4m in Figure 1.2). In this reaction, the 3-carbon of serine is transferred to THF, making CH_2-THF and also forming glycine. SHMT2 is ubiquitously expressed, being found in most adult tissues as well as embryos (Fujioka, 1969; Motokawa and Kikuchi, 1971; Thompson et al., 2001).

The oxidation and cleavage of glycine to form CH_2-THF is catalyzed by the glycine cleavage system (GCS, reaction 5 in Figure 1.2). The oxidative cleavage of glycine results in the formation of CO_2, NH_4, CH_2-THF, and NADH. GCS is a protein complex composed of four different subunits: glycine decarboxylase (GLDC or P-protein), aminomethyltransferase (AMT or T-protein), dihydrolipoyl dehydrogenase (GCSL or L-protein), and a hydrogen transfer protein known as the H-protein (GCSH) (Kikuchi, 1973). GCS is essential both in adults and during embryogenesis. Disruption of GCS causes the accumulation of glycine and can lead to a condition known as nonketotic hyperglycinemia (NKH), which can cause severe neurological symptoms (Hamosh and Johnston, 2001). In mice, deletion of either AMT or GLDC results in NKH-like symptoms and leads to neural tube defects (NTDs) (Narisawa et al., 2012; Pai et al., 2015).

Dimethylglycine and sarcosine, both intermediates in the oxidation of choline, can also serve as 1C donors in the mitochondria. The enzymes dimethylglycine dehydrogenase and sarcosine dehydrogenase catalyze the oxidative demethylation of dimethylglycine and sarcosine respectively, leaving glycine as the final product (Figure 1.2, reactions 8 and 9). The demethylation catalyzed by either enzyme will result in the formation of CH_2-THF when THF is present (Porter et al., 1985). In the absence of THF both enzymes are still active, but instead release the methyl group as formaldehyde (Wittwer and Wagner, 1980). Formaldehyde in the mitochondria can be oxidized to formate by a mitochondrial aldehyde dehydrogenase (ALDH2) and may provide a source of mitochondrial formate, particularly during folate deficiency (Dorokhov et al., 2015; Morrow et al., 2015).

Once CH_2-THF is formed, it can then be oxidized in two consecutive steps to 10-CHO-THF. Two mitochondrial bifunctional enzymes, MTHFD2 and MTHFD2L, carry both the CH_2-THF dehydrogenase (Figure 1.2, reaction 3m) and CH+-THF cyclohydrolase (Figure 1.2, reaction 2m) activities necessary to facilitate this conversion. It is currently unknown why mitochondria possess these redundant enzymatic activities. Of the two isozymes, less work has been done to characterize MTHFD2L. Our lab has shown that MTHFD2L is expressed in both embryonic and adult tissues, but the exact timing of its expression during development and tissue distribution in adults had not been fully elucidated prior to the work that will be described in Chapter 2 (Bolusani et al., 2011). MTHFD2L is NAD^+-dependent at saturating substrate concentrations, but work from our lab has shown that MTHFD2L can use NAD^+ or $NADP^+$ with almost equal affinity at physiological substrate concentrations (Shin et al., 2014).

Unlike MTHFD2L, MTHFD2 expression is almost entirely restricted to transformed cells and developing tissue (Di Pietro et al., 2004; Mejia and MacKenzie,

1985, 1988). MTHFD2 is essential for development in mice. By E12.5 embryos lacking MTHFD2 are smaller and more pale than their wild-type littermates, and live MTHFD2-null embryos are not observed past E15.5. Embryonic lethality appears to be caused by a defect in hematopoiesis (Di Pietro et al., 2002). Though the CH_2-THF dehydrogenase activity of MTHFD2 has been reported to be strictly NAD^+-dependent, these experiments were not carried out at physiological substrate concentrations (Mejia and MacKenzie, 1988). Recent unpublished work in our lab has shown that MTHFD2 can use either NAD^+ or $NADP^+$ in the oxidation of CH_2-THF at physiologically relevant substrate concentrations (Minhye Shin, personal communication). More work will be needed to identify differences in MTHFD2 and MTHFD2L that could explain the existence of two dehydrogenase/cyclohydrolase enzymes in the mitochondria.

Several potential fates await 10-CHO-THF formed in the mitochondria. It can be used for formylation of the initiator tRNA for synthesis of mitochondrial proteins (Figure 1.2, reaction 12), oxidized to CO_2 (Figure 1.2, reaction 11), or released as formate (Figure 1.2, reaction 1m). Like in bacteria, initiation of protein synthesis typically requires a formylated initiator tRNA (fMet-tRNA[Met]) (Kozak, 1983). In mammals this reaction is catalyzed by mitochondrial methionyl-tRNA formyltransferase (MTFMT). Although there is some indication from work with yeast that fMet-tRNA[Met] is not absolutely required for initiation of translation (Li et al., 2000), mutations have been identified in the human MTFMT that lead to defects in mitochondrial protein synthesis (Tucker et al., 2011).

Another possibility is that 10-CHO-THF can be oxidized to CO_2 and THF in an $NADP^+$ dependent reaction by the mitochondrial 10-CHO-THF dehydrogenase (formerly called FTD, encoded by the *Aldh1l2* gene). ALDH1L2 activity has been detected in the mitochondria of rat liver, retina, and brain (Barlowe and Appling, 1988; Neymeyer and

Tephly, 1994). Recent work has highlighted the importance of 1C metabolism in contributing to NADPH production in cancer cells (Ducker et al., 2016; Tedeschi et al., 2013). The total flux of 1C units generated from serine exceeds the synthetic requirements of cancer cells, so the oxidation of some of these 1C units to CO_2 and simultaneous production of NADPH by ALDH1L2 likely plays an important role in cancer cell proliferation (Tedeschi et al., 2013).

Finally, 10-CHO-THF can be oxidized to formate by the synthetase activity of MTHFD1L. In this reaction, ATP is produced from ADP and P_i and the formyl group is released as formate. Once produced, formate rapidly effluxes from the mitochondria into the cytoplasm (Barlowe and Appling, 1988; García-Martínez and Appling, 1993). MTHFD1L has been found to be expressed in both embryos and adult tissues (Pike et al., 2010; Prasannan et al., 2003). MTHFD1L is essential for embryonic development in mice (Momb et al., 2013), and mutations have been found in the human gene that are associated with an increased risk of NTDs (Minguzzi et al., 2014; Parle-McDermott et al., 2009). MTHFD1L expression may also be important in some types of cancer; MTHFD1L expression has been found to be upregulated in breast cancer cells (Selcuklu et al., 2012).

1.1.2.3 Cytoplasmic One-Carbon Metabolism

Formate released from the mitochondria into the cytoplasm can be reattached to THF by the synthetase activity of the cytoplasmic trifunctional MTHFD1 (Figure 1.2, reaction 1). This synthetase reaction forms 10-CHO-THF and consumes one ATP, meaning that there is no net synthesis of ATP from the mitochondrial 10-CHO-THF synthetase reaction. This 10-CHO-THF can again proceed in one of several directions. 10-CHO-THF can be oxidized to CO_2 and THF by the cytoplasmic 10-CHO-THF

11

dehydrogenase ALDH1L1. ALDH1L1 is highly expressed in adult livers, accounting for approximately 1.2% of the total cellular protein (Cook and Wagner, 1982). Unlike its mitochondrial homologue, ALDH1L1 is downregulated in most cancer cells (Krupenko, 2009; Krupenko and Oleinik, 2002).

One of the major roles of 10-CHO-CHF in the cytoplasm is as a substrate for *de novo* purine synthesis (Figure 1.2). Two reactions during *de novo* purine synthesis incorporate the formyl group from 10-CHO-THF into the growing purine ring. The reactions catalyzed by GAR transformylase and AICAR transformylase incorporate the formyl group into carbons 8 and 2 respectively of the purine ring (Barlowe and Appling, 1988; Pasternack et al., 1994; Tibbetts and Appling, 1997, 2000).

10-CHO-THF can also be reduced to CH_2-THF by the dehydrogenase and cyclohydrolase activities of MTHFD1, reversing the oxidation that was done in the mitochondria. This cytoplasmic CH_2-THF can be used as a substrate for thymidylate synthesis (Figure 1.2, reaction 10). Thymidylate synthase catalyzes the reductive methylation of dUMP forming dTMP and oxidizing THF to dihydrofolate (Hardy et al., 1987). THF can be reformed from dihydrofolate by DHFR. As growing cancer cells require dTMP synthesis to support proliferation, thymidylate synthase is a common target for chemotherapeutic agents (Hardy et al., 1987; Peters et al., 2002).

Finally, CH_2-THF can be irreversibly reduced to CH_3-THF by methylenetetrahydrofolate reductase (MTHFR) for use in the methylation cycle (Figure 1.2, reaction 6). Sufficient supply of 1C units to the methyl cycle is critical for proper cellular function, and disruption of MTHFR has been implicated in a variety of disorders including cardiovascular disease, neural tube defects, Alzheimer's disease, and autism (Liew and Gupta, 2015; Rai, 2016a, 2016b; Román, 2015; Sener et al., 2014; Yang et al., 2015). Increased risk for many of these disorders is associated with a common

polymorphism in MTHFR (C677T) which reduces the activity of MTHFR (Frosst et al., 1995). The frequency of the T allele is variable but can reach as high as 40% in some populations (Alluri et al., 2005; Li et al., 2005; Wang et al., 2005). Methionine synthase catalyzes the entry of the 1C unit from CH_3-THF into the methyl cycle by methylating homocysteine to form methionine in a vitamin B12-dependent reaction (Figure 1.2, reaction 7). Methionine is adenylated by S-adenosylmethionine synthetase to make the universal methyl donor S-adenosylmethionine (SAM) (Cantoni, 1951). SAM is involved in the methylation of a variety of biomolecules including proteins, DNA, RNA, and phospholipids (reviewed in (Chiang et al., 1996; Su et al., 2016)). S-adenosylhomocysteine (SAH) is released as a byproduct of the methylation reaction and broken down into homocysteine and adenosine by SAH hydrolase (Turner et al., 2000). This homocysteine can either be remethylated back to methionine or enter the transsulfuration pathway to synthesize cysteine (Mudd et al., 1965).

1.1.2.4 Nuclear One-Carbon Metabolism

Recent studies have shown that folate dependent synthesis of dTMP can also take place in the nucleus. During S-phase, several folate-dependent enzymes localize to the nucleus. Thymidylate synthase, DHFR, and SHMT1 all undergo sumoylation and localize to the nucleus (Anderson et al., 2007; Woeller et al., 2007). In addition, there is a splice variant of SHMT2 lacking exon 1 (SHTM2α) that has also been shown to localize to the nucleus (Anderson and Stover, 2009). Finally, MTHFD1 also localizes to the nucleus during S-phase (Field et al., 2014). Although MTHFD1 is not strictly required for dTMP synthesis, its transport to the nucleus could provide "on-site" production of CH_2-THF to enhance dTMP synthesis. This localization of a dTMP synthetic system to the

nucleus appears to be critical during S-phase as disruption of this system in the nucleus leads to increased accumulation of uracil in DNA (MacFarlane et al., 2011).

1.2 FOLATE METABOLISM IN EMBRYOGENESIS AND NEURULATION

1.2.1 Mammalian Neural Tube Closure

Embryogenesis is a highly complex process requiring the coordination of cell division, differentiation, and migration to form an organism composed of specialized organs and tissues from a single cell. One of the most important events during embryogenesis is neurulation. During neurulation, a region of surface ectoderm on the dorsal side of the embryo called the neural plate folds and fuses in order to form a hollow tube known as the neural tube. The neural tube is the precursor to the brain and spinal cord, which make up the central nervous system. Proper closure of the neural tube is critical for the development of a healthy and functional organism, and a variety of factors including genetics, maternal diet, and environment can adversely affect it.

Neurulation first begins around 18 days post conception in humans (day 8 in mice) with the thickening of the dorsal midline ectoderm to form the neural plate (reviewed in (Copp et al., 2003; Detrait et al., 2005). The neural plate first forms near the cranial region of the embryo and extends both towards the anterior (rostral) and posterior (caudal) ends of the embryo through a process known as convergent extension. During convergent extension, cells migrate medially and intercalate along the dorsal midline to both narrow and extend the neural plate. The two lateral edges of the neural plate (neural folds) begin to extend and then bend about a central axis known as the median hinge point (MHP). The extended neural folds then bend again about halfway from the MHP at the dorsolateral hinge points. This brings the ends of the neural folds together and allows them to fuse, forming the neural tube. In mice, fusion of the neural folds is initiated at a

minimum of three different sites along the length of the embryo, but there is likely only one initiation site in humans. In either species however, fusion of the neural folds extends both rostrally and caudally from the point of initiation. The neural tube is generally fully formed by day 28 in humans (day 10.5 in mice). When the neural folds fail to fuse correctly, it can lead to one of several types of NTDs depending on where the failure occurred. Failure of the neural tube to close in the mid/hindbrain region is called exencephaly and leaves brain tissue exposed outside of the skull. Exencephaly can develop into the more severe anencephaly where the brain tissue has degraded. If fusion on the spine fails to initiate, the neural tube remains open along the length of the spine and is called craniorachischisis. Spina bifida occurs when fusion is initiated on the spine, but caudal fusion fails before the tube can be fully closed.

Happening concurrently with neural tube closure is another important process known as neural crest cell (NCC) migration (reviewed in (Huang and Saint-Jeannet, 2004)). NCCs are transient cells that form below the ectoderm in proximity to the neural tube around the time of closure. Upon induction by a variety of signals originating from both the ectoderm and the mesoderm, NCCs will delaminate and migrate throughout the embryo, forming numerous tissues and structures. NCCs forming at different regions along the spine will give rise to different sets of derivatives. NCCs at the anterior of the neural tube form cranial crest cells. These will eventually form craniofacial bone and cartilage, connective tissue, and neurons in the face. Just posterior to the cranial crest cells are the vagal crest cells. These give rise to pigment cells, enteric neurons, and smooth muscle in the cardiovascular system. Trunk NCCs form pigment cells, much of the neurons that comprise the peripheral nervous system, and the adrenal medula. At the posterior of the neural tube, sacral NCCs form neurons of the lower intestines.

Disruptions to either formation, induction, or migration of NCCs are responsible for a range of birth defects including craniofacial, cardiovascular, and pigmentation defects.

1.2.2 History of Folic Acid Fortification in the United States

The link between low folate status in pregnant women and risk of NTDs first became apparent in the 1960s and 1970s (Hibbard, 1964, 1967; Smithells et al., 1976). Nearly two decades later, two randomized, controlled trials established that periconceptional folic acid supplementation could be preventative of NTDs. The first involved women who were at high risk of having an NTD affected pregnancy, due to a history of a previously affected pregnancy. It was found that folic acid supplementation reduced the risk of NTD reoccurrence by approximately 70% (MRC Vitamin Study Research Group, 1991). The following year, another study demonstrated that the first occurrence of NTDs could also be prevented by periconceptional supplementation of folic acid (Czeizel and Dudás, 1992). Consequently, the CDC recommended that all women who were capable of becoming pregnant consume 400 μg/day folic acid in an effort to prevent NTDs (Centers for Disease Control, 1992). Unfortunately, the success of the recommendation alone was limited; a survey found that as few as 29% of women consumed the recommended amount of folic acid by 1998 (Centers for Disease Control, 1999). In addition, up to 50% of pregnancies in the United States are unplanned, and many women may not discover they are pregnant until after the point of neural tube closure (Finer and Henshaw, 2006). In 1996, to try to ensure that all women of childbearing age received sufficient levels of folate in their diet, the US Food and Drug Administration mandated that all enriched cereal-grains be fortified with 140 μg folic acid /100 g (Food and Drug Administration, 1996). Several studies have evaluated the effectiveness of fortification on decreasing NTDs in the US and have found that NTDs

decreased by amounts ranging from 19-31% (Boulet et al., 2008; Honein et al., 2001; Williams et al., 2002). Despite this success, some cases of NTDs appear to be resistant to folate supplementation (as seen by the 30% reoccurrence rate in the MRC study). More work is needed to understand the mechanism of the protective effect of folate supplementation and why some NTDs cannot be rescued by folate supplementation.

1.2.3 Mouse Models of Folate Metabolism and Neural Tube Defects

One of the most common tools used to study mammalian neural tube closure is mouse mutants or strains that develop NTDs. As of 2010, over 240 such strains have been reported (Harris and Juriloff, 2010). Few of these mutants have been tested for responsiveness to folic acid and even fewer target genes directly involved in folate metabolism. Genes related to folate metabolism that have been targeted include *Folr1*, *Shmt1*, *Amt*, *Gldc*, and *Mthfd1l*. Only *Folr1* and *Shmt1* were found to be responsive to folate supplementation. Both these and the folate unresponsive genes will be discussed in more detail below.

1.2.3.1 NTD Mutants Responsive to Folate

Mouse embryos containing a homozygous deletion of either *Folr1* or *Shmt1* have both been shown to exhibit neural tube defects that are sensitive to folate status. Deletion of *Folr1* essentially renders embryos folate deficient by severely disrupting cellular uptake of folate. Homozygous deletion of *Folr1* is embryonic lethal, and *Folr1*$^{-/-}$ embryos do not survive past E10. *Folr1*$^{-/-}$ embryos are developmentally delayed and die before the point of neural tube closure (Piedrahita et al., 1999). Supplementation of dams with low doses of folate, in the form of either 5-CH$_3$-THF or 5-CHO-THF, improved survivability of *Folr1*$^{-/-}$ embryos, albeit with a plethora of developmental defects. Observed defects include NTDs (exencephaly, encephalocele, and craniorachischisis), craniofacial,

abdominal, and ocular defects. Larger doses of folate conferred a higher level of protection against these defects and allowed some $Folr1^{-/-}$ mice to survive until adulthood. Surviving $Folr1^{-/-}$ mice were found to have defects including brachycephaly, ocular defects, and teeth malocclusions. $Folr1^{-/-}$ mice also had much lower serum folate than their littermates (Spiegelstein et al., 2004).

When dams are fed a folate replete diet, $Shmt1^{-/-}$ mice appear to develop normally, suggesting that cytosolic SHMT activity is not essential for development under normal circumstances (Beaudin et al., 2012). When dams are placed on a folate deficient diet, both $Shmt1^{-/-}$ and $Shmt1^{+/-}$ embryos have NTDs at a higher rate than $Shmt^{+/+}$ littermates, though the rate is highest in $Shmt1^{-/-}$ embryos (14%) (Beaudin et al., 2011). The predominant NTD found in these mice is exencephaly. Due to the involvement of SHMT1 in thymidylate synthesis in the nucleus, the authors suggest that disruption of thymidylate synthesis may be one of the main factors leading to NTDs in these mice (Anderson and Stover, 2009).

1.2.3.2 NTD Mutants not Responsive to Folate

Perhaps more interesting than the folate responsive mouse models are the folate metabolism-related mutants that do not respond to folic acid supplementation. These mutants can give us a better understanding of NTDs in humans that are resistant to folate supplementation and may lead to alternate supplements or therapies that can further reduce the rate of NTDs in humans.

Our lab has recently reported the characterization of a homozygous deletion of $Mthfd1l$ in mice. We found that $Mthfd1l$ null ($Mthfd1l^{z/z}$) mice did not survive past E12.5 and had aberrant neural tube closure characterized by exencephaly, craniorachischisis, or wavy neural tubes (Momb et al., 2013). Supplementation of dams with 5-CHO-THF did

not rescue the NTD phenotype (Jessica Momb, unpublished data). However, maternal supplementation with formate, the end product of mitochondrial folate metabolism produced by MTHFD1L, not only increased the survival of embryos past E12.5, but also reduced the incidence of NTDs. Another folate resistant NTD mouse is the *curly tail* mouse (Seller, 1994). *Curly tail* mice are characterized by a hypomorphic allele of the *grainyhead-like 3 (Grhl3)* transcription factor. Increasing expression of *Grhl3* reduces spina bifida in the *curly tail* mouse but is not protective against exencephaly (Gustavsson et al., 2007). It has recently been shown that *curly tail* mice also express abnormally low levels of *Mthfd1l*, suggesting the possibility that it is the decreased MTHFD1L activity that is responsible for exencephaly in these mice. In support of this idea, it was found that maternal formate supplementation reduced the rates of both spina bifida and exencephaly in *curly tail* mice (Sudiwala et al., 2016).

Two other genes involved in mitochondrial folate metabolism have been found to be associated with NTDs. Deletion of either *Gldc* or *Amt*, both of which are found in the mitochondrial GCS, causes NTDs in embryos (Narisawa et al., 2012; Pai et al., 2015). The primary defect observed was exencephaly, but a smaller percentage of mice developed craniorachischisis. Folic acid supplementation in either mouse line was ineffective in rescuing the NTD phenotype. As with $Mthfd1l^{-/-}$ mice, maternal formate supplementation decreased NTDs in $Gldc^{-/-}$ mice (Pai et al., 2015). $Amt^{-/-}$ mice were not tested with formate, but another 1C metabolite, methionine, was shown to decrease NTDs (Narisawa et al., 2012).

Chapter 2: Characterization of expression of MTHFD gene family and alternative splicing of MTHFD2L

2.1 INTRODUCTION

For decades the only known mitochondrial CH_2-THF dehydrogenase/CH^+-THF cyclohydrolase was MTHFD2 (Mejia and MacKenzie, 1985; Mejia et al., 1986). This protein could only be detected in immortalized mammalian cells, embryos, or nondifferentiated tissues, but not in adult differentiated tissues (Christensen and Mackenzie, 2008). Although it had been shown that intact adult liver mitochondria were capable of oxidizing the 3-carbon of serine to formate and CO_2 in a THF dependent manner, the enzyme responsible for this activity remained unidentified (Barlowe and Appling, 1988).

In 2011 our lab reported the discovery of a new CH_2-THF dehydrogenase, MTHFD2L (Bolusani et al., 2011). MTHFD2L is homologous to MTHFD2, sharing 60-70% sequence identity. Using a V5 epitope-tagged rat MTHFD2L expressed in CHO cells it was shown that MTHFD2L is a mitochondrial protein that is localized to the matrix side of the inner mitochondrial membrane. Rat MTHFD2L expressed in yeast was shown to possess $NADP^+$-dependent CH_2-THF dehydrogenase activity. The study identified alternative splicing of two different exons, exon 2 and exon 8, in MTHFD2L in both humans and rats. Details of alternative splicing of these exons will be discussed in more detail below.

It is currently unknown why mammals might possess two mitochondrial CH_2-THF dehydrogenases. One possibility is that the two proteins differ enzymatically, either in activity or cofactor specificity. Another possibility is that they differ in their tissue distribution or expression profiles.

We have reported the enzymatic characterization of purified rat MTHFD2L (Shin et al., 2014). MTHFD2L possesses both CH_2-THF dehydrogenase and CH^+-THF cyclohydrolase activities. For its CH_2-dehydrogenase activity, MTHFD2L can use either $NADP^+$ or NAD^+ as a cofactor, but activity with NAD^+ also requires the presence of magnesium and inorganic phosphate. At saturating substrate concentrations, MTHFD2L shows a preference for NAD^+, but it appears to have equal preference for NAD^+ and $NADP^+$ at physiological substrate concentrations (Shin et al., 2014).

This chapter will describe my work on the characterization of the expression profile of MTHFD2L in developing mouse embryos and adult mice. It will also describe my investigation of the expression, enzymatic activity, and subcellular localization of MTHFD2L splice variants.

Portions of this work have been previously published. (Shin, M, **Bryant, JD**, Momb, J, Appling, DR (2014) *J. Biol. Chem.* 289(22): 15507-15517). These sections will be indicated by quotation marks and additional indentation.

2.2 METHODS AND MATERIALS

2.2.1 Materials

"All reagents were of the highest commercial grade available. NAD^+ and $NADP^+$ were purchased from U. S. Biological (Swampscott, MA) and Sigma, respectively. HRP-conjugated goat anti-rabbit IgG was from Invitrogen, and the ECL Plus chemiluminescence detection kit was from GE Healthcare Life Sciences. THF was prepared by the hydrogenation of folic acid (Sigma) using platinum oxide as a catalyst and purification of the THF product on a DEAE cellulose column (Sigma)(Blakley, 1957; Curthoys and Rabinowitz, 1971). CH_2-THF was prepared nonenzymatically from THF and formaldehyde (Fisher)(Appling and West, 1997). The yield of CH_2-THF was determined by solving the equilibria of THF, formaldehyde, and β-mercaptoethanol (Kallen and Jencks, 1966)."

2.2.2 Mouse Work

"All animals used within this study were maintained according to protocols approved by the Institutional Animal Care and Use Committee of The University of Texas at Austin and conform to the National Institutes of Health Guide for the Care and Use of Laboratory Animals."

2.2.3 RNA Isolation and cDNA Synthesis

"Tissue was collected from six male and six female C57BL/6 mice between 4 and 6 weeks of age. Embryos were dissected at the days indicated. For embryonic days 8.5–11.5, five embryos were pooled for each time point; for embryonic days 12.5–17.5, three embryos were pooled for each time point. Tissue and embryos were washed with PBS and then stored in RNAlater (Applied

Biosystems Inc. (ABI)). Embryos from each day were pooled prior to RNA isolation. RNA was isolated using TRI reagent (ABI) and treated with TurboDnase (Invitrogen) following the manufacturer's instructions. RNA quality was verified by confirmation of the presence of 28S and 18S rRNA bands on an agarose gel. cDNA was synthesized using SuperScript III (Invitrogen) and random hexamers."

2.2.4 Real Time PCR

"Primers against mouse MTHFD1, MTHFD1L, MTHFD2, MTHFD2L, eEF2 (eukaryotic translation elongation factor 2), and TBP (TATA-box-binding protein) were designed using Primer-BLAST (Ye et al., 2012) to yield an amplicon between 95 and 125 base pairs long and cross at least one exon-exon junction (see Table 2.1). Primers were checked individually against plasmids containing mouse MTHFD1, MTHFD1L, MTHFD2, and MTHFD2L to ensure that the primer pairs were specific to the target gene. Quantitative real-time PCR was performed using SYBR Green (Qiagen) on an ABI ViiA 7 using a two-step program (50 °C for 2 min and then 95 °C for 10 min followed by 40 cycles of 95 °C for 15 s and 60 °C for 15 s). The specificity of the reaction was verified by melt curve analysis. Relative expression values from embryos were calculated by normalizing to TBP (Willems et al., 2006), and values from adult tissues were normalized to eEF2 (Kouadjo et al., 2007).

"We have shown previously that MTHFD2L is alternatively spliced at exons 2 and 8 (Bolusani et al., 2011). To determine the abundance of the splice variants of MTHFD2L containing exon 2 or exon 8, we designed primer pairs that would bind in exons 2 and 3 or in exons 7 and 8, so that they would produce only

23

Primer name	Sequence	Location
MTHFD1 F	5'-TTCATCCCATGCACACCCAA-3'	Exon 6
MTHFD1 R	5'-ATGCATGGGTGCACCAACTA-3'	Exon 7
MTHFD1L F	5'-GGACCCACTTTTGGAGTGAA-3'	Exon 12
MTHFD1L R	5'-ATGTCCCCAGTCAGGTGAAG-3'	Exon 14
MTHFD2 F	5'-ACAGATGGAGCTCACGAACG-3'	Exon 5
MTHFD2 R	5'-TGCCAGCGGCAGATATTACA-3'	Exon 6
MTHFD2L F1	5'-GGCGGGAAGATCCAAGAACG-3'	Exon 6
MTHFD2L R1	5'-CGCTATCGTCACCGTTGCAT-3'	Exon 7
MTHFD2L F2	5'-GGCCAGCAGAGAGAAGAGACT-3'	Exon 2
MTHFD2L R2	5'-CCATGATTCCACTCCTTGCT-3'	Exon 3
MTHFD2L F3	5'-GAGGTGATGCAACGGTGAC-3'	Exon 7
MTHFD2L R3	5'-GAATACCCGCAGCCACTATG-3'	Exon 8
eEF2 F	5'-CGCATCGTGGAGAACGTCAA-3'	Exon 4
eEF2 R	5'-GCCAGAACCAAAGCCTACGG-3'	Exon 5
TBP F	5'-CATGGACCAGAACAACAGCC-3'	Exon 2
TBP R	5'-TAAGTCCTGTGCCGTAAGGC-3'	Exon 3

Table 2.1   Primers used for expression profiling of the MTHFD gene family in embryos and adult tissues.

a product from splice variants containing exon 2 or exon 8, respectively. The expression values for these primer pairs were normalized to the expression levels found using primers MTHFD2L F1 and R1, which bind in exons 6 and 7. There is no evidence for alternative splicing of these exons, and they are thus assumed to represent the total amount of MTHFD2L transcript, including all splice variants."

2.2.5 In situ hybridization of whole mouse embryos

"Mouse embryos ranging from E9.5 to 12.5 were hybridized as described previously using digoxigenin-labeled UTP RNA probes (Pike et al., 2010). Antisense probes were constructed as described previously (Pike et al., 2010) by in vitro transcription using T7 RNA polymerase to transcribe from Riken clone 1110019K23 (Kawai et al., 2001) linearized with BamHI. Sense probes were made by linearizing with XhoI and transcribing with T3 RNA polymerase."

2.2.6 5,10-Methylene-THF Dehydrogenase Assay

Full length rat MTHFD2L and MTHFD2L lacking exon 8 in the yeast expression vector yEP24 (see below) were transformed into *S. cerevisiae* strain MWY4.4 (*ser1 ura3–52 trp1 his4 leu2 ade3–65 Δmtd1*) using a high efficiency lithium acetate transformation procedure (Gietz and Woods, 2002; West et al., 1993). The preparation of yeast crude lysates was performed as described previously (Bolusani et al., 2011). 5,10 methylene-THF dehydrogenase activity of yeast crude lysate was measured using an endpoint assay as detailed in (Wagner et al., 2005). The final concentration of reagents in the reaction buffer was 50 mM HEPES (pH 8.0), 100 mM KCl, 5 mM $MgCl_2$, 0.4 mM CH2-THF, 40 mM β-mercaptoethanol, and either NAD^+ (1 mM) or $NADP^+$ (6 mM). Reactions using NAD^+ also contained 25 mM potassium phosphate. Reactions were carried out in PCR tubes then were transferred to a 96 well microplate for absorbance

measurements. 60 uL of reaction buffer was added to each tube. 20 uL of yeast crude lysate (see below) at a concentration of 7.75 mg/mL was added to each tube. 20 uL of THF (1 mM) was added to initiate the reactions. The tubes were incubated at 30°C for 5 minutes, then the reactions were quenched by the addition of 200 uL 3% perchloric acid. Blank reactions were also set up in which the perchloric acid was added before the yeast crude lysate. The PCR tubes were centrifuged to pellet the precipitated proteins, and the supernatant was transferred to a microplate and the absorbance at 350 nm, 900 nm, and 1,000 nm was measured. Near infrared measurements were used for path length correction (Palmer and Williams, 1974).

2.2.7 *In Vivo* Yeast Complementation Assay

"Exon 8 was removed from pET22b-rMTHFD2L by overlap extension PCR (Ho et al., 1989) using the primers rD2L-x8 5'/HindIII F (5'-ATCTAAGCTTATGGCGACGCGGGCCCGT-3'), rD2L-x8 5' R (5'-TAACAG CTGCAGCCACTATGATAATCT-3'), rD2L-x8 3' F (5'-CTGCAGCTGTTAA GAAGAAGGCCAGC-3'), and rD2L-x8 3'/BamHI R (V5) (5'-TGAT GGATCC A GTAGGTGATATTCTTGGCAGCCAG-3'). Following PCR, rMTHFD2L-x8 was subcloned into YEp24ES (Bolusani et al., 2011; Suliman et al., 2005) using the HindIII and BamHI restriction sites. Plasmids were transformed into the yeast strain MWY4.5 (ser1 ura3–52 trp1 leu2 his4 ade3–30/65 mtd1), and transformants were selected for uracil prototrophy. The *in vivo* complementation assay was performed in this yeast strain as described previously (Bolusani et al., 2011).

"Preparation of crude yeast lysates and immunoblotting were carried out as described previously (Bolusani et al., 2011). The protein concentration was determined by BCA assay (Thermo Fisher Scientific)."

2.2.8 Submitochondrial localization of MTHFD2L lacking exon 8

Rat MTHFD2L lacking exon 8 (see above) was subcloned into the pcDNA3.1 expression vector (Thermo Fisher Scientific) using the BamHI and HindIII restriction sites to make the pcDNA3.1/rD2L-x8 construct. The pcDNA3.1 vector contains a CMV promoter for expression in mammalian cell lines and introduces a C-terminal V5 epitope tag. pcDNA3.1/rD2L-x8 was transiently transfected into the glyB Chinese hamster ovary (CHO) cell line. To do this, the CHO cells were plated onto 6 6 well plates (36 wells in total) and grown to approximately 60% confluency. 26 µL of pcDNA3.1/rD2L-x8 DNA (1.42 µg/µL) was mixed with 714 µL OptiMEM (Thermo Fisher Scientific). In a separate tube, 74 µL was mixed with 666 µL OptiMEM. After leaving at room temperature for 5 minutes these tubes were combined and incubated at room temperature for 30 minutes. This mixture was then added to 29.6 mL OptiMEM that had been prewarmed to 37$^{\text{o}}$C. The media from all wells was aspirated and wells were washed with 2 mL PBS. After the PBS was aspirated, 840 µL of the OptiMEM/Lipofectamine/DNA mixture was added to 35 wells. Only OptiMEM was added to the 36th well to act as a negative control. Cells were incubated at 37$^{\text{o}}$C, 5% CO_2 for two days. The media was aspirated from all wells and wells were washed with PBS. Cells from 34 of 36 wells were trypsinized and pooled. Mitochondria were isolated from these cells as described previously (Bolusani et al., 2011). Cells from the remaining two wells (the negative control and one additional well) were treated with 200 µL NP-40 lysis buffer (50 mM Tris, 150 mM NaCl, 1% NP-40, pH 8.0) to create the whole cell lysate. The isolated mitochondria were pelleted by

27

centrifugation at 12,000 x g and resuspended in 100 µL HMS (0.25 M sucrose, 1 mM EGTA, 10 mM HEPES, pH 7.4) containing 0.5% Triton X-100 then incubated on ice for 30 minutes. This solution was centrifuged at 100,000 x g, and the supernatant was transferred to a new tube. The pellet was resuspended in 100 µL HMS (0.5% Triton X-100) and centrifuged again. The two supernatant fractions were combined to give the soluble mitochondrial fraction (MitoS), and the pellet was resuspended in 30 µL HMS (0.5% Triton X-100) to give the mitochondrial membrane fraction (MitoP).

2.3 RESULTS

2.3.1 Expression of MTHFD Genes During Mouse Embryonic Development

"It has been reported previously that the MTHFD2 gene is expressed in early embryos, but its expression declines as the embryo approaches birth, and the MTHFD2 enzyme is found only in nondifferentiated tissues in adults (Di Pietro et al., 2004; Pike et al., 2010). We determined the relative expression profiles of all four MTHFD gene family members in mouse embryos using real-time PCR, normalizing to TBP (TATA-box-binding protein) expression. TBP has been determined to be stably expressed at multiple stages of embryonic development, making it a suitable housekeeping gene for real-time PCR experiments involving embryos (Willems et al., 2006). MTHFD1 and MTHFD1L transcript expression was highest at E8.5 and subsequently decreased until expression increased again at E13.5–17.5 (Figure 2.1). MTHFD2 expression was low at all embryonic days examined. MTHFD2L was also expressed at all embryonic days examined. MTHFD2L expression was low at E8.5 but increased beginning at E10.5 (Figure 2.1). These profiles suggest that a switch between MTHFD2 and MTHFD2L
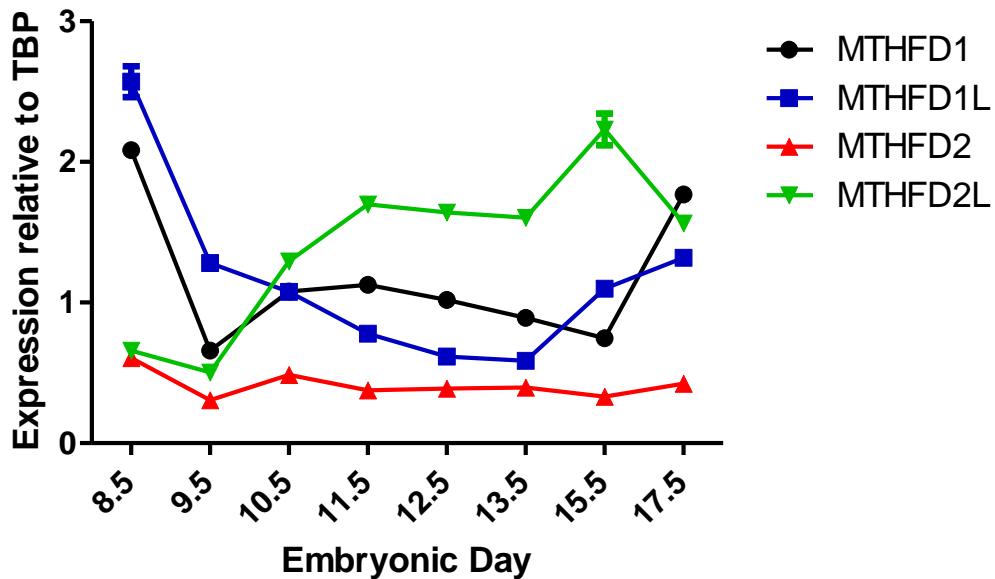
Figure 2.1   Temporal expression profile of MTHFD gene family in mouse embryos. The relative expression profiles of MTHFD1 (●), MTHFD1L (■), MTHFD2 (▲), and MTHFD2L (▼) was determined by real-time PCR as described under "Materials and Methods." The age of the embryos from which the RNA was obtained is indicated in embryonic days (birth occurs at E20.0). mRNA expression was normalized to that of the TBP transcript. Each point represents the mean +/- S.E. of triplicate determinations (error bars are included for all data points but are obscured by the data symbol when the scatter is small).

expression occurs approximately between embryonic days 8.5 and 10.5 during mouse embryogenesis.

"*In situ* hybridization of whole mouse embryos (Figure 2.2) revealed that MTHFD2L is expressed in the neural tube and the forebrain, midbrain, and hindbrain, suggesting a possible role in neural tube development. Other areas of intense staining included the branchial arches and limb buds, particularly along the progress zone."

2.3.2 Expression of MTHFD Genes in Male and Female Adult Mice

"Expression of adult MTHFD genes from male and female mice was normalized to the expression of eEF2, a housekeeping gene that is stably expressed in a wide array of adult tissues (Kouadjo et al., 2007). The MTHFD2L transcript was expressed in all of the tissues examined, with the highest expression observed in brain and lung and lower expression in liver and kidney (Figure 2.3). As has been reported previously, MTHFD1 showed the highest expression in liver and kidney (Thigpen et al., 1990). MTHFD1L was most highly expressed in brain and spleen. The MTHFD2 transcript could be detected at low levels in most tissues, but only testis and spleen expressed it at even a modest level. The expression patterns of the four transcripts were similar in males and females."

2.3.3 MTHFD2L Alternative Splicing

"*MTHFD2L* transcripts were analyzed by RT-PCR on RNA from human brain and placenta as described under 'Materials and Methods.' These analyses revealed alternative splicing of two exons in the human *MTHFD2L* gene. Doublets were observed with primers that flanked exon 2 or exon 8 in both brain
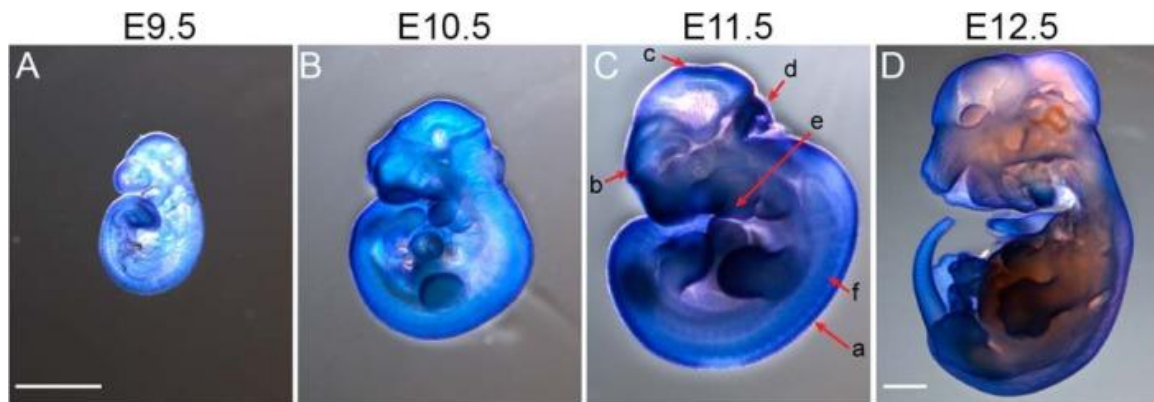
Figure 2.2   Spatial distribution of MTHFD2L expression in mouse embryos. "*In situ* hybridizations of whole mount embryos ranging from E9.5 to E12.5 (*A–D*) were performed using digoxigenin-labeled UTP RNA probes as described under 'Materials and Methods.' *C*, as shown on the E11.5 embryo, *MTHFD2L* is especially prominent in the neural tube (*a*), forebrain (*b*), midbrain (*c*), hindbrain (*d*), branchial arches (*e*), and somites (*f*). Embryos *A–C* were imaged at the same magnification (×20). Embryo *D* was imaged at ×12.5 magnification. *Scale bars* correspond to 1 mm."
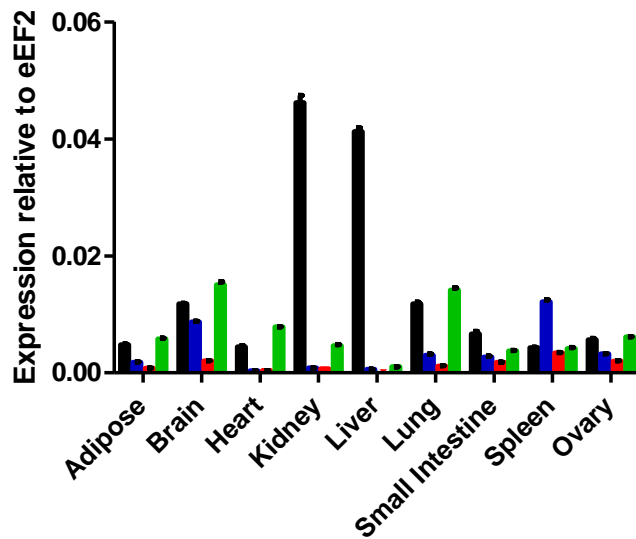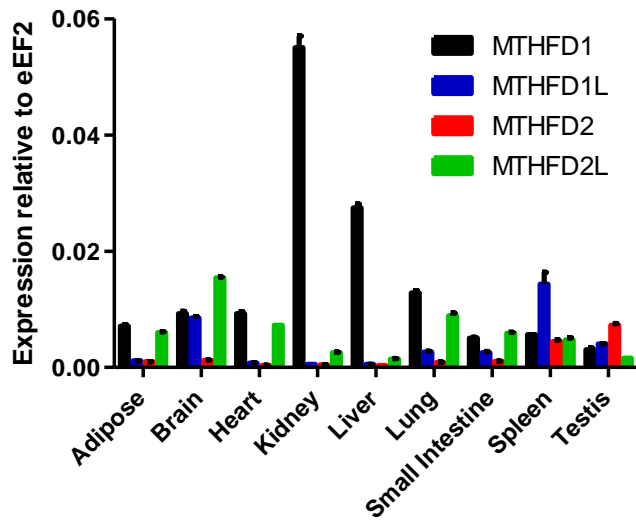
Figure 2.3   Tissue specific expression of the MTHFD gene family. The relative expression of MTHFD1, MTHFD1L, MTHFD2, and MTHFD2L was determined as described under "Materials and Methods." mRNA expression was normalized to that of the eEF2 transcript in female (top) and male (bottom) adult mice. Each bar represents the mean +/- S.E. of triplicate determinations.

and placenta RNA (Figure 2.4, *B* and *C*). The band intensity of the exon 8 doublet was always weak with placenta RNA. Sequence analysis of the cloned PCR products confirmed that the larger product of each doublet included the alternate exon (2 or 8), and the smaller product of each doublet lacked the alternate exon. This alternative splicing thus produces at least three classes of transcripts from the human *MTHFD2L* gene (Figure 2.4, *A*). In class I transcripts, the 34-bp exon 2 is skipped, giving an mRNA that encodes the 347-amino acid protein… In class II transcripts, exon 2 is retained; translation of this mRNA from the first AUG codon in exon 1 would produce an early termination product of only 60 amino acids. However, translation of the class II mRNA from an AUG codon in exon 3 would give a protein identical to the last 289 amino acids of the class I protein. In class III transcripts, both exon 2 and exon 8 are skipped. Based on sequenced RT-PCR clones and expressed sequence tags in the NCBI EST databases, all three transcript classes are expressed in both brain and placenta from adult humans." (Bolusani et al., 2011)

"RT-PCR analysis of RNA isolated from adult rat tissues revealed that the *MTHFD2L* gene is widely expressed (Figure 2.5). The 34-bp exon 2 is also found in the mouse and rat *MTHFD2L* genes. Although the majority of mouse and rat expressed sequence tags in the NCBI EST database lack exon 2, there are several that contain this exon. RT-PCR on rat brain RNA using primers in exons 1 and 3 produced two products, although the longer product (containing exon 2) was the minor species (data not shown). RT-PCR using primers in exons 7 and 9 also produced two products with rat RNAs, a 338-bp product containing exon 8 and a 212-bp product lacking exon 8 (Figure 2.5). Sequence analysis of the 212-bp product indicated precise splicing of exon 7 to exon 9 with the reading frame

intact. In all tissues examined, the exon 8 skipped transcript is the minor species." (Bolusani et al., 2011)

We also examined alternative splicing of MTHFD2L during development. "Using total embryo RNA from embryos ages E8.5 to E17.5, we observed that exon 2 was present in less than 10% of the transcripts in all of the embryonic days examined (Figure 2.5), indicating that the vast majority of MTHFD2L transcripts encode a mitochondrial targeting sequence. Exon 8, on the other hand, was found to be missing in 20– 45% of the MTHFD2L transcripts throughout embryogenesis (Figure 2.5).

"To determine what effect the removal of exon 8 would have on MTHFD2L activity, MTHFD2L lacking exon 8 was expressed in yeast. NAD-dependent CH_2-THF dehydrogenase activity could not be detected in crude yeast lysate from yeast cells transformed with the truncated construct (YEp-rD2L-x8; Figure 2.6). NAD-dependent CH_2-THF dehydrogenase activity was easily detectable in lysate from yeast cells transformed with the full-length construct.

"We next asked whether MTHFD2L lacking exon 8 was active *in vivo*, using a yeast complementation assay (Bolusani et al., 2011). Briefly, this assay uses yeast strain MWY4.5, which lacks cytoplasmic CH_2- THF dehydrogenase activities as well as the 10-formyl-THF synthetase activity of the cytoplasmic trifunctional C1-THF synthase (West et al., 1996). Wild-type yeast can produce 10-CHO-THF for de novo purine biosynthesis from serine using either cytoplasmic or mitochondrial 1C pathways (36) (see Figure 1.2). However, MWY4.5 is blocked in both pathways to 10-CHO-THF. This blockage creates a requirement for adenine in the growth medium (West et al., 1996).
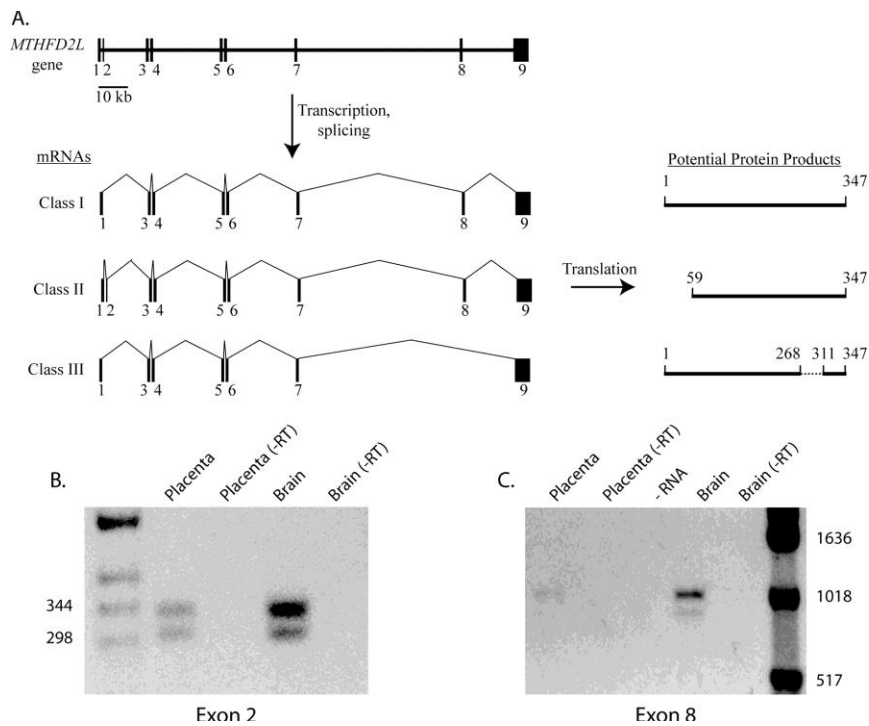
Figure 2.4   MTHFD2L gene structure and alternative splicing. "*A*, gene structure, alternative splicing, and potential protein products. The entire gene spans 145 kbp on chromosome 4 at 4q13.3. Exons are shown as *numbered black bars*; introns are shown as *thin horizontal lines*. Exons are not drawn to scale. Three alternative splicing patterns due to skipping of exon 2 and/or 8 are observed in human brain and placenta….*B*, RT-PCR analysis of exon 2 splicing using primers binding in exons 1 and 3... The expected sizes of the two products are 335 bp (including exon 2) and 301 bp (excluding exon 2). −*RT*, minus reverse transcriptase control. *C*, RT-PCR analysis of exon 8 splicing using primers binding in exons 1 and 9... The expected sizes of the two products are 980 bp (including exon 8) and 852 bp (excluding exon 8). DNA size markers are indicated."(Bolusani et al., 2011)
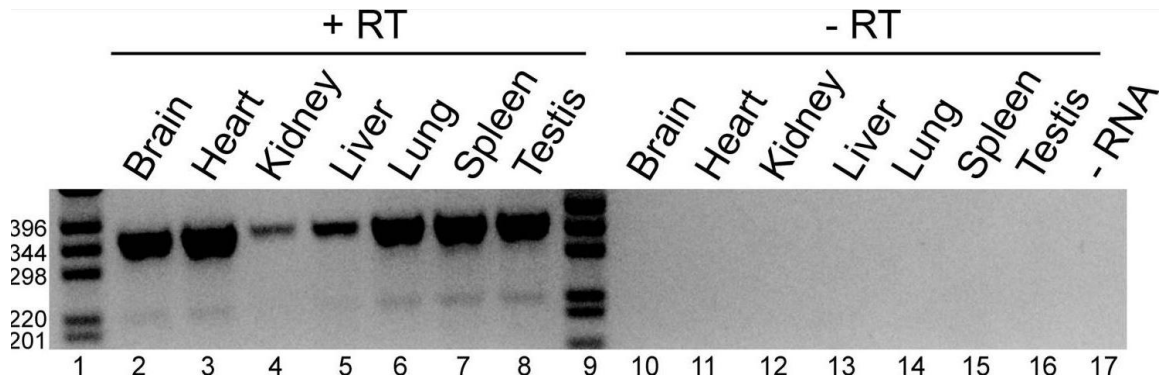
Figure 2.5   "MTHFD2L expression in adult rat tissues. Total RNA isolated from the indicated adult rat tissues was analyzed by RT-PCR as described under "Materials and Methods" using primers binding in exons 7 (5'-CGGTGACCATAGCTCACAGA) and 9 (5'-GCTCTCCCCTGCGATC-TAGTA). The expected sizes of the two products are 338 bp (including exon 8) and 212 bp (excluding exon 8). *Lanes 1* and *9* contain DNA size markers (sizes indicated on *left*). *Lanes 2–8,* reverse transcriptase samples (+ *RT*); *lanes 10–16,* minus reverse transcriptase controls (− *RT*); *lane 17,* minus RNA control (− *RNA*; contained reverse transcriptase). The image is overexposed to reveal the smaller band." (Bolusani et al., 2011)
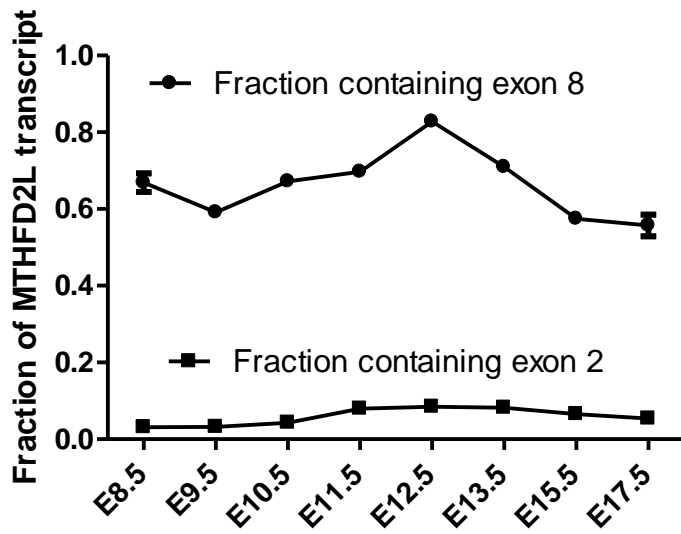
Figure 2.6   Temporal expression profile of MTHFD2L splice variants containing exon 2 (■) and exon 8 (●) in mouse embryos. *MTHFD2L* transcripts was determined by real-time PCR and analyzed as described under "Experimental Procedures." Each *point* represents the mean ± S.E. of triplicate determinations ('*bars* are included for all data points but are obscured by the data symbol when the scatter is small).
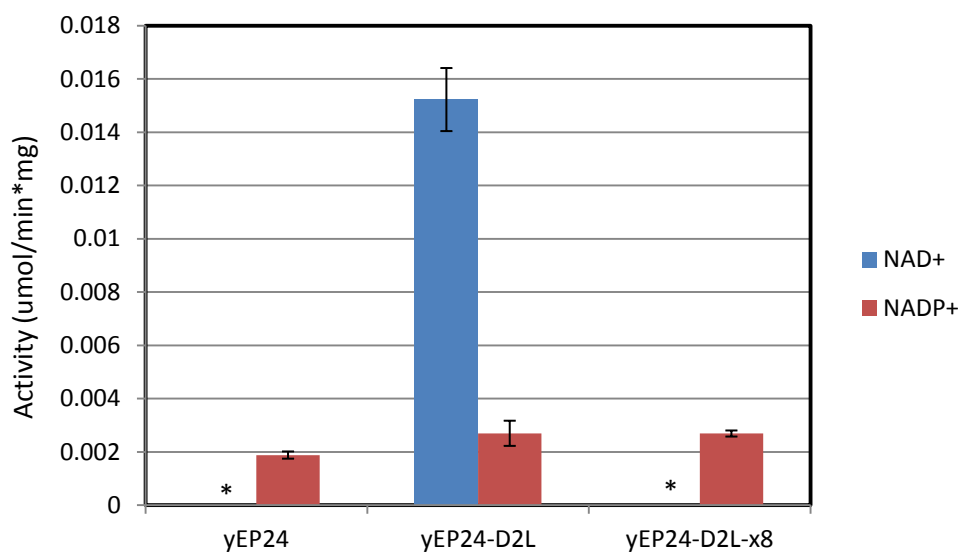
Figure 2.7   Dehydrogenase activity of rat MTHFD2L lacking exon 8. *S. cerevisiae* strain MWY4.4 (*ser1 ura3–52 trp1 his4 leu2 ade3–65 Δmtd1*) was transformed to uracil prototrophy with YEp-D2L (wild-type), YEp-D2L-x8 (lacking exon 8), or empty vector (YEp24). Crude lysates were assayed for CH2-THF dehydrogenase activity as described in "Materials and Methods." Each bar represents the mean +/- S.D. of duplicate determinations. * indicates no activity detected.

Cytoplasmically localized MTHFD2L lacking exon 8 should rescue the adenine requirement of MWY4.5 if it is catalytically active in vivo. Transformants of MWY4.5 harboring YEp-rD2L-x8, YEp-rD2L (full-length MTHFD2L) (Bolusani et al., 2011), or empty vector (YEp24ES) were streaked onto yeast minimal plates containing serine as a one-carbon donor or serine adenine and incubated at 30 °C. As shown in Figure 2.7, full-length MTHFD2L, expressed from YEp-rD2L as a positive control, fully complemented the adenine requirement of MWY4.5, as observed previously (Bolusani et al., 2011). However, MTHFD2L lacking exon 8, expressed from the rD2L-x8 plasmid, did not complement the adenine requirement. An immunoblot of crude yeast lysates from these transformants confirmed that the truncated protein was expressed at a level similar to that of the full-length protein in control cells (Figure 2.7, inset). These *in vitro* and *in vivo* results suggest that the MTHFD2L variant lacking exon 8 does not function as a CH_2-THF dehydrogenase."

Full-length MTHFD2L (containing exon 8 but lacking exon 2) localizes to the inner mitochondrial membrane. We sought to determine if MTHFD2L lacking exon 8 would behave similarly *in vivo*. CHO cells were transiently transfected with rat MTHFD2L lacking exon 8 (pcDNA3.1/rD2L-x8) tagged with a V5 epitope. Isolated mitochondria were treated with 0.5% Triton X-100 to solubilize the mitochondrial membranes then were spun at 100,000 x g in an ultracentrifuge to separate mitochondrial matrix (soluble) and membrane (pellet) fractions. The resulting fractions were analyzed by immunoblotting with an anti-V5 antibody (Figure 2.8). MTHFD2L lacking exon 8 was found predominantly in the mitochondrial pellet fraction indicating it still localizes to the mitochondria and suggesting association of MTHFD2L with the mitochondrial

39
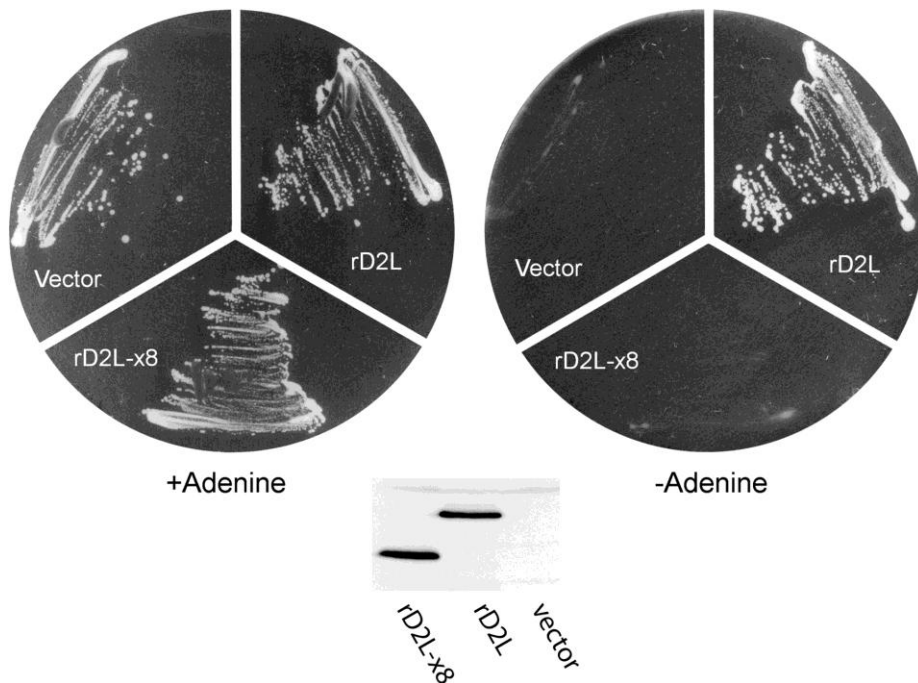
Figure 2.8   Expression of MTHFD2L lacking exon 8 in yeast. "*S. cerevisiae* strain MWY4.5 (ser1 ura3 trp1 leu2 his4 ade3–30/65 Δmtd1) was transformed to uracil prototrophy with YEp-rD2L (wild type), YEp-rD2L-x8 (lacking exon 8), or empty vector (YEp24ES). Ura+ transformants were streaked onto yeast minimal plates containing serine as a one-carbon donor plus adenine (left) or serine alone (right) and incubated at 30 °C for 4 days. Both plates also contained leucine, tryptophan, and histidine to support the other auxotrophic requirements of MWY4.5. Inset, immunoblot of whole cell lysate from MWY4.5 transformed with the indicated plasmids. Each lane was loaded with 50 μg of protein. The blot was probed with polyclonal antibodies against MTHFD2L (1:1000 dilution)."

40
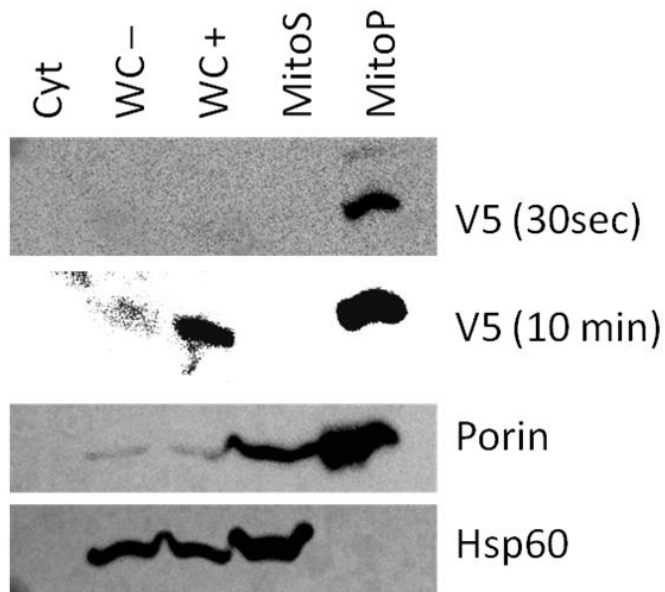
Figure 2.9   Submitochondrial localization of epitope tagged rat MTHFD2L lacking exon 8. Protein from the cytoplasmic fraction (Cyt), whole cell lysate of untransfected cells (WC-). whole cell lysate of pcDNA3.1/rD2L-x8 transfected cells (WC+), soluble mitochondrial fraction (MitoS), and mitochondrial pellet (MitoP) were subjected to SDS-PAGE and analyzed by immunoblotting using anti-V5, anti-porin, and anti-Hsp60. MTHFD2L migrated at an apparent molecular mass of 30 KDa, Porin migrated at 30 KDa, and Hsp60 at 60 KDa. The immunoblot with anti-V5 was overexposed (V5 (10 min)) in order to show the expression of the epitope tagged MTHFD2L in the WC+ fraction.

41

membrane is unaffected by loss of exon 8. Antibodies against porin (a mitochondrial membrane marker) and Hsp60 (a mitochondrial matrix marker) were used to verify the integrity of the subfractionation.

2.4 DISCUSSION

"We determined expression profiles for the entire *MTHFD* family of genes during mouse embryogenesis (Figures 2.2 and 2.3) and in adult tissues (Figure 2.4). The results for *MTHFD1* (cytoplasmic reactions **1–3** (Figure 1.3)) and *MTHFD1L* (mitochondrial reaction **1m**) are qualitatively similar to previously reported transcript expression patterns in mouse embryos based on a staged Northern blot (Pike et al., 2010). Both transcripts are highest in early embryos and decrease during embryonic days 9.5–15.5, only to increase again as the embryo approaches birth. MTHFD2 and MTHFD2L, on the other hand, exhibit very different expression profiles. MTHFD2 expression was low in all embryonic days examined, whereas expression of the MTHFD2L transcript increased beginning at E10.5 and remained elevated through birth (Figure 2.2). These data reveal a switch from MTHFD2 to MTHFD2L expression at about the time of neural tube closure in mouse embryos. The spatial expression of MTHFD2L is localized to the neural tube, developing brain, branchial arches, and limb buds (Figure 2.3). These regions are also areas where *MTHFD2* and *MTHFD1L* are expressed (Pike et al., 2010), suggesting a role for the mitochondrial folate pathway in these embryonic tissues."

The widespread expression of MTHFD2L in adult tissues is of particular relevance to cancer research. The related mitochondrial isozyme of MTHFD2L, MTHFD2, has been identified in a screen of 19 cancer cell types as a protein that is highly associated with proliferating cancer cells (Nilsson et al., 2014). Increased MTHFD2 expression is associated with increased breast cancer cell migration and invasion (Lehtinen et al., 2012) and poor prognosis in patients with breast cancer (Liu et al., 2014). MTHFD2 has been suggested as a novel target for anticancer therapy (Tedeschi et al., 2015). A BLAST sequence alignment of human MTHFD2L and MTHFD2 reveals that the two proteins share 72% sequence identity. While the strong association of increased MTHFD2 expression in proliferating cancer cells may make it attractive target for anticancer drugs, the high similarity between MTHFD2 and MTHFD2L could result in unintended off target effects on MTHFD2L in other tissues. Inhibition of MTHFD2L may have negative consequences for the proper function of organs such as the brain, heart, and lungs where MTHFD2L is most highly expressed. Care would need to be taken when implementing any anticancer drug targeting MTHFD2.

"Why might mammals possess these two distinct mitochondrial dehydrogenase/cyclohydrolase isozymes? It appears that under most conditions, the majority of 1C units for cytoplasmic processes are derived from mitochondrial formate (Tibbetts and Appling, 2010). Oxidation of mitochondrial CH_2-THF is essential for the production of 10-CHO-THF, which is processed by MTHFD1L to provide formate for cytoplasmic export (Figure 1.3). This formate is then

43

reattached to THF for use in *de novo* purine biosynthesis or further reduced for either thymidylate synthesis or remethylation of homocysteine to methionine. Modeling studies suggest that the oxidation step (reaction **3m** (Figure 1.3)), catalyzed by either MTHFD2 or MTHFD2L, is a critical control point for mitochondrial 1C metabolism. Using an *in silico* model, Nijhout *et al.* (Nijhout et al., 2006) observed that the exclusion of CH_2-THF dehydrogenase and CH^+-THF cyclohydrolase activities from the mitochondrial folate pathway results in loss of formate export and a dramatic increase in mitochondrial serine production for gluconeogenesis. When CH_2-THF dehydrogenase and CH^+-THF cyclohydrolase activities are included in the model, the mitochondrial folate pathway produces formate for cytosolic export, where it is incorporated into purines, thymidylate, and the methyl cycle (Nijhout et al., 2006). Christensen and MacKenzie (Christensen and MacKenzie, 2006) have proposed that the level of MTHFD2 expression could act as a metabolic switch to control the balance between serine and formate production.

"We suggest that the existence of two mitochondrial dehydrogenase/cyclohydrolase isozymes in mammals (MTHFD2 and MTHFD2L) reflects the need to tightly regulate flux through this oxidation step in response to changing metabolic conditions and needs. For example, *de novo* purine biosynthesis is especially important in rapidly dividing cells, such as during embryogenesis. Thus, early embryos express both MTHFD2 and MTHFD2L isozymes, ensuring that mitochondrial formate production is adequate to

support *de novo* purine biosynthesis. Indeed, embryonic growth and neural tube closure requires mitochondrial formate production . Compared with embryos, however, adult mammals do not have a high demand for *de novo* purine biosynthesis (Alexiou and Leese, 1992). The loss of expression of MTHFD2 as the embryos approach birth may reflect the lower demand for *de novo* purine biosynthesis in neonate and adult mammals."

"In addition to switching between expressing one or two mitochondrial CH_2-THF dehydrogenase/CH^+-THF cyclohydrolase enzymes, there may be other ways of regulating MTHFD2L expression such as alternative splicing." I report here the relative abundances of MTHFD2L splice variants either containing or lacking exons 2 and 8 in mouse embryos. The splice variant containing exon 2, which would introduce an early stop codon, was at low abundance at all time points examined. We have previously shown that the splice variant lacking exon 8 is present in a variety of adult tissues. We show here that this splice variant accounts for up to 45% of total MTHFD2L transcripts. Although the loss of exon 8 did not appear to affect mitochondrial sublocalization, this splice variant was found to be catalytically inactive *in vitro* and *in vivo*. Expressing a catalytically inactive splice variant may represent one means of regulating dehydrogenase/ cyclohydrolase activity in the mitochondria. There is also the possibility that this splice variant has a protein binding or structural function that does not require it to be catalytically active. A recent study has reported that MTHFD2 localizes to the nucleus near sites of DNA synthesis and enhances cell proliferation independently of its catalytic activity (Gustafsson Sheppard et al., 2015). Given the sequence similarities between

MTHFD2L and MTHFD2, it is possible that a similar function may exist for MTHFD2L

or its splice variants.

Chapter 3: Characterization of loss of function of MTHFD1L in adult mice

3.1 INTRODUCTION

There has long been a known association between disruptions to folate metabolism and cognitive dysfunction (Melamed et al., 1975; Strachan and Henderson, 1967). Disruptions to folate metabolism can be caused by environmental factors, such as folate deficiency, or genetic factors. Undoubtedly, the best characterized folate gene with regards to cognitive dysfunction is MTHFR. MTHFR catalyzes the conversion of CH_2-THF to CH_3-THF for use in the methyl cycle. A common polymorphism of MTHFR (C677T) reduces the enzymatic activity of MTHFR and disrupts the methyl cycle (Frosst et al., 1995). Both folate deficiency and mutations in MTHFR have been found to be associated with increased risk for Alzheimer's disease, Parkinson's disease, vascular dementia, and depression (Bjelland I, 2003; Jadavji et al., 2015; Kim et al., 2008; Mattson et al., 1999).

One of the main culprits implicated in the etiology of diseases caused by either folate deficiency or MTHFR mutations is elevated homocysteine (Araújo et al., 2015). 1C units generated in the mitochondria serve as substrates for synthesis of methionine from homocysteine. Methionine, when converted to S-adenosylmethionine in the methyl cycle, can serve as a source of methyl groups for DNA methylation, histone methylation, and synthesis of neurotransmitters, all of which are important for cognitive function (Chiang et al., 1996; Grillo and Colombatto, 2008; Su et al., 2016). Similar to folate deficiency and MTHFR mutations, increased homocysteine is an independent risk factor

for dementia, Alzheimer's disease, depression, and cardiovascular disease (Araújo et al., 2015; Bjelland I, 2003; Luchsinger et al., 2004; Refsum et al., 1998; Seshadri et al., 2002; Van Dam and Van Gool, 2009). Whether this association is only due to the fact that elevated homocysteine is a symptom of altered methionine metabolism or homocysteine itself is responsible for the negative effects is still not fully understood. Both cases are likely true depending on the situation. For example, folate deficient rats show cognitive impairment that can be reversed with methionine supplementation; however, homocysteine remains elevated (Troen et al., 2008). In some cases though, homocysteine may be directly responsible for neurodegeneration. It has been reported that homocysteine induces apoptosis in neurons through DNA damage (Kruman et al., 2000). Homocysteine has also been shown to sensitize hippocampal neurons to amyloid toxicity in a mouse model of Alzheimer's disease (Kruman et al., 2002).

Although MTHFR is the most commonly studied folate-related gene in regards to cognitive dysfunction, recent studies have implicated MTHFD1L as well. Three independent studies have identified a single nucleotide polymorphism (SNP, rs11754661) in the gene encoding MTHFD1L that is associated with increased risk for late onset Alzheimer's disease (LOAD), but the underlying mechanisms have not yet been identified (Ma et al., 2012; Naj et al., 2010; Ramírez-Lorca et al., 2011; Ren et al., 2011). The same SNP has also been implicated in increased rumination in patients with major depressive disorder (Eszlari et al., 2016). Because mitochondrial MTHFD1L provides 1C units to the cytoplasm for methionine synthesis from homocysteine (Pike et al., 2010), we hypothesize that loss of MTHFD1L activity could result in elevated homocysteine and

altered cellular methylation leading to downstream effects on behavior and memory in mice.

In this chapter, I investigate the loss of MTHFD1L in adult mice in conjunction with a folate deficient diet using experiments designed to test for anxiety-related behaviors and memory defects. I also examine alterations in methyl cycle metabolites in serum and brain tissue.

3.2 MATERIALS AND METHODS

3.2.1 Mouse Work

All protocols used within this study were approved by the Institutional Animal Care and Use Committee of The University of Texas at Austin and conform to the National Institutes of Health Guide for the Care and Use of Laboratory Animals. Mice were maintained on the C57BL/6 background. Genotyping was carried out using a modified PCR method (Stratman et al., 2003). A forward primer (5′-GAGTATGTGATTGCTTGGACCCCCAGGTTCC-3′) binding in the 5' region outside of the floxed cassette (see below) and reverse primer (5′-TGGCTCCCGAGGTTGTCTTCTGGCTATGAT-3′) binding 5' to exon 5 within the floxed cassette would yield a 444-bp amplicon for the wild-type allele, a 543-bp amplicon for the floxed allele, and no product when the conditional cassette was removed. Cre recombinase was detected using the forward (GCATTACCGGTCGATGCAACGAGTGATGAG-3') and reverse (GAGTGAACGAACCTGGTCGAAATCAGTGCG-3') primers which yield a 408-bp amplicon.

For the preliminary study, MTHFD1L mutant mice (see below) were treated after weaning with 1 mg tamoxifen per day by gavage for 5 days. Mice were maintained on standard chow for the duration of the study. Experiments were started after the mice reached approximately 1 year of age. In the main study, mice aged 1.5-3 months old were placed on a diet containing 333mg/kg tamoxifen (Harlan Teklad, TD.09548) for 1 month. After tamoxifen treatment, mice were started on either control (CD) or folate deficient diets (FD) (Harlan Teklad, TD.04194 and TD.95247 respectively). The diets were identical except that CD contained 2 mg/kg folic acid and FD did not contain any folate. 3 months later, behavioral testing was started. Mice were euthanized at approximately 10-11 months of age. Serum was collected by cardiac puncture, and brain, liver, and spleen tissues were rinsed with PBS and stored at -70°C.

3.2.2 MTHFD1L conditional knock out

Because homozygous deletion of MTHFD1L is embryonic lethal (Momb et al., 2013), we generated a conditional knockout to study loss of MTHFD1L in adult mice. A mouse line containing a conditional cassette consisting of loxP sites on either side of exon 5 of Mthfd1l in both alleles was bred with mice expressing Cre-ERT2 under control of the ubiquitin C promoter. Cre-ERT2 is a fusion protein of Cre recombinase and a mutant form of the estrogen receptor (ER) that is activated by tamoxifen but is not affected by estrogen (Feil et al., 1997). When activated by tamoxifen, Cre-ERT2 will translocate into the nucleus and recombine out the region between the two loxP sites. Deletion of exon 5 introduces a frame shift that disrupts translation of the rest of the

protein. Mice containing the floxed alleles and expressing Cre-ERT2 will be referred to as "mutant" mice and control mice containing the floxed alleles but lacking Cre-ERT2 will be referred to as "WT" in the following work.

3.2.3 Behavioral experiments

Mice were brought to the testing room at least one hour prior to each experiment to be allowed to acclimate to the testing environment. During each experiment, movement was recorded with a digital camera. Movement data was analyzed using the Any-maze software (Stoelting Co.; Wood Dale, IL).

3.2.3.1 Open Field Test

The testing chamber consisted of a 40 x 40 cm box. The walls were made of 35 cm high opaque plastic. The chamber was lit from above by a diffuse light source. To initiate the test, mice were placed in a corner of the testing chamber facing the outer wall. Mice were observed for 30 minutes. The center was defined as an 18.5 x 18.5 cm zone in the center of the chamber.

3.2.3.2 Elevated Plus

The plus-shaped maze consisted of four arms each 30 cm in length and 5 cm in width. Two arms were "closed" with walls 13 cm in height, and the other two arms were "open." The maze was on a stand set approximately 130 cm above the floor. The maze was lit from above with a diffuse light source. Mice were placed in the one of the closed arms facing the outside of the apparatus to begin the test. Mice were observed for 10 minutes.

3.2.3.3 Delay Fear Conditioning

The testing chamber consisted of a box lit with a white light and a metal grate for the floor. The back of the box contained an infrared camera to track the movement of the mice. After cleaning the box with a Clorox wipe, the box was wiped with ethanol. The fear conditioning procedure took place over three days. Freezing behavior was scored using a pixel-change algorithm (VideoFreeze, Med Associates Inc., St. Albans, VT).

Day 1 - Cue and context fear conditioning

Mice were placed in the testing chamber and the testing procedure was initiated. The testing procedure began with a 120 second pre-tone habituation period followed by four tone-shock pairings occurring at 120, 204, 314, and 409 seconds. Each tone-shock pairing consisted of a 20 second tone (CS, 5000 Hz, 85 db) with a 1 second shock (US, 0.75 mA) during the final second of the tone.

Days 2 and 3 - Context and Cue testing

On day 2, one randomly selected group of mice was tested for context-dependent fear conditioning, and the other group was tested for cue-dependent conditioning. On day 3, the groups were switched. For the context test, mice were placed in a chamber identical to the chamber on day 1. Freezing was measured for 5 minutes in the absence of any tones or shocks. For the cue test, the testing chamber was altered to have an uneven grate for the floor, a triangular roof insert, the white light was turned off, and the chamber was wiped with acetic acid instead of ethanol. During the test, tones identical to those played on day 1 were played at the same intervals but without the shocks.

3.2.3.4 Morris Water Maze

Mice were first pre-trained to locate the platform beneath the surface of the water. A small bucket was filled with water (21°C) and a circular platform (8 cm in diameter) was submerged 1 cm beneath the surface. The water was made opaque with white

tempera paint. Mice were placed on the platform for 10 seconds. If the mice jumped off of the platform, they were guided back to the platform by hand. This procedure was carried out three times a day for three consecutive days. After each trial, the mice were dried with paper towels and placed in a cage warmed with an infrared heating lamp and a heating pad.

Hidden platform training was started one week after the first day of pre-training. A circular tank 120 cm in diameter was filled with water (21°C) made opaque with tempera paint. The platform was submerged 1 cm below the surface in the center of one of four quadrants of the tank. The tank was surrounded by black curtains, and each quadrant had a different object that varied in shape, size, and color affixed to the curtain. At the beginning of each trial, the mouse was placed in the tank near the wall in one of the four quadrants. The trial would last for two minutes or until the mouse reached the hidden platform. If the mouse was unable to find the platform after two minutes, the mouse would be guided by hand to the platform. Four trials per mouse were conducted each day for five consecutive days. The starting location for each subsequent trial was moved to a different quadrant each time. One week after the start of training, the mice were subjected to a two minute probe trial, in which the platform was removed.

3.2.4 Immunoblotting

Mitochondria were isolated from brain tissue as previously described (Pike et al., 2010). Protein concentration was determined by BCA assay (Thermo Fisher Scientific). Proteins were separated by SDS-PAGE and immunoblotted using rabbit polyclonal anti-MTHFD1L (1:1,000) (Prasannan and Appling, 2009). After incubation with HRP-conjugated goat anti-rabbit IgG (1:5,000) (Invitrogen), reacting bands were detected using ECL Prime (GE Healthcare Life Sciences).

3.2.5 Statistics

Unpaired t-tests were performed in Microsoft Excel. All other analyses were performed with JMP Pro 12 (SAS Institute). Grouped data was analyzed by two-way ANOVA, and Tukey's HSD test was used for *post hoc* pairwise comparisons. The mixed-effects restricted maximum likelihood (REML) model was used for experiments with repeated measures.

3.3 RESULTS

3.3.1 Preliminary Study

A small pilot study consisting of 8 mutant and 6 WT mice was conducted to assess the effects of loss of MTHFD1L in adult mice. The mice were subjected to a battery of tests designed to assess anxiety-like behavior and memory. The open field test and elevated plus maze were used to evaluate spontaneous exploration and anxiety-like behavior (Denenberg, 1969; Hogg, 1996; Pellow et al., 1985). In the open field test, mice are placed in a box with high walls that is open to the ceiling. The elevated plus maze consists of four arms elevated above the ground. Two of these arms are enclosed by walls and the other two are completely open. Mouse movements are tracked by a digital camera and the time spent and distance travelled in open versus closed areas are compared. Mice have an innate exploratory drive but also tend to avoid open spaces, and these tests evaluate the competition among these two drives. Mouse models of AD have shown increased exploratory behavior (Bryan et al., 2009).

In the pilot study, the open field test seemed to indicate the mutant mice were more active, with a trend for them to travel a longer total distance during the test (Figure 3.1). Though mutant mice travelled the same distance through the center as WT mice, they spent less time in the center (Figure 3.1). This means that though mutant mice did venture into the center of the field, they traversed more quickly than WT mice, possibly indicating an anxiety phenotype. A similar anxiety phenotype was seen in the elevated plus maze, with Mutant mice spending less time and travelling a shorter distance on the open arms (Figure 3.1).

55

Delay fear conditioning and the Morris water maze were used to test associative and spatial memory in these mice. Fear conditioning is a Pavlovian learning task in which mice learn to associate a conditioning stimulus (CS), like a tone, with an aversive unconditioned stimulus (US), such as a foot shock, that takes place immediately after the CS. After being trained to associate the US with the CS, mice can be exposed to either the CS alone (alternate context) or the context (lighting, shape of the enclosure, smells, etc.) in which they experienced the US, and fear response, as indicated by freezing behavior, can be observed. Lesions in the amygdala have been shown to prevent association of the US with the CS, while lesions in the hippocampus prevent association of the US with the context in which the US is delivered (reviewed in (Maren, 2001)). Atrophy of both the amygdala and the hippocampus have been associated with AD (Chow et al., 2012; Poulin et al., 2011). We did not observe any significant differences during training, but mutant mice in the context test showed higher freezing early in the test, possibly indicating increased anxiety. Overall there were no significant differences in the alternate context test, but mutant mice showed a trend towards decreased pre-tone freezing (Figure 3.2).

The Morris water maze is a spatial learning test that was first described by Morris (Morris, 1984). In this test, mice are placed in a large water tank containing a single platform just beneath the surface of the water. The water is made opaque so that the platform cannot be seen, and mice must rely on external visual cues to orient themselves in relation to the platform's location. Mice are trained with multiple trials per day over several days (acquisition) to learn the location of the platform. After acquisition training,

mice are tested in a probe trial in which the platform is removed and the number of times the mice cross the area where the platform used to be is recorded (real platform). The number of crossings of an area the same size as the platform in the opposite quadrant of the tank (false platform) is measured as a negative control. If the mice learn and remember the location of the platform, they will be expected to cross the real platform more frequently than the false platform. Folate deficiency Mice were trained with 4 trials per day for 5 days. There was a trend for mutant mice to acquire the platform's location more slowly than WT ($p = 0.25$, Figure 3.3). In the probe trial, WT mice crossed the real platform location significantly more frequently than the false location ($p = 0.039$), whereas mutant mice did not ($p = 0.61$) (Figure 3.3).

The pilot study suggested some interesting potential changes in mice with decreased MTHFD1L activity, but many of the trends we observed were not statistically significant. We speculated that this could be due to one or more of several factors. First, the number of mice used may have been too small to have sufficient power to detect the behavioral differences in the mice. Second, though there was no detectable expression of MTHFD1L in brain tissue, several tissues retained expression of MTHFD1L (not shown). It has been reported that in conditional knockouts using the Cre-ERT2 system, expression of the target gene can recover over time, especially in proliferative tissues (Ruzankina et al., 2007). It is possible that the long delay between tamoxifen treatment and the start of the experiments allowed enough recovery of MTHFD1L expression to rescue some of behavioral alterations. A final possibility is that differences we saw were artifacts caused by the low number of mice used in the study. With these factors in mind, we planned a

larger scale follow-up study. This study would consist of approximately 60 total mice, 30 WT and 30 mutant. Half of these mice (15 WT and 15 mutant) would be placed on a folate deficient diet with the intent of exacerbating any potential phenotype associated with loss of MTHFD1L. Finally, the behavioral experiments would be conducted much sooner after tamoxifen treatment. The rationale was that if the behavioral alterations are a result of metabolic changes caused by loss of MTHFD1L, conducting the experiments before expression of MTHFD1L had a chance to recover may improve our chances of detecting behavioral changes.
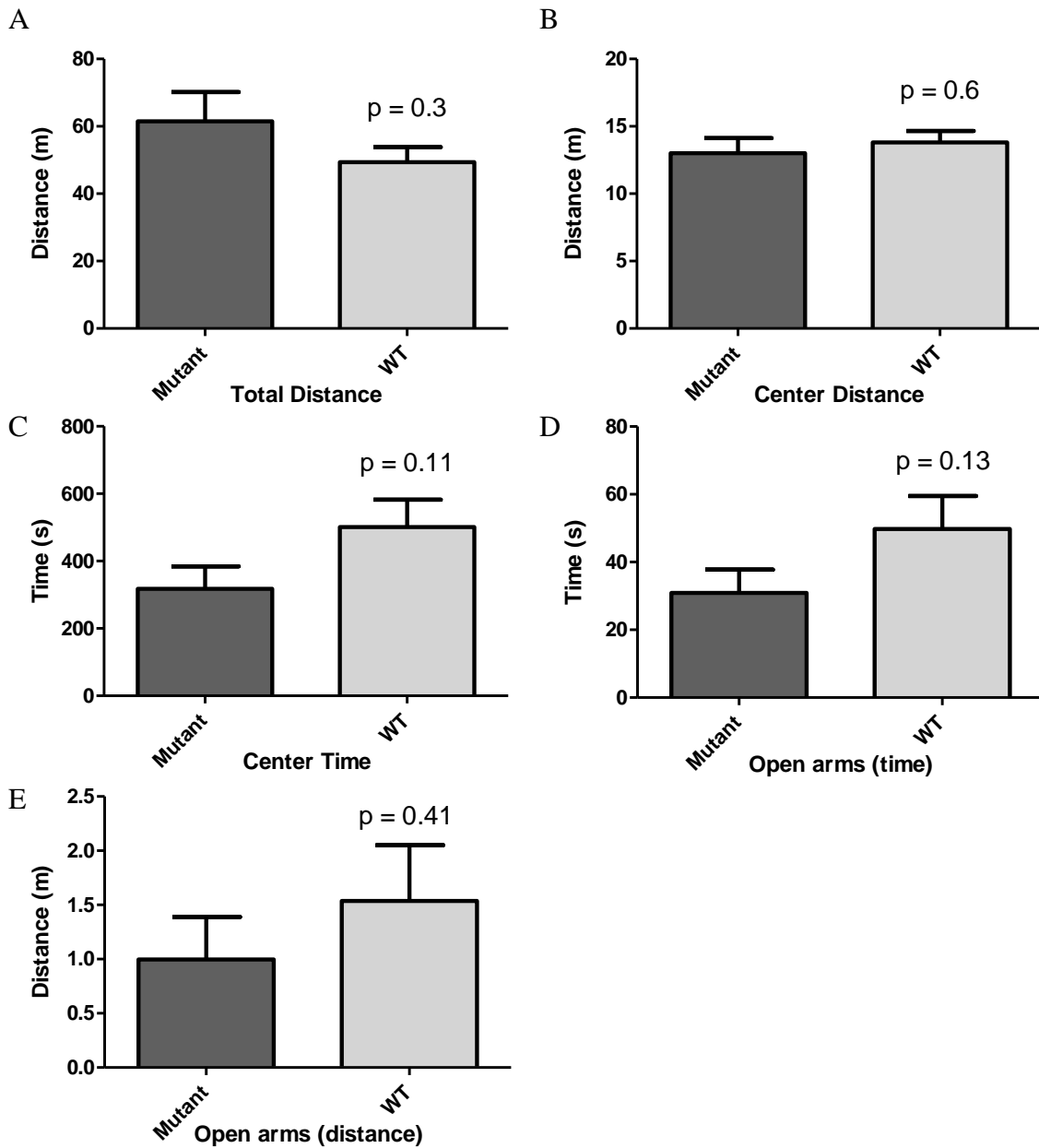
Figure 3.1   Preliminary results of open field and elevated plus tests. In the open field

test (A-C) mutant mice showed a trend for a longer total distance and

moving through the center more quickly. In the elevated plus maze (D,E),

mutant mice showed a trend for avoiding the open arms.
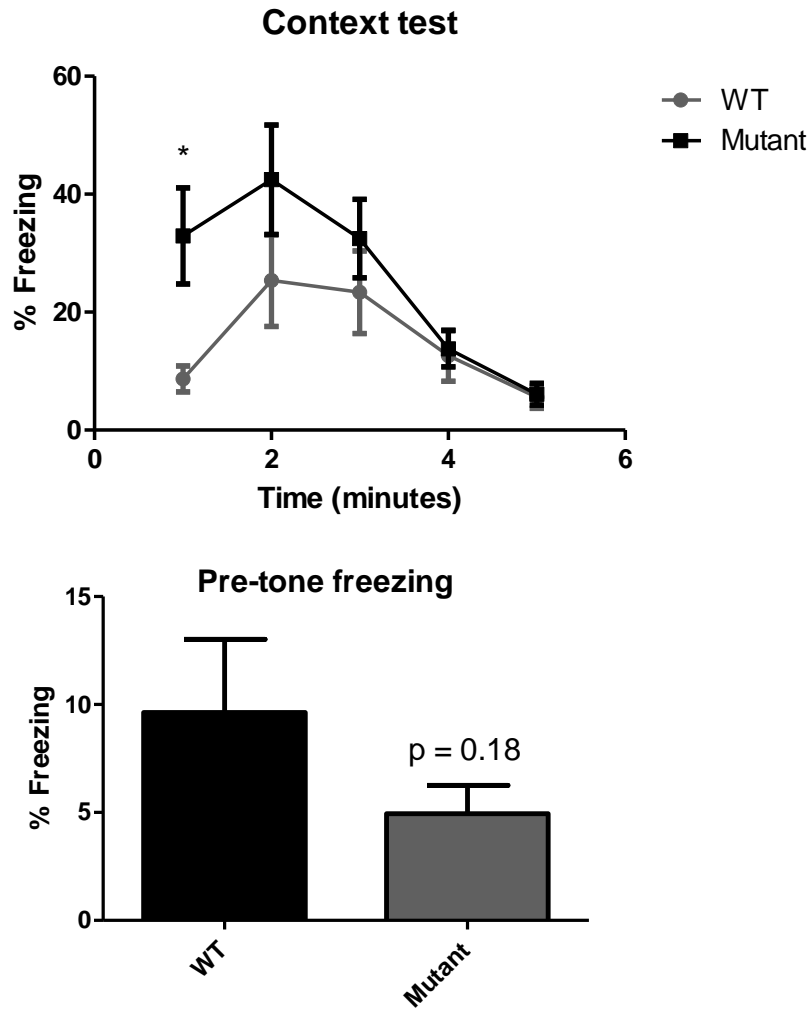
Figure 3.2   Preliminary fear conditioning. (Top) Context test. Test was conducted in the same context as the tone-shock training. * indicates $p < 0.05$ for that time point. (Bottom) Pre-tone freezing in alternate context test. Test was conducted in a different context from tone-shock training (different floor shape, roof shape, scent, and lighting). Error bars in both graphs represent +/- SEM.
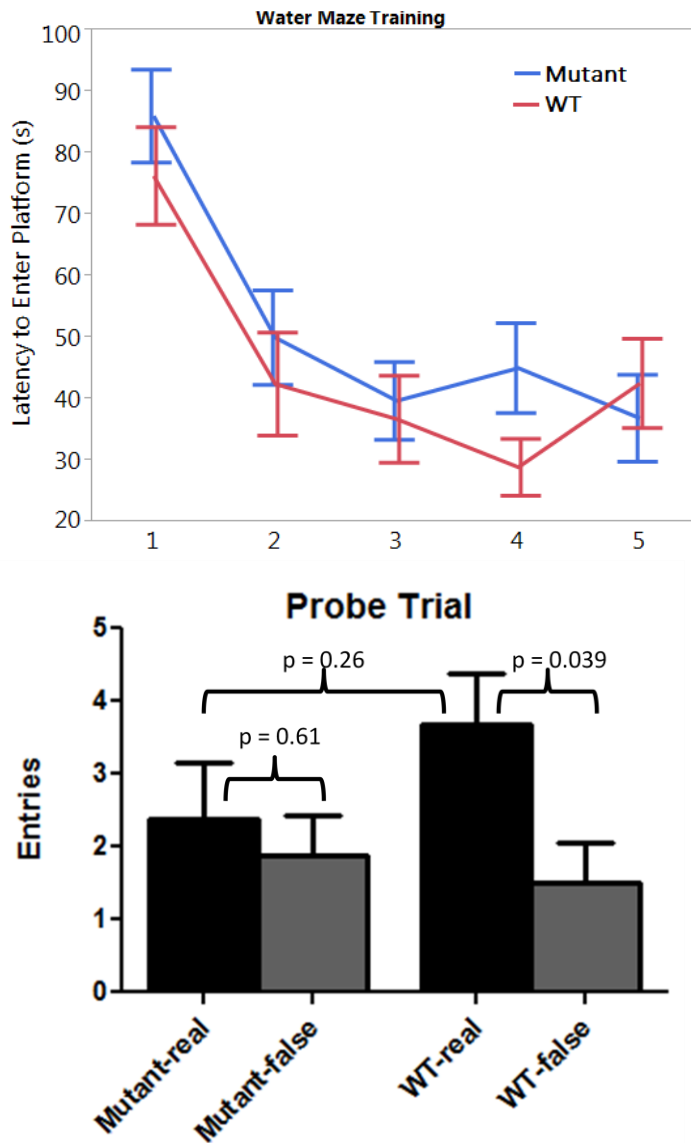
Figure 3.3   Preliminary results of Morris water maze. (Top) Hidden platform training.

Each point represents the mean time required to find the hidden platform.

Error bars represent +/- SEM. (Bottom) Probe Trial. Bars represent mean

number of entries into real or false platform area +/- SEM.

3.3.2 Main Study

3.3.2.1 Open Field Test

Mice were first tested on the open field apparatus (Figure 3.4). An initial 3 way ANOVA showed there was a sex effect where female mice travelled a longer total distance (p = 0.008), distance along the margin (p = 0.0015), and distance through the center (p = 0.026), so results from male and female mice were analyzed separately. Mutant male mice appeared to be more active than male WT mice, travelling a longer total distance independently of diet (p = 0.012). There was no significant difference in total distance in female mice. Female mice on the FD tended to spend more time on the margin of the apparatus (p = 0.015) and there was a trend for a shorter distance travelled through the center (p = 0.074) (center distance was corrected for the total distance travelled). There were no significant effects in male mice for time spent on the margins or distance travelled through the center.

3.3.2.2 Elevated Plus

Next, mice were tested on the elevated plus maze (Figure 3.5). We did not observe any significant differences in time spent or distance travelled on either the open or the closed arms of the maze, nor did the total distance travelled during the test significantly differ with regards to sex, diet, or genotype.

3.3.2.3 Delay Fear Conditioning

On the first day of the fear conditioning experiment, the mice were trained to associate a foot shock with a tone. The tone plays for 20 seconds with the foot shock applied during the last second of the tone. There were four of these tone-shock pairings during the course of the approximately 8 minute training period. The average freezing during the pre-tone period and during each tone was examined (Figure 3.6). We found a significant sex x time interaction ($p = 0.0351$), so results from male and female mice were analyzed separately. In both male and female mice, freezing behavior changed significantly over time ($p < 0.0001$). In male mice, there was a significant genotype x time interaction ($p = 0.0123$), but female mice only showed a significant diet effect ($p = 0.0218$), with female mice on the FD exhibiting higher freezing.

Over the next two days, mice were tested for context-dependent and cue-dependent (alternate context) fear conditioning. We did not observe any significant effects due to diet, sex, or genotype in the context test (Figure 3.7). In the alternate context test, freezing increased over time in response to the CS ($p < 0.001$), but freezing did not significantly differ between groups (Figure 3.8).

3.3.2.4 Mouse weights and immunoblots

At the conclusion of behavioral experiments, mice were weighed prior to dissection and tissue collection (Table 3.1). Male mice weighed more than female mice ($p < 0.0001$), but weights were not significantly affected by genotype or diet.

Mitochondria were isolated from brain tissue and an immunoblot for MTHFD1L expression was performed on mitochondrial extracts. MTHFD1L expression was markedly decreased in CD mutant mice, though some mice still retained a degree of MTHFD1L expression (Figure 3.9). Surprisingly, mutant mice on the FD appeared to retain much more expression of MTHFD1L than mutant mice on the CD.

3.3.2.5 Serum and brain metabolites

Whole brain samples (one hemisphere) and serum samples were analyzed to determine the concentrations of folate and metabolites related to the methyl cycle (Bottiglieri Lab, UT Southwestern). 5-CH$_3$-THF and homocysteine (Hcy) were measured in serum; and methionine, S-adenosylmethionine (SAM), S-adenosylhomocysteine (SAH), cystathionine, betaine, and choline were measured in brain tissue. Male and female mice seemed to respond differently to both loss of MTHFD1L and the effects of the folate deficient diet. Female mice on the FD had significantly lower 5-CH$_3$-THF in serum ($p < 0.0001$, Figure 3.10). Although there was no significant genotype effect on 5-CH$_3$-THF levels in female mice, there was a significant diet x genotype interaction ($p = 0.0148$). Male mice on the FD also had lower 5-CH$_3$-THF in serum ($p < 0.0001$, Figure 3.10), but there was also a genotype effect where male mutant mice on the CD had lower 5-CH$_3$-THF than WT mice on the CD ($p = 0.0257$, Figure 3.10). Serum homocysteine in female mice showed a trend for a diet x genotype interaction ($p = 0.094$), but *post hoc* analysis did not show any significant differences between groups (Figure 3.10). Hcy was elevated in response to both the mutant genotype ($p = 0.0145$) and FD ($p = 0.001$) in male

mice; however, *post hoc* pairwise comparisons indicated that only mutant mice on the FD significantly differed.

Genotype did not appear to have any significant effects on the metabolites measured in brain tissue; however, several were altered in response to the FD. In the brain tissue of female mice, methionine was the only metabolite to significantly differ (p = 0.0007), decreasing in mice on the FD (Table 3.2). In male mice, methionine was unchanged, but SAM increased (p = 0.0425) and SAH decreased (p = 0.010) in mice on the FD (Table 3.3). There was also a decrease in choline (p = 0.0007) in male mice on the FD. Cystathionine and betaine were not significantly changed.
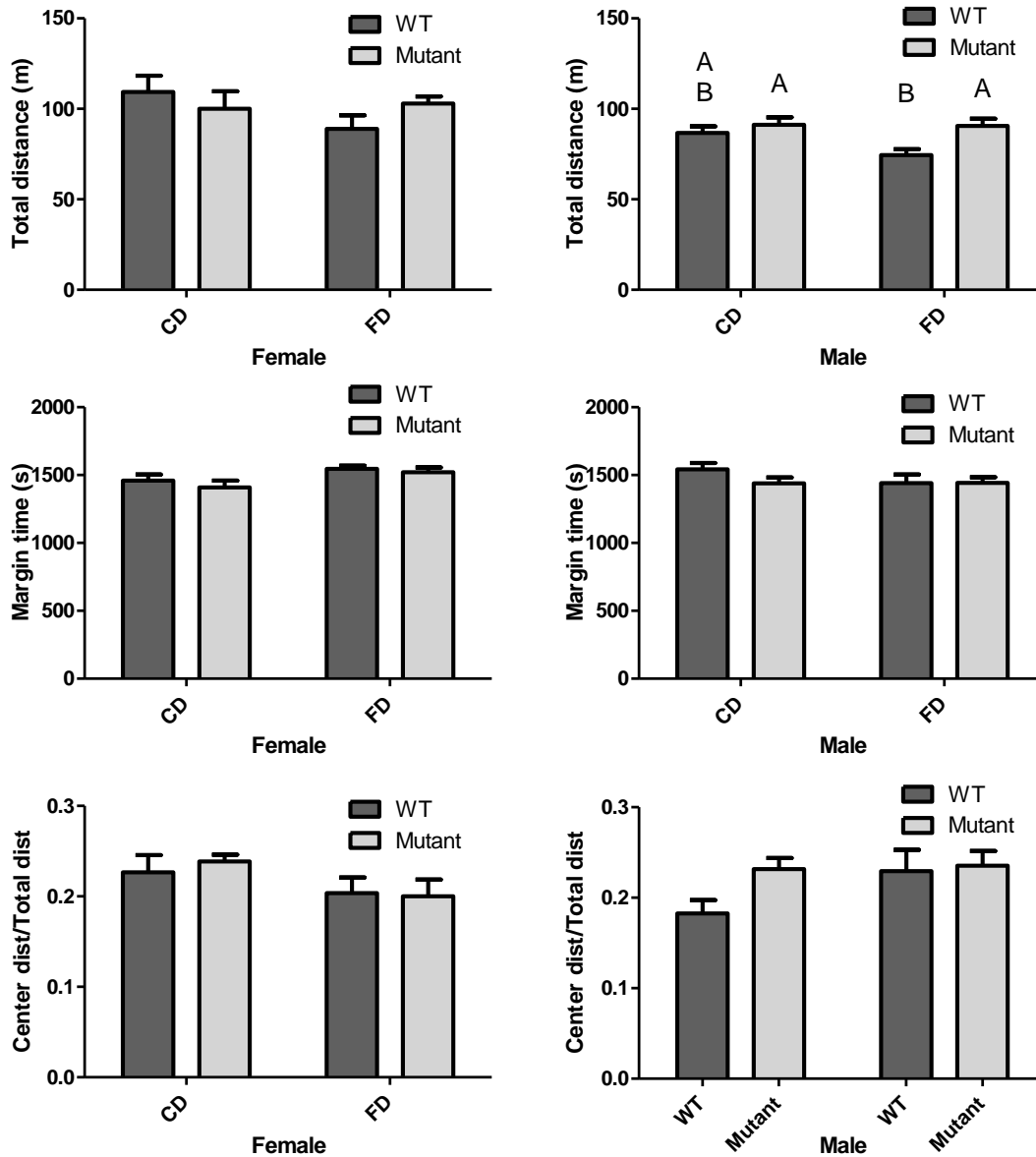
Figure 3.4   Open field test. Where significant differences were found either based on genotype or diet, Tukey's test was used for *post hoc* pairwise comparisons. Bars that share the same letter do not significantly differ. Where letters are omitted, no significant differences were found in the *post hoc* analysis. Bars represent the mean +/- SEM.
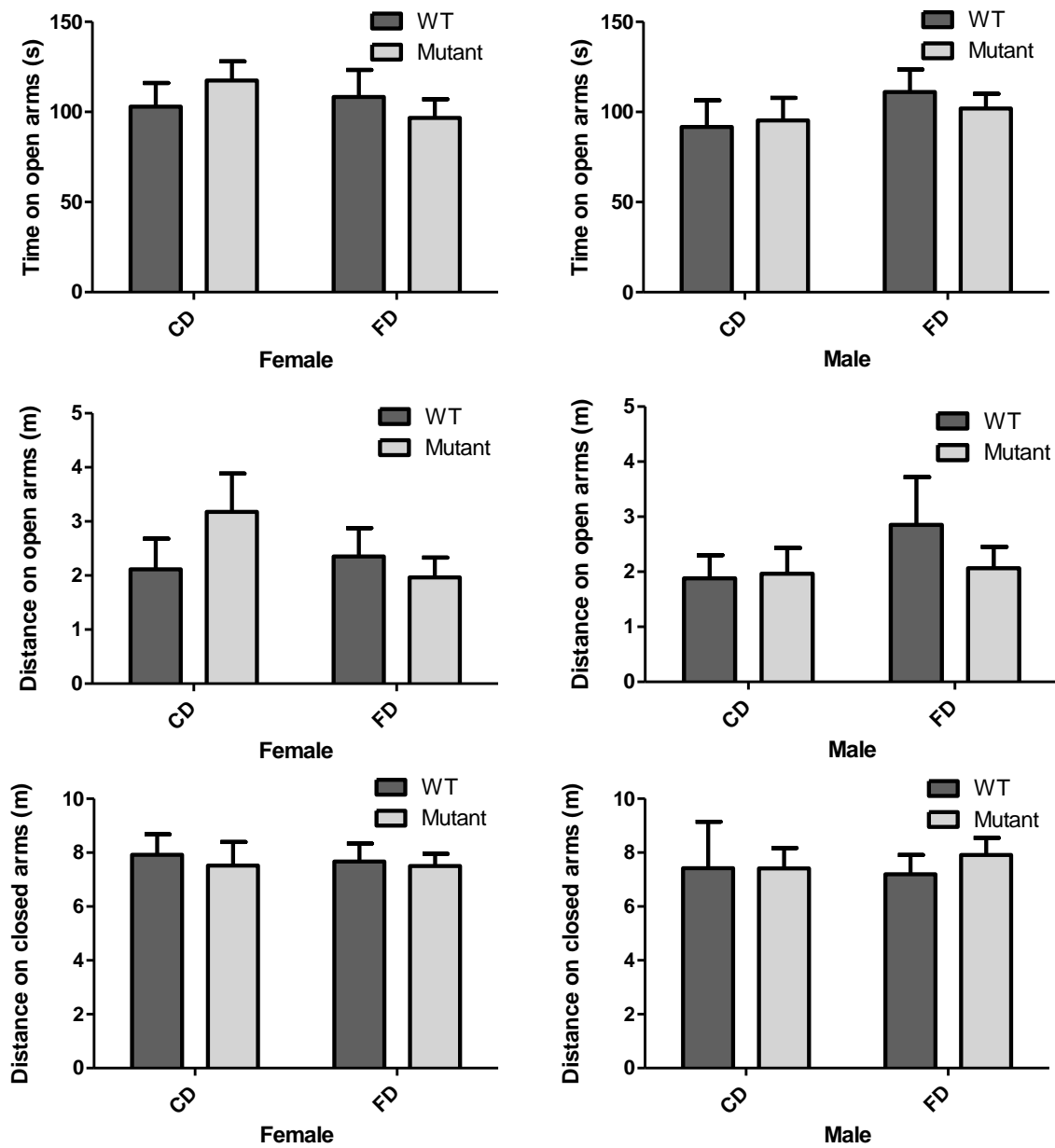
Figure 3.5   Elevated plus maze. Bars represent the mean +/- SEM.
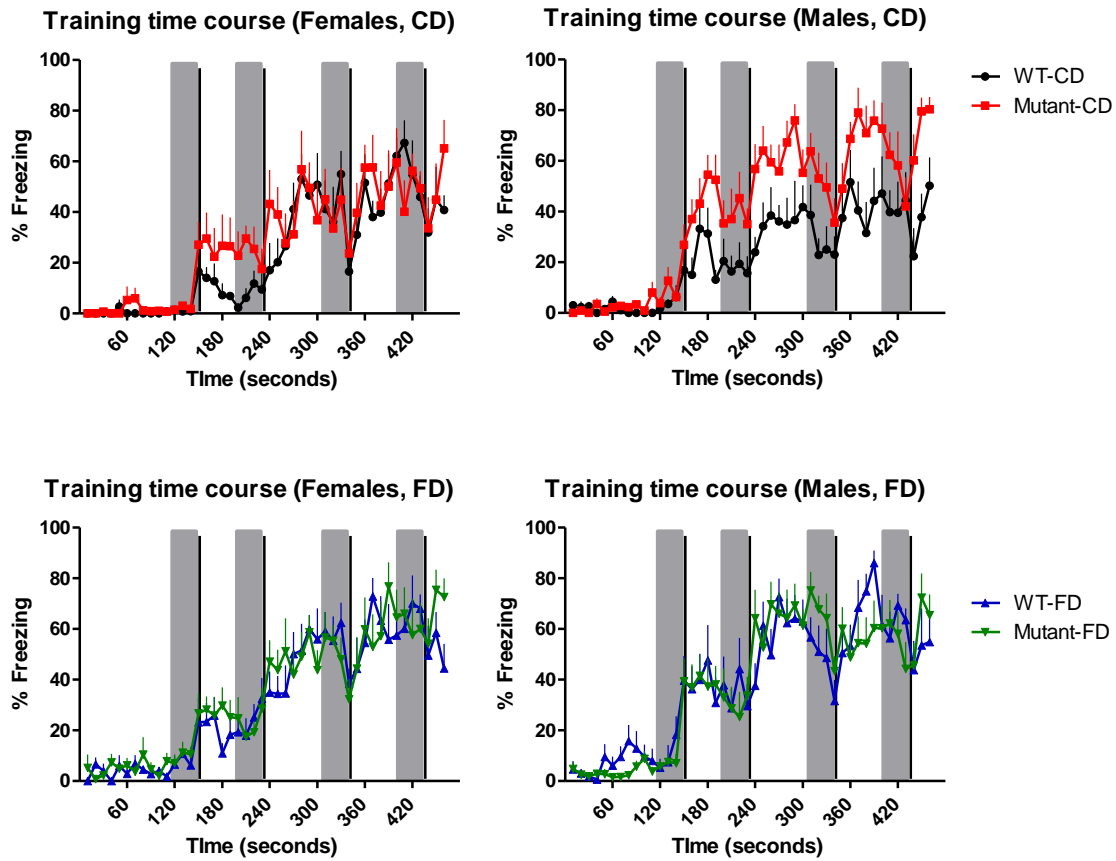
Figure 3.6   Fear conditioning training. Each point represents mean % freezing for a 10 second time bin. Error lines represent SEM. Vertical grey bars indicate tone periods and vertical black lines represent the foot shock. Mice of the same sex were analyzed together but have been separated here by diet for ease of viewing.
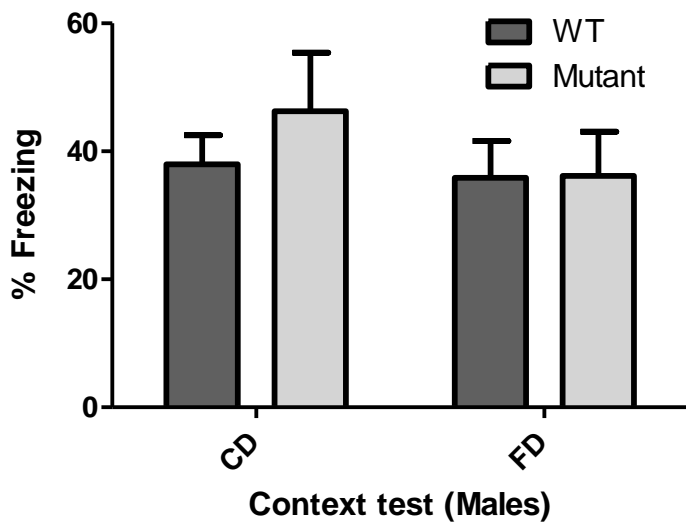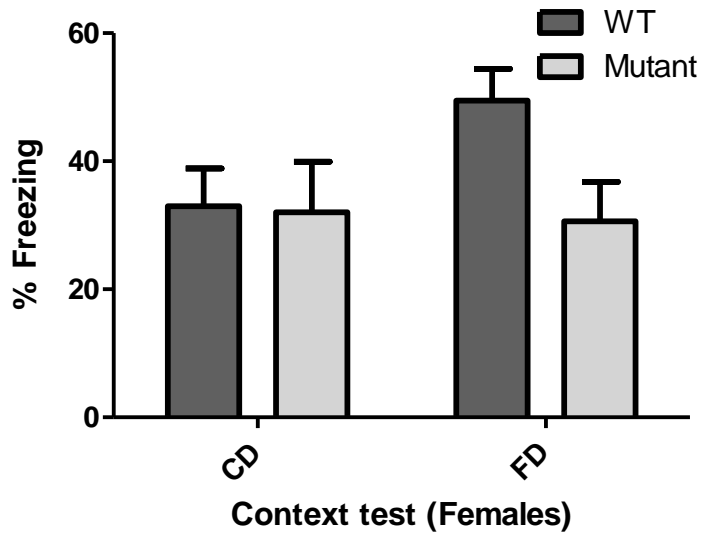
Figure 3.7   Fear conditioning context test. Test was conducted in the same context as the tone-shock training. Bars represent mean % freezing over 5 minute period +/- SEM.
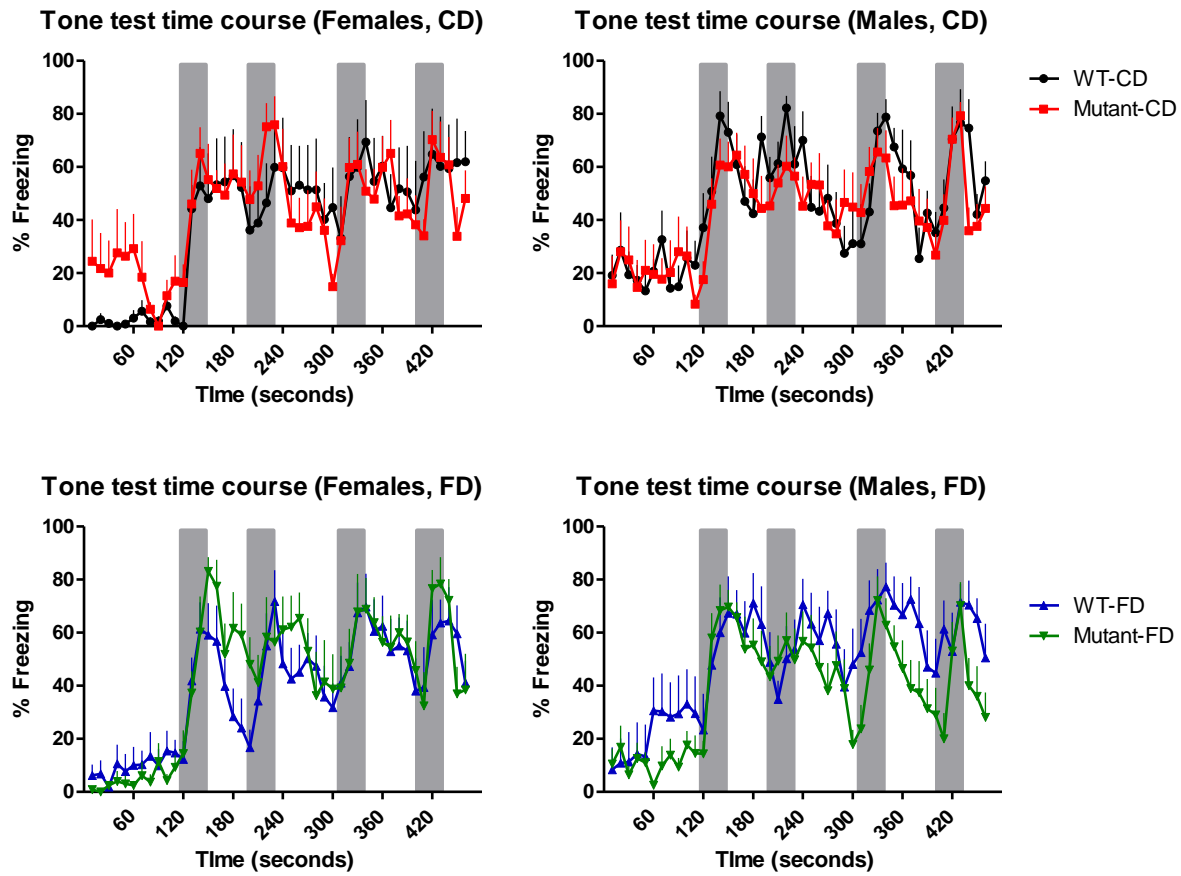
Figure 3.8   Fear conditioning alternate context test. Test was conducted in a different context from tone-shock training (different floor shape, roof shape, scent, and lighting). Each point represents mean % freezing for a 10 second time bin. Error lines represent SEM. Vertical grey bars indicate tone periods. Mice of the same sex were analyzed together but have been separated here by diet for ease of viewing.

70
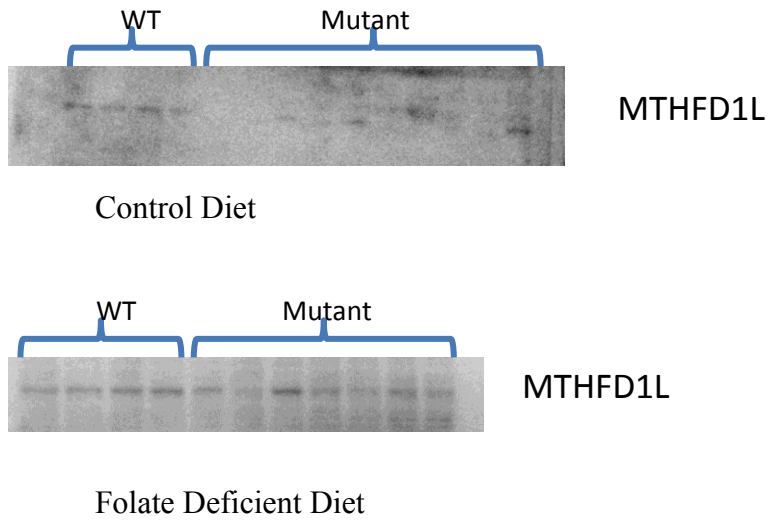
Figure 3.9   Representative immunoblots of MTHFD1L expression in the brains of mice

on control and folate deficient diets.
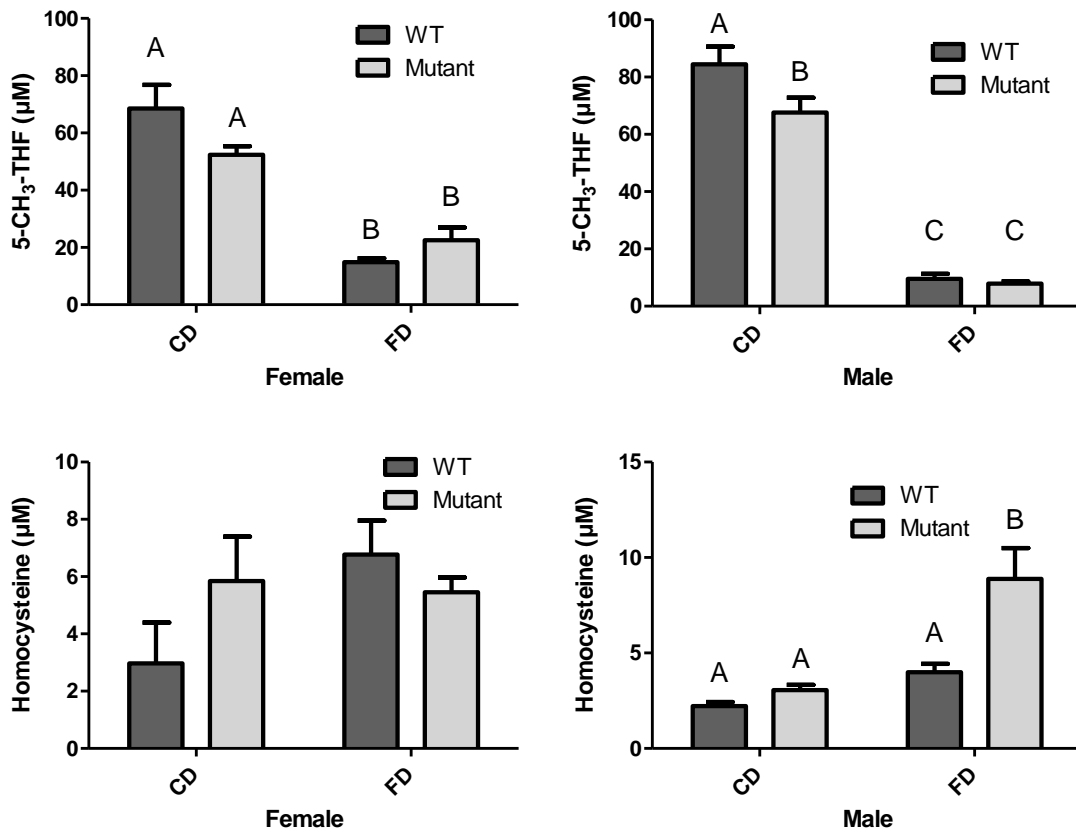
Figure 3.10 Serum 5-CH$_3$-THF and homocysteine. Where significant differences were found either based on genotype or diet, Tukey's test was used for *post hoc* pairwise comparisons. For each metabolite, identical letters over two bars signify that those samples do not significantly differ (e.g. 5-CH$_3$-THF in female WT-FD and Mutant-FD mice does not significantly differ). Bars represent the means +/- SEM. CD = control diet. FD = folate deficient diet.

	Female				Male			
	CD		**FD**		**CD**		**FD**	
	WT	Mutant	WT	Mutant	WT	Mutant	WT	Mutant
# of mice	6	7	8	7	6	10	8	10
Weight (g)	25.0 +/- 2.1	25.7 +/- 1.7	27.4 +/- 3.8	27.0 +/- 2.2	33.6 +/-6.6	32.1 +/- 6.0	34.8 +/-4.9	34.2 +/- 4.3

Table 3.1   Numbers and weights of mice used in study. The number of mice in each

group is given. Average mouse weights at the time of dissection +/- SD are

shown.

Female	CD		FD		2-way ANOVA P-value		
	WT	Mutant	WT	Mutant	Genotype	Diet	G*D
Methionine (nmol/g)	76.3 ± 14.8[a]	68.1 ± 9.9[ab]	57.1 ± 8.9[b]	57.0 ± 6.1[b]	0.287	<0.001	0.298
SAM (nmol/g)	24.0 ± 3.8	24.0 ± 3.8	22.0 ± 2.6	22.1 ± 3.0	0.953	0.143	0.974
SAH (nmol/g)	4.5 ± 1.0	4.1 ± 0.3	4.6 ± 1.1	3.9 ± 0.6	0.103	0.939	0.557
SAM/SAH	5.7 ± 1.8	5.8 ± 0.8	5.1 ± 1.7	5.8 ± 1.2	0.413	0.606	0.633
Cystathionine (nmol/g)	22.8 ± 11.7	20.3 ± 3.4	23.3 ± 24.6	26.1 ± 18.6	0.982	0.635	0.690
Betaine (nmol/g)	21.7 ± 11.3	22.9 ± 5.4	20.8 ± 6.5	23.5 ± 3.7	0.469	0.953	0.795
Choline (nmol/g)	262 ± 102	263 ± 87	265 ± 75	255 ± 53	0.882	0.920	0.862

Table 3.2   Methyl cycle metabolites from the brains of female mice.

Male	CD		FD		2-way ANOVA P-value		
	WT	Mutant	WT	Mutant	Genotype	Diet	G*D
Methionine (nmol/g)	71.0 ± 21.5	66.2 ± 8.1	64.5 ± 15.0	62.9 ± 9.1	0.492	0.297	0.743
SAM (nmol/g)	20.6 ± 2.1	20.6 ± 2.2	23.0 ± 3.5	23.1 ± 3.5	0.975	0.026	0.993
SAH (nmol/g)	5.0 ± 0.9	4.7 ± 0.7	4.2 ± 0.8	4.0 ± 0.6	0.324	0.008	0.798
SAM/SAH	4.2 ± 0.9^a	4.5 ± 0.9^{ab}	5.7 ± 1.4^{ab}	5.9 ± 1.3^b	0.538	0.002	0.913
Cystathionine (nmol/g)	21.4 ± 9.8	28.3 ± 20.5	29.4 ± 12.3	34.7 ± 26.5	0.381	0.308	0.903
Betaine (nmol/g)	26.8 ± 11.1	26.6 ± 8.2	22.2 ± 13.6	18.2 ± 9.4	0.567	0.087	0.608
Choline (nmol/g)	390 ± 138^a	309 ± 91^a	190 ± 52^{ab}	251 ± 64^b	0.750	<0.001	0.027

Table 3.3   Methyl cycle metabolites from the brains of male mice.

3.4 DISCUSSION

We report here a model of the loss of MTHFD1L in adult mice. While there were no major changes to the behavior or memory of the mice, there were some subtle differences in how male and female mice responded to the folate deficient diet (FD) and loss of MTHFD1L. Female mice appeared to be more affected by the folate deficient diet, with female mice on the FD appearing to show an aversion to open spaces in the open field test, and showing higher freezing during the training period of the delay fear conditioning experiment. Male mice did not show any diet-dependent effects in the behavioral experiments; however, male mutant mice appeared to be more active in the open field test than WT, and there was a significant genotype x time interaction during the training period in the fear conditioning test. Sex-dependent effects have been reported in other models of folate metabolism dysfunction. A study looking at methylenetetrahydrofolate reductase (MTHFR) heterozygote mice found that male MTHFR heterozygotes were hyperactive during the open field test, but female mice were not (Levav-Rabkin et al., 2011). This is reminiscent of the increased activity of male mutant mice in the open field test that we have observed, but the lack of increased activity in the elevated plus maze makes it difficult to draw any firm conclusions. A similar increase in activity without an increase in anxiety has been seen in mice fed a diet deficient in choline and vitamins B2, B9, B12, though no sex-dependent differences were reported (Lalonde et al., 2008). Another study found that homocysteine concentrations in patients with the MTHFR C>T genotype was associated with interactions between

76

genotype and folate status in males but only folate status in females (Stanisławska-Sachadyn et al., 2008).

In addition to the sex-dependent behavioral differences, we also observed different sex-dependent responses to genotype and diet effects on serum 5-CH$_3$-THF and homocysteine. While both male and female mice had lower 5-CH$_3$-THF on the FD, only male mutant mice on the CD had significantly lower 5-CH$_3$-THF than WT. Additionally, male mice appeared to be more susceptible to increased serum homocysteine, with homocysteine increasing due to both genotype and diet. These results were unexpected, as folate deficiency is typically reported to increase homocysteine in both male and female mice (Jadavji et al., 2015; Martínez-Vega et al., 2016). Also unexpected, was our finding that brain SAM/SAH increased on the FD in male mice, despite the rise in serum homocysteine. Typically an increase in serum homocysteine is accompanied by a decrease in SAM/SAH (Chen et al., 2001; Yi et al., 2000). Increased serum homocysteine in male mice may provide an explanation for the apparent hyperactivity in male mice during the open field test; high homocysteine has been associated with hyperactivity in various mouse models (Lalonde et al., 2008; Middaugh et al., 1976), but it is unclear how this could be reconciled with the increase in brain SAM/SAH.

This study had several limitations. First, the tamoxifen treatment to knock down expression of MTHFD1L was not done until after weaning, so any deleterious effects caused by MTHFD1L dysfunction during development would not be seen in these experiments. Since deletion of MTHFR is not lethal, studies looking at the effects of MTHFR deletion on behavior do not have this limitation (Jadavji et al., 2012; Levav-

Rabkin et al., 2011). Due to the embryonic lethality caused by complete loss of MTHFD1L, the homozygous deletion of the gene during development is not feasible for studies of adult mice; however, the use of a mouse expressing Cre recombinase under the control of a tissue specific promoter may allow embryos to survive until birth. Another option is to use MTHFD1L heterozygotes, which are viable and have been shown to express lower levels of the MTHFD1L protein as embryos (Momb et al., 2013). Another limitation is that the knockdown of MTHFD1L was variable and incomplete, especially in the FD mice. This could be due to incomplete knockdown from the initial Tamoxifen treatment, or the subsequent recovery of expression of MTHFD1L over time after Tamoxifen treatment. Because the degree of Tamoxifen exposure is dependent on how much of the diet is consumed, the actual Tamoxifen dosage for each mouse could be highly variable. Administering the Tamoxifen by gavage would provide a more consistent means of treating the mice. Recovery of expression of MTHFD1L over time could also cause inconsistencies between mice. Recovery of the expression of the target gene in conditional knockdowns using the Cre-ERT2 system, particularly in proliferative tissues, has been reported (Ruzankina et al., 2007). One strategy to minimize this effect would be to use mice that are heterozygous-null for MTHFD1L, with the other allele containing the floxed exon. Since only one allele per cell would need to be recombined by Cre recombinase, the chances of getting a complete knockout of MTHFD1L would be increased. It is unclear why expression of MTHFD1L would be higher in mutant mice on the FD than mutant mice on the CD. Since mice were not placed on the FD until after the Tamoxifen treatment, the higher level of MTHFD1L expression is likely due to recovery

of expression of MTHFD1L rather than a difference in the efficiency of the initial knockdown.

We did not detect any deficits in cue or context dependent memory due to either diet or genotype; however, more stringent experiments may have revealed effects not tested by delay fear conditioning. Trace fear conditioning, where there is a short period of time between the conditioned stimulus and the unconditioned stimulus, may reveal differences between groups that are not apparent with delay fear conditioning. For example, hippocampal lesions may only result in deficits in trace, but not delay, fear conditioning (James et al., 1987; McEchron et al., 1998, 2000; Quinn et al., 2002). In addition, trace fear conditioning has been shown to require higher cognitive functions, such as awareness or attention, that are not required for delay fear conditioning (Clark and Squire, 1998; Han et al., 2003; Weike et al., 2007). Another alternative is the Morris water maze. Mice in the main study were not tested on the water maze due to time and budgetary constraints. The Morris water maze could reveal deficits in spatial learning and memory that are not tested in fear conditioning experiments (reviewed in (Vorhees and Williams, 2014)). Finally, older mice than those used in this study may have additional or more severe phenotypes than those observed in the current study.

Chapter 4: Metabolic characterization of MTHFD1L null embryos

4.1 INTRODUCTION

Neural tube defects have a complex etiology, involving both environmental and genetic factors. The link between low folate status in pregnant women and risk of NTDs was first recognized in the 1960s and 1970s (Hibbard, 1964, 1967; Smithells et al., 1976). Since then, maternal supplementation with folic acid has been shown to reduce NTDs by as much as 70% (MRC Vitamin Study Research Group, 1991), but this still leaves 30% of NTD cases that are resistant to folic acid supplementation. Understanding the role of folic acid in neural tube closure is important for learning how folate supplementation prevents NTDs and why some NTDs are resistant. An essential tool for studying NTDs is mutant mouse models that develop NTDs; however, only a handful of null mutants of folate-related genes form NTDs (Harris and Juriloff, 2010). Mice lacking either *Folr1* or *Shmt1* both develop NTDs that are sensitive to folate status (Anderson and Stover, 2009; Beaudin et al., 2011; Piedrahita et al., 1999; Spiegelstein et al., 2004). Deletion of *Amt* or *Gldc* in mice also results in NTDs, but these mice do not respond to folic acid (Narisawa et al., 2012; Pai et al., 2015). If the mechanisms in these mice, or other folate resistant mouse models, leading to NTDs are better understood, therapies could be developed to prevent NTDs that are resistant to folic acid in humans.

Metabolomic profiling has been used to identify metabolic defects in several mouse models of NTDs. Mice nullizygous for LRP6 develop exencephaly and spina bifida (Pinson et al., 2000). LRP6 mutants were found to have decreased concentrations of the methyl cycle metabolites methionine, homocysteine, and, SAH. The purine base

hypoxanthine was also decreased (Hansler et al., 2014). A study looking at valproate-induced NTDs in mice found that a range of purines and pyrimidines were decreased, and the methyl cycle/1C metabolites methionine, SAM, SAH, serine, and glycine were all reduced (Akimova et al., 2016). Another study has profiled folate species in GLDC-null mice, and found an increase in free THF and DHF accompanied by a decrease in 5-CH$_3$-THF. The same mice also had significantly increased levels of glycine (Pai et al., 2015).

Our lab has previously reported a mouse model containing a homozygous deletion of MTHFD1L. Embryos lacking MTHFD1L were found to exhibit aberrant neural tube closure, craniofacial defects, developmental delay, and embryonic lethality by embryonic day 12.5 (E12.5) (Momb et al., 2013). The aberrant neural tube closure occurs with 100% penetrance without feeding a folate deficient diet and includes defects such as wavy neural tube, exencephaly, and craniorachischisis. Treating the mice with folinic acid (5-CHO-THF) had no effect on the incidence of neural tube defects (Jessica Momb, unpublished data). This result makes intuitive sense, because if the protein MTHFD1L is missing, adding additional cofactor will have no effect on the missing enzymatic activity. The lack of 10-CHO-THF synthetase activity is expected to result in a loss of mitochondrial production of formate, so pregnant dams were supplemented with formate. We found that maternal supplementation with sodium formate reduced the incidence of neural tube defects, partially rescued the growth restriction, and allowed survival past the previous point of lethality. It has since been found that rescue with formate occurs in a dose dependent manner. Embryos at E15.5 were dissected from a series of matings in which the dams were supplemented with a calculated dose of either 250, 500, 1,500,

2,500, or 3,500 mg·kg^{-1}·d^{-1} calcium formate. *Mthfd1l*$^{z/z}$ embryos were observed at all doses of calcium formate, and the number of embryos did not significantly differ from the expected Mendelian ratio. The crown-rump length of *Mthfd1l*$^{z/z}$ embryos increased significantly at the 1,500 and 2,500 doses. As the dose of formate increased, up to 2,500 mg·kg^{-1}·d^{-1}, there was a concomitant increase in the proportion of *Mthfd1l*$^{z/z}$ embryos observed which did not have any obvious morphological defects (Jessica Momb, unpublished data).

Despite these results, the exact metabolic defects caused by loss of MTHFD1L that could be leading to NTDs remain unknown. Given the role of MTHFD1L in generating 1C units for cytoplasmic synthetic reactions, I hypothesize that metabolism of purines, thymidylate, and methionine will be disrupted by loss of MTHFD1L and that formate supplementation will rescue that disruption. In this chapter, I investigate formate production from mitochondria missing MTHFD1L and identify metabolic defects associated with loss of MTHFD1L that could contribute to the occurrence of NTDs.

4.2 MATERIALS AND METHODS

4.2.1 Mice and Formate Supplementation

All protocols in this study were approved by the Institutional Animal Care and Use Committee of The University of Texas at Austin and conform to the National Institutes of Health Guide for the Care and Use of Laboratory Animals. Mice were maintained on a C57BL/6 background.

Where indicated, matings of $Mthfd1l^{z/+}$ mice were set up in cages equipped with a water bottle containing calcium formate. The concentration of calcium formate was adjusted to deliver a calculated dose of 2,500 mg·kg^{-1}·d^{-1} based on the assumption that a 25 g C57BL/6 mouse consumes water at a rate of 5 mL/d(Whiting et al., 1991). The female mice had access to the supplemented water a minimum of one day prior to the observation of a vaginal plug.

4.2.2 Cell Lines and Media

Wild type and nullizygous MTHFD1L MEFs were derived as described below. The cell lines were not immortalized, so all experiments were conducted low passage numbers (fewer than four passages). Cells were grown in either DMEM (Sigma) supplemented with 10% Fetal Bovine Serum (FBS) or MEM (MP Bio 1641454) supplemented with 15% dialyzed FBS. Cells were grown in a humidified cabinet at 37°C under 5% CO_2 on 100 mm dishes. Cells were typically passaged at 95% confluency at no more than a 1:4 dilution.

4.2.3 Mitochondrial Formate Synthesis Assay

Due to the requirement for large amounts of mitochondria for this assay, pregnant dams were supplemented with 2,500 mg/kg calcium formate to allow survival of $Mthfd1l^{z/z}$ embryos past the typical point of lethality at E12.5. Embryos were dissected between E14.5 and E16.5. The embryos were genotyped using yolk sack tissue as previously described (Momb et al., 2013). Embryos of the same genotype were pooled and mitochondria were isolated using differential centrifugation as previously described. Mitochondrial protein content was quantified by BCA assay (ThermoFisher Scientific). Measurement of mitochondrial synthesis of formate from serine was carried out essentially as described previously (García-Martínez and Appling, 1993). In short, 1mg of mitochondria was incubated with either L-[3-^{14}C]Serine or L-[2-^{14}C]Glycine (1000 dpm/nmol, Moravek Biochemicals, Brea, CA) at the indicated concentration in a shaking incubator for 20 minutes at 37°C. The reactions were quenched by centrifugation at 10,000xg at 4°C for 10 minutes to remove the mitochondria. The resulting supernatant was incubated at 95°C to remove any ^{14}C labeled CO_2 that may have been formed.

4.2.4 MEF Derivation

Mouse embryonic fibroblasts (MEFs) were derived essentially as described in (E Michalska, 2007). Dams that had been supplemented with a calculated dose of 2,500 mg/kg calcium formate were euthanized at E14.5 with CO_2 asphyxiation followed by cervical dislocation. The mice were thoroughly sprayed with 70% ethanol then moved to a laminar flow cabinet for dissection. The uterus was dissected and washed with sterile

PBS. Individual embryos were placed into separate wells of a 6 well plate containing PBS. The yolk sac was saved separately for genotyping. Using two pairs of fine forceps, the heads were removed along with the heart and liver. The remaining tissue was moved to a 15 mL tube containing 3 mL Trypsin-EDTA (0.25%) and kept overnight at 4°C. The next morning, most of the Trypsin was aspirated off, leaving about twice the volume of the tissue. The tubes were placed at 37°C for 30 minutes to activate the Trypsin. 8 mL of DMEM (10% FBS, Pen/Strep) was added and the tissue was thoroughly disrupted by pipetting. Large pieces of tissue were allowed to sediment for 1 minute, then the supernatant was moved to a new tube. 6 mL of media was added to sedimented tissue and the disruption and sedimentation were repeated. This supernatant was combined with the original supernatant then was distributed onto 5 100 mm plates and incubated at 37°C and 5% CO_2. These cells were considered passage number 0. After isolation, MEFs were genotyped as described previously (Momb et al., 2013). MEFs were tested for mycoplasma infection using a PCR test kit (SouthernBiotech). Expression of the MTHFD1L protein was determined by immunoblotting. Proteins were extracted by disrupting cells with NP-40 lysis buffer (50 mM Tris, 150 mM NaCl, 1% NP-40, pH 7.5). Proteins were separated by SDS-PAGE and immunoblotted as described previously (Pike et al., 2010). Blots were probed with anti-MTHFD1L (Prasannan and Appling, 2009) (1:1000) and reacting bands were detected with ECL Prime (GE Healthcare Life Sciences).

4.2.5 MEF Growth Curves

Mthfd1l$^{+/+}$ and *Mthfd1l*$^{z/z}$ MEFs were plated onto six 96 well plates (one for each time point) at a density of 5 x 10^3 cells per well with four replicate wells per genotype for each condition tested. Basal media (referred to as MEM) was made from a formulation of Modified Eagle's Medium lacking methionine, cysteine, and cystine (MP Bio 1641454) and contained additional 15% dialyzed FBS, 500 μM serine, 20 μM methionine, and the following amino acids: 25 mg/L alanine, 50 mg/L asparagine, 30 mg/L aspartate, 75 mg/L glutamate, 292 mg/L glutamine, 40 mg/L proline, 100 mg/L cysteine, 31 mg/L cystine. Additional 30 μM hypoxanthine, 30 μM thymidine, or 1 mM sodium formate were added as indicated. Cell growth was monitored using the cell viability assay Cell Titer Blue (Promega).

4.2.6 Methanol Chloroform Extraction of Polar Metabolites

Prior to starting the extraction, solutions were prechilled in a -80°C freezer for 30 minutes. Embryos or cells were suspended in 1 mL of a 1:1 water:methanol solution and were disrupted by pipetting. The lysate was added to a 2 mL glass vial containing 500 μL choloroform and vortexed for 20 minutes. Glass vials were centrifuged at 6,000 x g for 20 minutes at 4°C. The upper aqueous phase containing the polar metabolites was transferred to a 1.5 mL tube using a Hamilton syringe. Samples were desiccated until dryness in a Centrivap vacuum concentrator at 4 °C (Labconco, Kansas City, MO, USA), then re-suspended in 150 μL of water with 0.1% FA and filtered through a Nanosep 3K ultra centrifugal filter (Pall Co. Port Washington, NY, USA) at 8000 rpm for 2 h at 4 °C.

4.2.7 Embryo Metabolite Analysis

4.2.7.1 LC-MS

Chromatographic separation was performed on a Thermo Scientific (Thermo Fisher Sci., San José, CA, USA) Accela HPLC system equipped with a quaternary pump, vacuum degasser and an open autosampler with a temperature controller. Separation of metabolites was achieved through a 100 ×2.1 mm i.d., 2.6 μm particle size Kinetex biphenyl C18 column (Phenomenex Inc, Torrance, CA, USA). Separation conditions were: solvent A, water/FA (99.8:0.2); solvent B, MeOH; separation gradient, initially 1% B, then linear to 100% B in 4 min, washing with 100% B for 1 min and column equilibration with 1% B for 10 min; flow rate, 0.3 mL/min; injection volume, 3 μl; autosampler temperature, 6℃; column temperature, 22℃. Mass spectrometry analysis was carried out on a Thermo Scientific (Thermo Fisher Sci., Bremen, Germany, EU) Q Exactive benchtop Orbitrap detector loading an electrospray (ESI) source operating in positive ionization mode. The detector run in Full scan MS analysis under the following conditions: spray voltage, 4.0 kV; capillary temperature, 300℃; sheath gas, 55 (arbitrary units); auxiliary gas, 30 (arbitrary units); microscans, 1; AGC target, $1e^{6}$; maximum injection time, 100 ms; mass resolution, 70,000; considered *m/z* range, 145-165. The MS device was calibrated through the commercial calibration solution provided by the manufacturer to keep mass tolerance below 3 ppm at any time. The LC-MS platform of analysis was controlled by a PC loading the software Xcalibur v. 2.2 SP1.48 (Thermo Scientific, San Jose, CA, USA).

Following LC-MS acquisition, Thermo *.raw files were processed for untargeted analysis using two commercially available software packages from Thermo Scientific. Thermo SIEVE (v2.2) was used for the tissue culture experiments and Compound Discoverer (v2.0) was used for the embryos, both in conjunction with an in-house library of approximately 300 compounds. Deuterium incorporation into IMP and hypoxanthine was scored by hand in Xcalibur. Customized settings were as follows: maximum RT shift, 0.25 minutes; minimum base peak intensity 50,000; mass tolerance, 5 ppm, peak integration, ICIS; smoothing, 3 points; adduct formation, ± H. Spectral alignment above 0.9 was considered acceptable for all data sets. Retention times were used to reduce multiple assignments of spectral features and to confirm metabolite assignment. Data was normalized by the total spectral area (TSA) of the features that had a reproducibility greater than 75% (CV<0.25) in the pooled quality control (QC). When a QC was not available, targeted data analysis was done following normalization to the internal standard, d5-tryptophan.

4.2.7.2 NMR

One dimensional ^{1}H NMR spectra were acquired using a Bruker Avance III 500 MHz with 1.7 mm TCI MicroCryoProbe system (Bruker BioSpin Corp., Billerica, MA) equipped with an autosampler at 300 K. The excitation sculpting pulse sequence was used to suppress the water resonance signal. NRMLab and MetaboLab were used to process the raw data. Metabolite identification and quantification was done using Chenomx 8 NMR Suite (Chenomx Inc., Edmonton, Alberta, Canada) referencing the

Birmingham Metabolite Library (Ludwig et al.), and the Human Metabolome Databse (Wishart et al., 2007).

4.2.8 Mitochondrial Respiration and Glycolysis Assays

Oxygen consumption rate (OCR) and extracellular acidification rate (ECAR) were measured using the Seahorse XFp Flux Analyzer (Seahorse Bioscience–Agilent Technologies, Billerica, MA). Cells at a density of 2.10^5 cells/mL were seeded in 80µL DMEM+10%SVF+PSQ on XFp 8-well micro-plates and incubated for 24h at 37°C, 5% CO_2.

For mitochondrial function analysis, based on OCR, cells were washed two times with XF media freshly supplemented with 2.5mM of Glucose, 2mM of Glutamine, 1mM of Pyruvate and adjusted at pH 7.4. Cells were then incubated in that same media for 1h at 37°C in a CO_2-free incubator. After calibration, the device first measures a baseline then levels of OCR and ECAR after sequential addition of different compounds to each well: Oligomycin (an ATP coupler, final concentration of 2µM), Carbonyl cyanide-4 (trifluoromethoxy) phenylhydrazone (FCCP, an uncoupling agent, final concentration of 1µM), Antimycin A/Rotenone (Complex I and III inhibitors, final concentration of 1µM).

For the glycolysis assay, based on ECAR, cells were washed and incubated as above except that the media lacked glucose. The treatments were as follows: Glucose (final concentration of 10mM), Oligomycin (final concentration of 2µM), 2-deoxyglucose (2-DG, glucose competitive inhibitor, final concentration of 50mM).

After each assay, the media was removed from each well and the plates were frozen at -80°C overnight. Cells were then lysed by adding 10µl of lysis buffer (10mM Tris pH8, 0.1% Triton X-100) in each well. To determine total protein levels, a Bradford assay was carried out adding 200 µL of 1X dye Bradford reagent (Bio-Rad #5000205) to each well and using a bovine serum albumin (BSA) standard scale (Bio-Rad #5000207). Data from each well were normalized by total protein concentration. Assays were analyzed using the Seahorse Data Analysis Software (Seahorse Bioscience–Agilent Technologies).

4.2.9 Deuterated Serine Tracer Experiment

Labeling of MEFs with 2,3,3-D3-L-serine was performed essentially as previously described (Pike et al., 2010). Cells were plated onto 10 cm dishes in triplicate at a density of 1 x10^6 cells per dish. Labeling media was identical to the basal MEM used for the growth curve experiments (see above) except methionine was at 10 µM. 1 µM cyanocobalamin was added as indicated. Cells were grown in the labeling media for a total of four days, with fresh media added after two days. Cells were washed with PBS and collected by trypsinization. At the time of cell collection, aliquots of the labeling media were collected and stored at -70°C to be used for metabolite analysis. Cell pellets were snap frozen in liquid nitrogen and stored at -70°C until the metabolites could be extracted using methanol/chloroform as described above.

4.2.10 Statistical analysis

Growth curves and Seahorse experiments were analyzed in Graphpad Prism using a mixed model two-way ANOVA for repeated measures, and Bonferroni post-tests were used for pairwise comparisons at individual time points. Unpaired t-tests tests were calculated in Microsoft Excel. False discovery rate (q) for the metabolite analyes was calculated using the method described by Benjamini and Hochberg (1995). Principal component analysis (PCA) was performed with Jmp Pro12 (SAS Institute). Pathway analysis was performed using MetaboAnalyst (Xia and Wishart, 2011; Xia et al., 2009). Data were log transformed and mean centered prior to PCA and pathway analysis. α was set to 0.05 for all experiments.

4.3 RESULTS

4.3.1 Formate production in isolated mitochondria

It has been show that isolated mitochondria are capable of producing formate from either serine or glycine (Bao et al., 2016; García-Martínez and Appling, 1993; Pike et al., 2010). We hypothesized that mitochondria lacking MTHFD1L would be unable to produce formate when given serine or glycine as a substrate. Embryos at E14.5-E16.5 were dissected from dams that had been supplemented with 2500 mg/kg calcium formate. Mitochondria from these embryos were incubated with either 0.2 mM, 0.5 mM or 1 mM L-[3-^{14}C]Serine or L-[2-^{14}C]Glycine. *Mthfd1l*$^{z/z}$ mitochondria showed a reduction in formate produced from serine (Figure 4.1A), but surprisingly there was no difference with glycine as a substrate (Figure 4.1B). Formate production increased linearly with L-

[3-^{14}C]Serine and L-[2-^{14}C]Glycine concentrations, indicating that serine and glycine were not saturating at these conditions. Immunoblots confirmed the absence of any detectable MTHFD1L expression (Figure 4.1C). We observed that ALDH1L2 expression was increased in *Mthfd1l*$^{z/z}$ mitochondria (Figure 4.1 C,D). ALDH1L2 has been reported to have 10-CHO-THF hydrolase activity *in vitro*, converting 10-CHO-THF to formate and THF (Krupenko et al., 2010; Strickland et al., 2011), and increased expression of ALDH1L2 may account for some of the formate production we have observed.

4.3.2 Embryo metabolites

In order to try to identify specific metabolic defects associated with loss of MTHFD1L that could be contributing to the defects that we have observed and the effects of formate supplementation, we collected *Mthfd1l*$^{+/+}$ and *Mthfd1l*$^{z/z}$ embryos from either unsupplemented dams or dams that had been supplemented with 2,500 mg/kg calcium formate (n=5 for each group). We conducted a non-targeted metabolomics screen using both NMR and MS and identified a total of 98 metabolites in unsupplemented embryos and 117 in supplemented embryos.

4.3.2.1 Unsupplemented

We first analyzed metabolite data from embryos from unsupplemented dams in order to identify defects associated with loss of MTHFD1L. Metabolites from NMR and MS were combined and analyzed by PCA (Figure 4.2). There was clear separation of the groups, primarily along Component 1. Metabolite differences were also analyzed by t-test, and p values were corrected for the false discovery rate (Benjamini and Hochberg,

1995). We found that 24 of the 98 detected metabolites were significantly altered by loss of MTHFD1L (Table 4.1, see Appendix II for full list of metabolites). The 1C metabolites serine, glycine, and formate were significantly different. Serine was elevated, and glycine and formate were decreased, consistent with decreased utilization of serine for formate synthesis. There were also indications of disrupted energy metabolism. Lactate was reduced in $Mthfd1l^{z/z}$ embryos, possibly indicating decreased flux through glycolysis. To further explore this possibility, we used the lactate:pyruvate ratio to estimate the cytoplasmic NAD^+:NADH ratio using the method described by Krebs (Williamson et al., 1967). This method assumes that the conversion of pyruvate + NADH to lactate + NAD^+ is in chemical equilibrium. Assuming a pH of 7.0 and $K_{eq} = 1.11 \times 10^{-4}$, we estimated the NAD^+:NADH ratio in $Mthfd1l^{z/z}$ and $Mthfd1l^{+/+}$ embryos. We found that the NAD^+:NADH ratio in $Mthfd1l^{z/z}$ embryos (116.2 +/- 12.3) was significantly higher than $Mthfd1l^{+/+}$ embryos (88.4 +/- 7.1, p = 0.0024), consistent with decreased flux through glycolysis (Lim et al., 2010). The tricarboxylic acid (TCA) cycle also appeared to be affected. The entry metabolite into the cycle, citrate, was elevated; whereas the downstream metabolites fumarate and (Table 4.2) succinate (Appendix II, q = 0.077) were both decreased in $Mthfd1l^{z/z}$ embryos. The ATP pool was also disrupted. In $Mthfd1l^{z/z}$ embryos, there was a depletion of the low energy AMP and an accumulation of high energy ADP and ATP.

In order to get a picture of the metabolic pathways affected by loss of MTHFD1L we performed a pathway analysis using MetaboAnalyst (Xia and Wishart, 2011; Xia et al., 2009). We identified 12 pathways that were significantly altered in $Mthfd1l^{z/z}$

93

embryos (Impact > 0.2, FDR < 0.05, Table 4.2). Consistent with the previously mentioned metabolites, perturbations to pathways involving 1C metabolism (Methane metabolism and Serine, Glycine, and Threonine metabolism) and energy metabolism (Pyruvate metabolism and TCA cycle) were identified. In addition, seven pathways involving amino acid metabolism were identified as significantly altered (Table 4.2). Leucine, isoleucine, valine, phenylalanine, tyrosine, glycine, and arginine were all depleted in *Mthfd1l*$^{z/z}$ embryos, though not all reached statistical significance after correcting for the FDR (Table 4.1, Appendix II). Aspartate, serine, and threonine (q = 0.085) were elevated in *Mthfd1l*$^{z/z}$ embryos.

4.3.2.2 Formate Supplementation

We next compared metabolites of *Mthfd1l*$^{z/z}$ and *Mthfd1l*$^{+/+}$ embryos from calcium formate supplemented dams to see if any of the metabolites that were altered in unsupplemented embryos were normalized with formate supplementation. Indeed, of the 117 detected metabolites only 9 were significantly different, 4 of which matched metabolites that were altered in unsupplemented embryos (Table 4.3, see Appendix III for full list). Serine remained elevated, and glycine remained depleted (Table 4.3); however, formate was no longer significantly different (Appendix III). Taurine abundance was reversed; it was elevated in unsupplemented *Mthfd1l*$^{z/z}$ embryos but is lower in supplemented *Mthfd1l*$^{z/z}$ embryos. AMP remained depleted in *Mthfd1l*$^{z/z}$ embryos. Metabolites were analyzed by PCA, and while there was still separation between the groups, there appeared to be more overlap along Component 1 (Figure 4.2).

We performed a pathway analysis with MetaboAnalyst and looked specifically at the pathways that had been identified in unsupplemented embryos. Of the 12 pathways that were altered in unsupplemented embryos, 6 were "restored" in supplemented embryos and did not significantly differ (Table 4.2). These include both pathways involved in energy metabolism (though Pyruvate metabolism was close to significance at FDR = 0.057).

4.3.3 MEF growth curves

In order to assess any dysfunction in the synthesis of purines and thymidylate, we conducted a series of growth curves using MEFs derived from *Mthfd1l*$^{z/z}$ and *Mthfd1l*$^{+/+}$ embryos. The basal media, MEM, contained serine as a source of one carbon units, but lacked any nucleotides. Cell growth was monitored using the cell viability assay Cell Titer Blue and is shown as the fluorescent signal from the resorufin dye. Although null MEFs were viable in MEM, WT cells grew significantly better ($p < 0.0001$) (Figure 4.3 A). Addition of thymidine alone to the media resulted in only a small improvement in the growth of null MEFs as compared to WT (Figure 4.3 B), though WT MEFs still grew better ($p = 0.0023$). The addition of hypoxanthine alone yielded a larger improvement in growth, with null MEFs matching or surpassing the growth of WT MEFs at later time points (Figure 4.3 C), and the overall genotype effect was no longer significant ($p = 0.13$). With the addition of hypoxanthine and thymidine together or formate alone, the growth of null MEFs was almost indistinguishable from that of WT (Figure 4.3 D,E; $p = 0.64$ and 0.30 respectively). Neither cell line was able to grow when methionine was

replaced with homocysteine and vitamin B12 (not shown). The knockdown of MTHFD1L in *Mthfd1l*$^{z/z}$ MEFs was confirmed by genotyping and immunoblotting (Figure 4.3 F).

4.3.4 Deuterated serine labeling

Despite the fact that mitochondrially derived 1C units are generally the primary source of carbon for methionine synthesis from homocysteine (Davis et al., 2004; Pike et al., 2010), loss of MTHFD1L did not significantly alter the concentrations of methionine or homocysteine in embryos (Appendix II). To further explore this result, I employed a tracer experiment utilizing 2,3,3-D3-L-serine (Herbig et al., 2002). This experiment relies on the principle that 1C units derived from carbon 3 of serine which are processed in the mitochondria before being incorporated into methionine will only contain one deuterium atom (D1) due to the dehydrogenase activity of MTHFD2(L). One-carbon units incorporated into methionine via SHMT1 in the cytosol will retain both deuterium atoms (D2). We found that singly deuterated methionine in *Mthfd1l*$^{z/z}$ MEFs accounted for almost three-fold less of the total methionine pool as compared to *Mthfd1l*$^{+/+}$ (Table 4.4). *Mthfd1l*$^{z/z}$ MEFs also showed a trend for an increase in doubly deuterated methionine, suggesting the cells are compensating for the loss of MTHFD1L by increasing flux of cytosolic serine through SHTM1. Similar results have been seen in HEK293 cells, where a block in the mitochondrial folate pathway leads to increased incorporation of 1C units from serine into dTTP via the cytosolic pathway, though incorporation into methionine was not reported (Ducker et al., 2016). Consistent with previously reported values, about

98% of labeled methionine in *Mthfd1l*^{+/+} cells was mitochondrially derived (Davis et al., 2004; Pike et al., 2010). The proportion of D1 methionine in *Mthfd1l*[z/z] cells was lower at only 85% (Table 4.4).

Previous labeling experiments with deuterated serine were carried out using a modified αMEM as the labeling medium, which contains 1 μM vitamin B12 (Herbig et al., 2002; Pike et al., 2010). B12 is a required cofactor for the function of methionine synthase (Loughlin et al., 1964). DMEM does not typically contain additional B12, so we repeated the labeling experiment using the same conditions as before but with the addition of 1 μM cyanocobalamin. We found that overall the total amount of labeled methionine produced was approximately doubled in both cells lines with the addition of B12 (Table 4.5). The differences in singly and doubly deuterated methionine were also much more pronounced. The methionine pool in *Mthfd1l*^{+/+} cells contained five times as much singly deuterated methionine as the *Mthfd1l*[z/z] cells. Conversely, doubly deuterated methionine was five-fold higher in *Mthfd1l*[z/z] cells than *Mthfd1l*^{+/+} cells. Singly deuterated methionine still made up most of the labeled methionine in *Mthfd1l*^{+/+} cells but only accounted for 27% of labeled methionine in *Mthfd1l*[z/z] cells.

We also looked at deuterium incorporation into hypoxanthine and IMP as an indicator of *de novo* purine synthesis. 1C units derived from serine can be incorporated into purines in one of two ways, either as 10-CHO-THF or as glycine formed by SHMT. As is the case with methionine, a mitochondrially derived 1C unit from either glycine or 10-CHO-THF would contain a single deuterium. 10-CHO-THF derived from the cytoplasmic pathway would contain two deuterium atoms. Higher order labeling is

97

possible, with IMP or hypoxanthine incorporating a combination of labeled 10-CHO-THF and glycine, but only singly deuterated species were detected. We found that $Mthfd1l^{+/+}$ cells had a much higher proportion of labeled hypoxanthine and IMP than $Mthfd1l^{z/z}$ cells (Table 4.6), suggesting that $Mthfd1l^{+/+}$ cells are utilizing *de novo* purine synthesis, while $Mthfd1l^{z/z}$ cells have to rely more on the salvage pathway. It should be noted that while we cannot distinguish whether the deuterium label is derived from 10-CHO-THF or glycine, in either case a singly deuterated species is indicative of synthesis in the *de novo* purine synthesis pathway rather than the salvage pathway.

Finally, we examined deuterium labeled serine in both cellular extracts and the labeling media in which the cells had been grown. The only external source of serine was the 2,3,3-D3-L-serine provided in the labeling medium. Serine could also be synthesized intracellularly through several routes. Serine could be synthesized from glycine and CH_2-THF by SHMT, which would have the potential to generate serine with 0, 1, 2 or 3 deuterium atoms depending on the degree of labeling of glycine and CH_2-THF. Serine could also be derived from protein degradation or synthesized *de novo* from the glycolytic intermediate 3-phosphoglycerate (Snell, 1986). Serine derived from either of these sources would most likely not be deuterated. We found that the abundance of singly and doubly deuterated serine did not significantly differ between $Mthfd1l^{z/z}$ and $Mthfd1l^{+/+}$ MEFs (not shown). However, unlabeled serine was more abundant than the triply deuterated species in extracts from $Mthfd1l^{z/z}$ MEFs as well as in the labeling media (Table 4.7), suggesting that *de novo* synthesis of serine is increased in these cells.

98

4.3.5 Energy metabolism in *Mthfd1l$^{z/z}$* MEFs

Our metabolic analysis of *Mthfd1l$^{z/z}$* embryos suggested that these embryos may have impaired energy metabolism. We utilized the Seahorse XFp Flux Analyzer to measure mitochondrial respiration via oxygen consumption rate (OCR) and glycolytic flux via extracellular acidification rate (ECAR). *Mthfd1l$^{z/z}$* MEFs showed similar respiratory function to *Mthfd1l$^{+/+}$* MEFs (Figure 4.4, $p = 0.62$). Both cell lines showed well coupled mitochondria after addition of rotenone and the maximal respiration rates after the addition of FCCP did not significantly differ. In the glycolysis test, *Mthfd1l$^{z/z}$* MEFs showed lower rates of glycolysis (Figure 4.4, $p = 0.010$). ECAR did not increase in either cell line after the addition of oligomycin, indicating little to no glycolytic reserve in these cells. ECAR only significantly differed after the glucose injection and prior to the 2-DG injection, indicating that the difference in ECAR was due to decreased glycolytic flux, rather than acidification of the media by some other cellular process. These results are consistent with the perturbations to energy metabolism that we observed in *Mthfd1l$^{z/z}$* embryos.
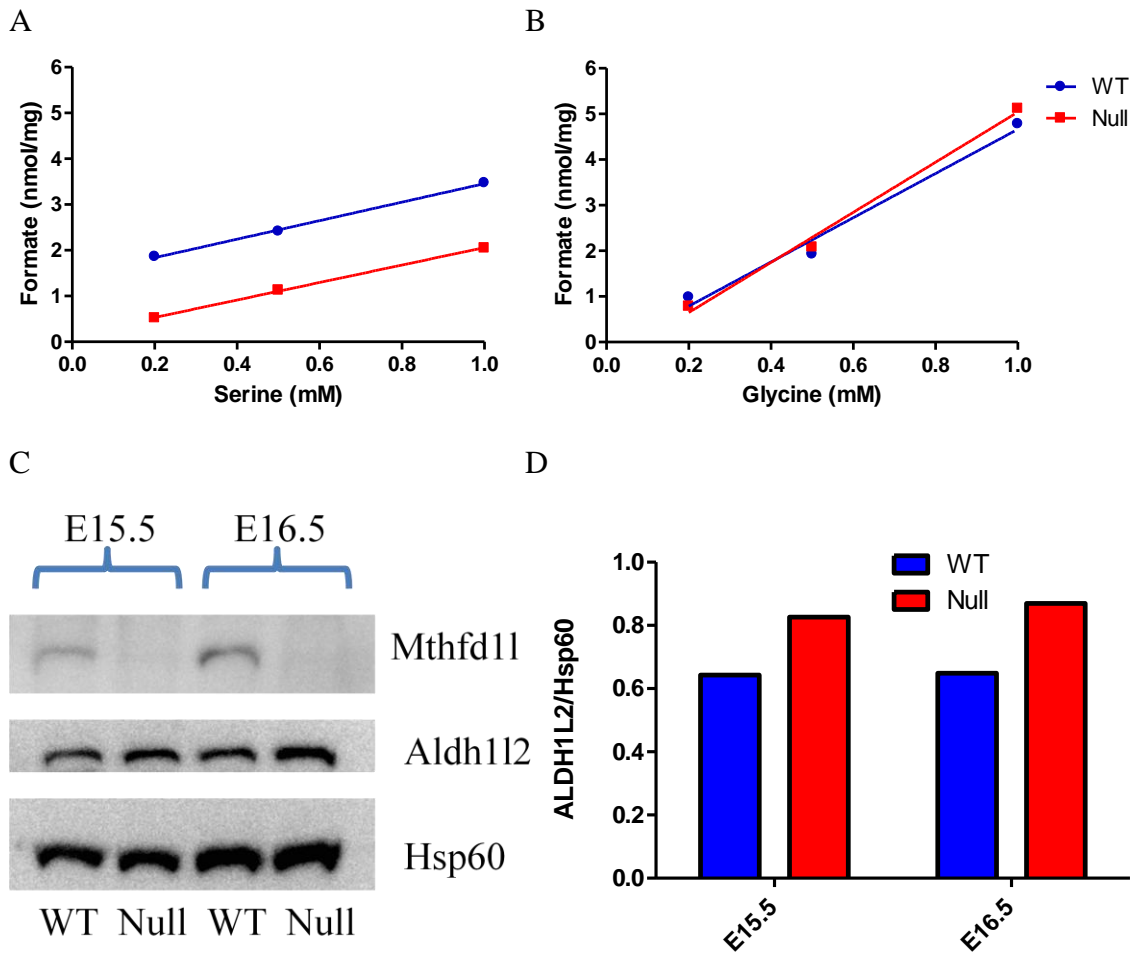
Figure 4.1   Formate production in isolated mitochondria. ^{14}C formate produced from either L-[3-^{14}C]Serine (A) or L-[2-^{14}C]Glycine (B) in isolated mitochondria. (C) Representative immunoblot of MTHFD1L and ALDH1L2 expression in mitochondria isolated from E15.5 and E16.5 embryos. (D) Densitometry of the expression of ALDH1L2 in (C) normalized to the Hsp60 signal.
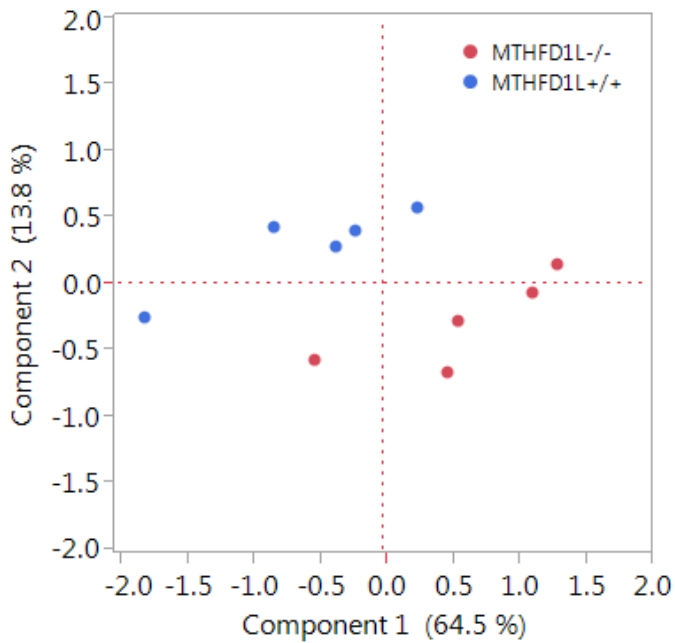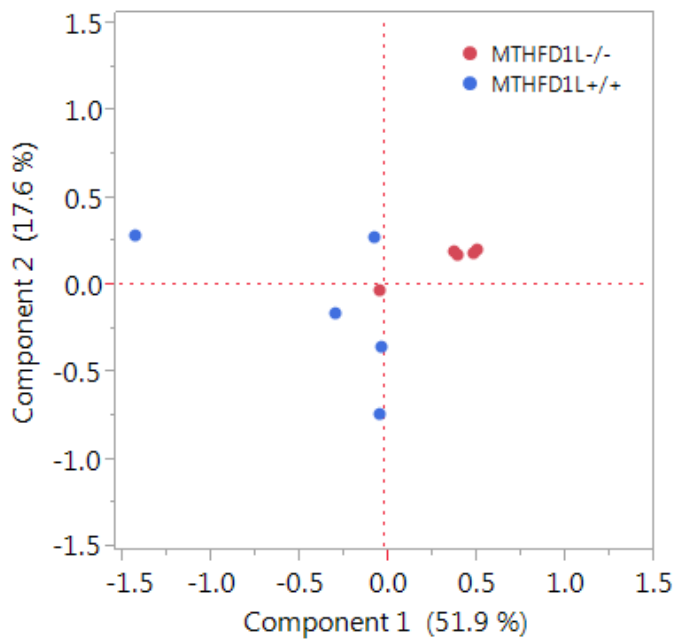
Figure 4.2   Principal component analysis of embryo metabolites. PCA plots were generated for metabolites from embryos from unsupplemented (top) and formate supplemented (bottom) dams. Each point represents an individual embryo.
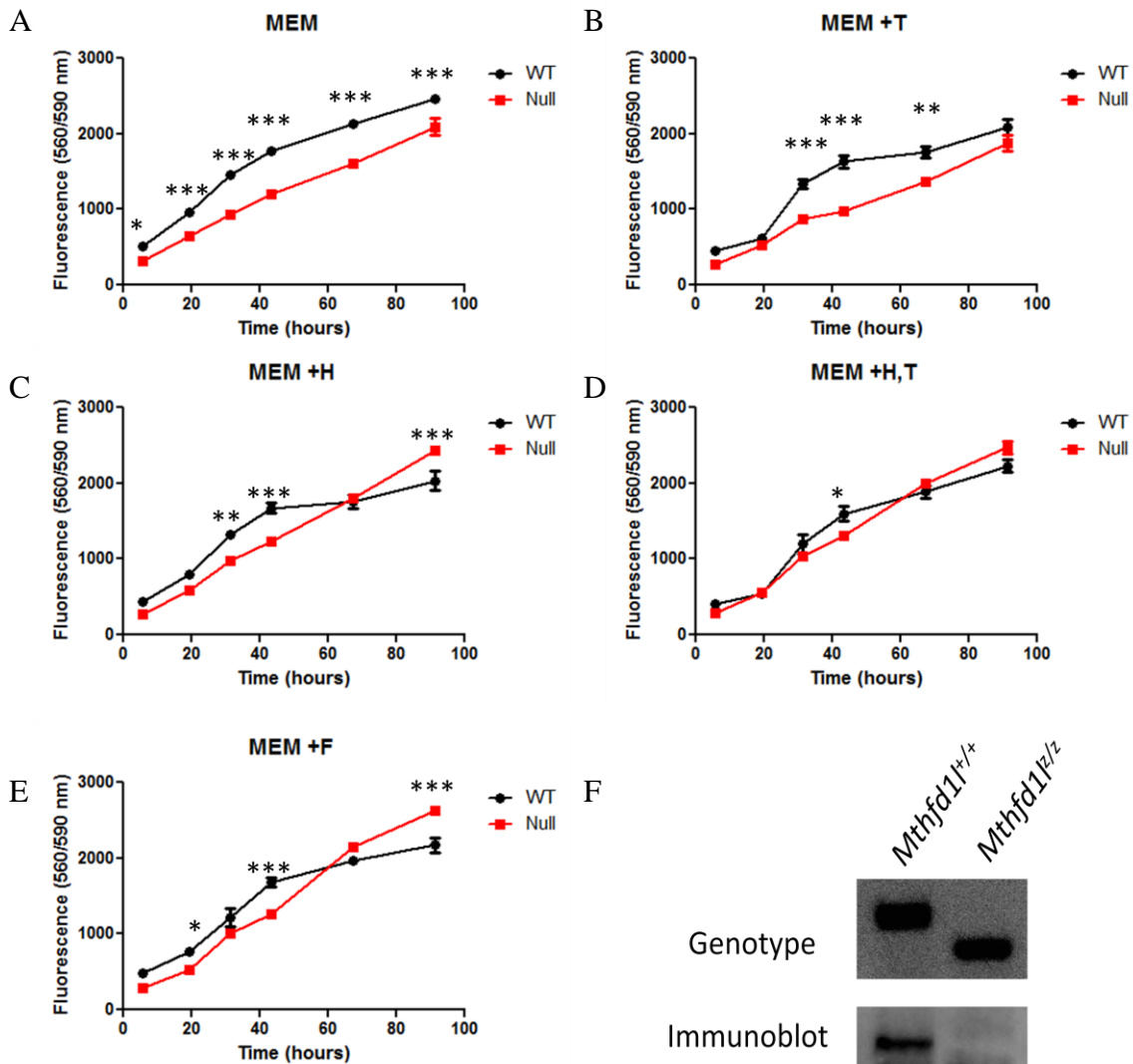
Figure 4.3   MTHFD1L null MEF growth curves. Cell growth was monitored using the cell viability assay CellTiter Blue. (A-E) Cells were grow in basal MEM (described in "Materials and Methods") with additional 30 μM thymidine (T), 30 μM hypoxanthine (H), or 1 mM formate (F) as indicated. (F) Knockdown of MTHFD1L expression was confirmed by genotyping and immunoblotting. * = $p < 0.05$, ** = $p < 0.001$, *** = $p < 0.0001$ as determined by Bonferroni post test.
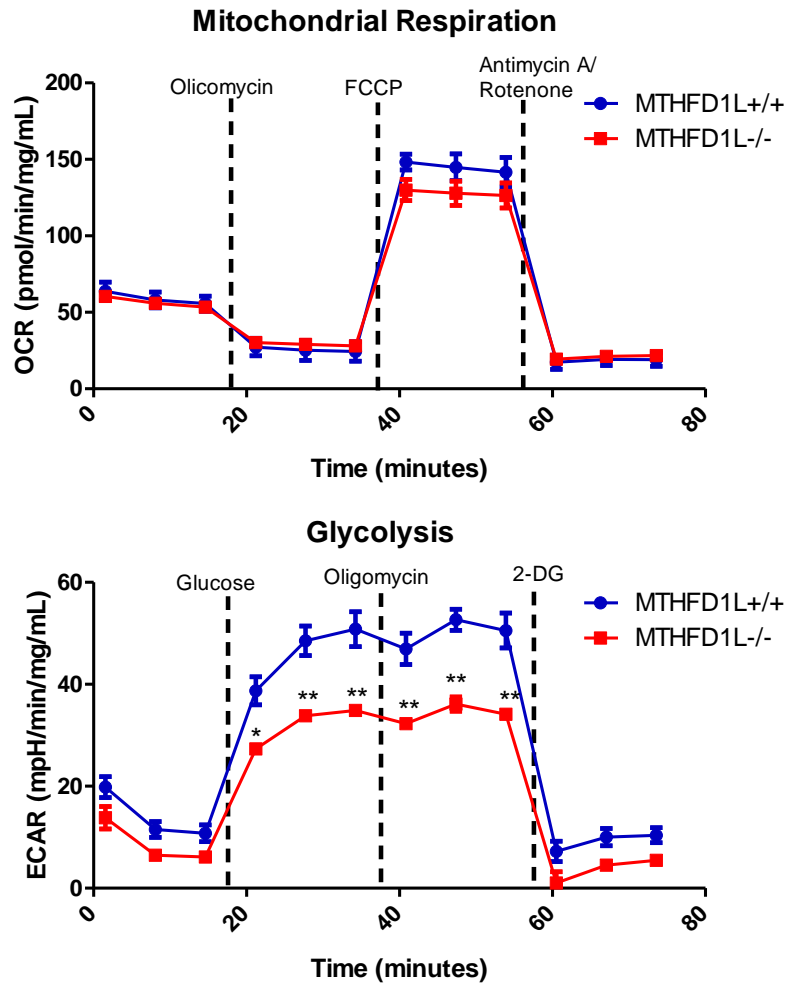
Figure 4.4   Energy metabolism in *Mthfd1l*$^{z/z}$ MEFs. Mitochondrial respiration (top) and glycolysis (bottom) were analyzed in MEFs using the Seahorse XFp Flux Analyzer as described in "Materials and Methods." Data points represent the mean rates of triplicate determinations +/- SD. Dashed lines represent injections of the indicated compounds. * $p < 0.01$, ** $p < 0.0001$ as determined by Bonferroni post test.

Metabolite	$Mthfd1l^{z/z}/Mthfd1l^{+/+}$	q value
Taurine	1.07	0.0089
Fumarate	0.84	0.0067
Arginine	0.86	0.0052
Glycine	0.85	0.013
Lactate	0.82	0.012
ADP	1.26	0.013
Serine	1.16	0.013
Glutathione	1.05	0.017
Leucine	0.87	0.017
ATP	1.33	0.016
Fucose 1-phosphate*	1.27	0.016
Creatine	1.09	0.020
5-Hydroxymethyl-2-furanoate*	1.29	0.020
Isoleucine	0.81	0.021
AMP	0.76	0.023
Valine	0.88	0.029
Formate	0.93	0.028
Citrate	1.28	0.027
Uracil	0.82	0.026
Acetate	0.90	0.030
Phosphocholine	1.11	0.032
Ascorbic acid*	1.26	0.039
Phosphoethanolamine	1.15	0.044
Aspartate	1.28	0.044

Table 4.1   Significantly altered metabolites in $Mthfd1l^{z/z}$ embryos. The ratio of the abundance of the given metabolite in $Mthfd1l^{z/z}$ embryos relative to the abundance in $Mthfd1l^{+/+}$ embryos is shown. False discovery rate (q value) was calculated from p values using the method described by Benjamini and Hochberg (Benjamini and Hochberg, 1995). * indicates metabolites detected by LC-MS; all others were detected by NMR.

Pathway	Total Compounds	Hits	Unsupp FDR	Supp FDR
Methane metabolism[a]	9	3	2.76E-06	5.32E-06
Citrate cycle (TCA cycle)[c]	20	6	0.0028	0.52
Alanine, aspartate and glutamate metabolism[b]	24	8	0.0054	0.027
Arginine and proline metabolism[b]	44	10	0.0057	0.13
Glyoxylate and dicarboxylate metabolism	18	4	0.0057	0.39
Valine, leucine and isoleucine biosynthesis[b]	11	4	0.0057	0.63
Pyruvate metabolism[c]	23	4	0.0063	0.057
Glycine, serine and threonine metabolism[ab]	31	7	0.012	5.32E-06
Histidine metabolism[b]	15	2	0.018	0.020
Phenylalanine metabolism[b]	11	2	0.026	0.023
Phenylalanine, tyrosine and tryptophan biosynthesis[b]	4	2	0.026	0.023
beta-Alanine metabolism	17	4	0.028	0.13

Table 4.2   Pathway analysis by MetaboAnalyst. Metabolic pathways that were found to be significantly altered (based on FDR) in *Mthfd1l*[z/z] embryos from unsupplemented dams. The rightmost column shows how each pathway has responded to formate supplementation (supplemented *Mthfd1l*[z/z] vs supplemented *Mthfd1l*^{+/+}). Pathways involved in 1C (a), amino acid (b), and energy metabolism (c) were identified. Red text indicates pathways that were "restored" with formate supplementation.

Metabolite	$Mthfd1l^{z/z}/Mthfd1l^{+/+}$	q value
Serine	3.06	1.33E-06
Glycine	0.59	0.0029
Diethyl fumarate*	1.89	0.0051
Asparagine	1.32	0.0074
Taurine	0.84	0.011
3-Methyladipic acid/Ethyl methyl succinate*	1.19	0.026
Histidine	1.35	0.049
AMP	0.57	0.043
Glycerophosphocholine	0.72	0.045

Table 4.3 Significantly altered metabolites in $Mthfd1l^{z/z}$ embryos from calcium formate supplemented dams. The ratio of the abundance of the given metabolite in supplemented $Mthfd1l^{z/z}$ embryos relative to the abundance in supplemented $Mthfd1l^{+/+}$ embryos is shown. False discovery rate (q value) was calculated from p values using the method described by Benjamini and Hochberg (Benjamini and Hochberg, 1995). * indicates metabolites detected by LC-MS; all others were detected by NMR.

	Fraction of Total (M+D1+D2)			Fraction of Labeled (D1+D2)	
	D1	D2	D1+D2	D1	D2
Mthfd1l$^{+/+}$	0.12 +/- 0.0007	0.0025 +/- 0.0003	0.12 +/- 0.007	0.98 +/- 0.002	0.0210 +/- 0.002
Mthfd1l$^{z/z}$	0.045 +/- 0.002	0.0080 +/- 0.003	0.0531 +/- 0.001	0.85 +/- 0.05	0.15 +/- 0.05
p value	0.0006	0.1051	0.0007	0.0501	0.0501

Table 4.4   Methionine labeling with deuterated serine. MEFs were plated in triplicate in 10 cm dishes at a density of 1 x 10^6 cells per dish and were grown in labeling media for four days as described in "Materials and Methods." Incorporation of the deuterium label into methionine was measured by LC-MS. Means of triplicate determinations +/- SD are shown. M = unlabeled methionine, D1 = methionine + 1 deuterium, D2 = methionine + 2 deuterons. P values were calculated using two tailed t-tests.

	Fraction of Total (M+D1+D2)			Fraction of Labeled (D1+D2)	
	D1	D2	D1+D2	D1	D2
MTHFD1L$^{+/+}$	0.18 +/- 0.008	0.020 +/- 0.01	0.20 +/- 0.009	0.90 +/- 0.05	0.10 +/- 0.05
MTHFD1L$^{z/z}$	0.033 +/- 0.001	0.092 +/- 0.009	0.12 +/- 0.008	0.27 +/- 0.03	0.73 +/- 0.03
p value	6.70E-06	0.0011	5.80E-04	5.60E-05	6.00E-05

Table 4.5   Methionine labeling with deuterated serine and B12. MEFs were plated in triplicate in 10 cm dishes at a density of 1 x 10^6 cells per dish and were grown in labeling media for four days as described in "Materials and Methods." Incorporation of the deuterium label into methionine was measured by LC-MS. Means of triplicate determinations +/- SD are shown. M = unlabeled methionine, D1 = methionine + 1 deuteron, D2 = methionine + 2 deuterons. P values were calculated using two tailed t-tests.

	Fraction of Total (IMP + IMP+D)		Fraction of Total (Hyp + Hyp+D)	
	IMP	IMP+D	Hyp	Hyp+D
MTHFD1L$^{+/+}$	0.18 +/- 0.02	0.82 +/- 0.02	0.22 +/- 0.01	0.78 +/- 0.01
MTHFD1L$^{-/-}$	0.90 +/- 0.009	0.1 +/- 0.009	0.81 +/- 0.03	0.19 +/- 0.03
p value	5.87E-06	5.87E-06	0.00024	0.00024

Table 4.6   Purine labeling with deuterated serine and B12. MEFs were plated in triplicate in 10 cm dishes at a density of 1×10^6 cells per dish and were grown in labeling media for four days as described in "Materials and Methods." Incorporation of the deuterium label into IMP and hypoxanthine (Hyp) was measured by LC-MS. Means of triplicate determinations +/- SD are shown. IMP+D = IMP + 1 deuteron, Hyp+D = Hyp + 1 deuteron. P values were calculated using two tailed t-tests.

	Fraction of total serine (S + D1 + D2 + D3)	
Intracellular	**S**	**D3**
Mthfd1l$^{+/+}$	0.25 +/- 0.02	0.41 +/- 0.04
Mthfd1l$^{z/z}$	0.34 +/- 0.03	0.31 +/- 0.01
p value	0.012	0.012
Media	**S**	**D3**
Mthfd1l$^{+/+}$	0.12 +/- 0.04	0.88 +/- 0.04
Mthfd1l$^{z/z}$	0.34 +/- 0.07	0.66 +/- 0.07
p value	0.0087	0.0087

Table 4.7   *De novo* serine synthesis in *Mthfd1l*$^{z/z}$ MEFs. MEFs were plated in triplicate in 10 cm dishes at a density of 1×10^6 cells per dish and were grown in labeling media for four days as described in "Materials and Methods." Deuterium labeling of serine from cellular extracts and serine effluxed into the media was measured by LC-MS. Means of triplicate determinations +/- SD are shown. S = unlabeled serine, D1 = serine + 1 deuteron, D2 = serine + 2 deuterons, D3 = serine + 3 deuterons. P values were calculated using two tailed t-tests.

4.4 DISCUSSION

We had hypothesized that isolated, intact mitochondria from $Mthfd1l^{z/z}$ embryos would produce minimal formate from glycine or serine. We found that labeled formate production from $Mthfd1l^{z/z}$ mitochondria using L-[3-^{14}C]Serine as a substrate was reduced, but some formate was still being formed. This suggests some alternate means of making formate from the 3-carbon of serine exists in the mitochondria. One possibility is that cytoplasmic MTHFD1 and SHMT1 are being copurified on the outside of the mitochondria. This is unlikely to account for the activity, however, as the concentrations of the necessary cofactors $NADP^+$, THF, and ADP outside the mitochondria are likely too low allow for any copurified proteins to be catalytically active. This is supported by a study from our lab in which extracts from sonicated mitochondria were given L-[3-^{14}C]Serine and formation of labeled formate was measured. Production of formate was only detected when the appropriate cofactors were added back to the system (García-Martínez and Appling, 1993). Another possibility is that formate is being produced from 10-CHO-THF by the hydrolase activity of ALDH1L2 (Krupenko et al., 2010; Strickland et al., 2011). Although 10-CHO-THF hydrolase activity in ALDH1L2 has only been demonstrated *in vitro*, if it occurs *in vivo*, it could account for the ability of $Mthfd1l^{z/z}$ mitochondria to produce formate from L-[3-^{14}C]Serine. We observed that expression of ALDH1L2 was increased in $Mthfd1l^{z/z}$ embryos. This increase in expression is likely the cell compensating for the bottleneck at 10-CHO-THF caused by loss of MTHFD1L, but whether that compensation is simply to regenerate THF by releasing the 1C unit as CO_2 or to provide supplementary formate production has yet to be determined. Work is

111

currently underway to assess what role, if any, ALDH1L2 plays in mitochondrial formate production.

With L-[2-^{14}C]Glycine as a substrate, formate production in $Mthfd1l^{z/z}$ mitochondria was indistinguishable from that of $Mthfd1l^{+/+}$ mitochondria. This was a surprising result and likely indicates that at least some of the formate produced from glycine is obtained via a different route from that of serine. If the only pathway for production of formate from glycine was through the folate-dependent pathway involving GCS and the intermediate 10-CHO-THF, we could reasonably expect to see a similar reduction in formate production that is seen with serine. There is evidence for a folate independent pathway that can produce formate from glycine via a glyoxylate intermediate (Nakada et al., 1955). There are several potential routes for formation of glyoxylate from glycine. The most likely route seems to be through D-amino acid oxidase, which is typically a peroxisomal protein but has also been found to localize with the mitochondria (Sacchi et al., 2011). D-amino acid oxidase catalyzes the deamination of glycine to form glyoxylate (de Marchi and Johnston, 1969). There is also evidence for nonenzymatic transamination reactions under physiological conditions between glyoxylate and several different amino acids to form glycine, though it was not shown whether or not these reactions would proceed in the direction of glycine catabolism (Nakada and Weinhouse, 1953). Another possibility is the mitochondrial alanine:glyoxylate aminotransferase (AGT2) which catalyzes a transamination between alanine and glyoxylate to form pyruvate and glycine. However, this reaction has been reported to proceed exclusively in the direction of glycine synthesis *in vitro*, so it is

112

unlikely that AGT2 would contribute to glyoxylate synthesis in mitochondria (Noguchi et al., 1978; Thompson and Richardson, 1967). Once glyoxylate is formed, it is oxidized to CO_2 and formate (Nakada et al., 1955). This oxidation can occur either enzymatically or nonenzymatically. After a search of the existing literature, the enzymatic pathway of glyoxylate oxidation does not appear to be fully described, but is has been shown to require NAD^+, does not require folate (Nakada and Sund, 1958), and appears to involve a condensation with α-ketoglutarate (Kawasaki et al., 1966). Alternatively, glyoxylate can react non-enzymatically with H_2O_2 to form CO_2 and formate (Kenten and Mann, 1952).

Even though $Mthfd1l^{z/z}$ mitochondria retain some formate production capacity, it is apparently insufficient to support proper embryonic development, since formate supplementation of the dams partially rescues the NTD and growth defects (Momb et al., 2013). It's possible that the flux of formate from the mitochondria is simply too low to supply cellular 1C needs. This is supported by the decrease in formate in $Mthfd1l^{z/z}$ embryos and a lower abundance of labeled methionine in $Mthfd1l^{z/z}$ MEFs. An alternate possibility is that there exists a mechanism of channeling formate made by MTHFD1L in the mitochondria into MTHFD1 in the cytoplasm. The total cellular formate concentration could remain relatively low, but formate would still be available for synthetic reactions in the cytoplasm. Mitochondrial formate produced either by ALDH1L2 or via glyoxylate would not be channeled to MTHFD1, and cellular formate would remain too dilute to supply cellular synthetic requirements.

The etiology of NTDs in $Mthfd1l^{z/z}$ embryos is likely influenced by numerous factors, making it difficult to identify any one factor that is causing the NTDs.

113

Nevertheless, we identified a variety of metabolic defects associated with loss of MTHFD1L that are likely contributing to the abnormal neural tube closure and growth delay seen in $Mthfd1l^{z/z}$ embryos. In a stable isotope tracer experiment with deuterated serine we identified disruptions to methionine synthesis which could have downstream effects on the methyl cycle. We also observed an apparent decrease in *de novo* purine synthesis in $Mthfd1l^{z/z}$ MEFs. Using growth curves we found that the growth of $Mthfd1l^{z/z}$ MEFs could be rescued with supplementation of nucleotide precursors. Proper function of both the methyl cycle and nucleotide synthesis are essential for development. Inhibiting SAM synthesis from methionine and inhibiting DNA methylation both cause NTDs in mice (Dunlevy et al., 2006; Matsuda, 1990). Inhibition of *de novo* purine synthesis with lometrexol induces NTDs in 30% of mouse embryos (Xu et al., 2016), and defects in purine synthesis have been found in a mouse model of NTDs (Hansler et al., 2014). Disruption of thymidylate synthesis by knocking out SHMT1 is also associated with NTDs (Beaudin et al., 2011). Finally, disruptions to both purine and thymidylate synthesis are associated with valproate-induced NTDs in mice (Akimova et al., 2016).

Using a non-targeted metabolomics screen and pathway analysis with MetaboAnalyst, we also identified disruptions to the metabolism of multiple amino acids as well as energy metabolism. Many of the affected amino acids were depleted in $Mthfd1l^{z/z}$ embryos, which could have negative effects on protein synthesis required for rapid cell growth and division during neural tube closure. The disruption of so many amino acids beyond the 1C metabolites glycine and serine is interesting and warrants further study. Metabolites involved in both glycolysis and the TCA cycle were also

affected. Though we did not detect any differences in mitochondrial respiration in $Mthfd1l^{z/z}$ MEFs, we did observe significantly decreased flux through glycolysis compared to $Mthfd1l^{+/+}$ MEFs. Disruptions to glycolysis have also been implicated in NTDs. Cultured embryos treated with 100 μM 2-DG develop NTDs with 100% penetrance (Hunter and Tugman, 1995).

Formate supplementation appeared to normalize many of the metabolites that were perturbed by loss of MTHFD1L. All of the TCA cycle intermediates that were disrupted in unsupplemented $Mthfd1l^{z/z}$ embryos appeared to be rescued by formate supplementation. In addition, calculation of the NAD^+:NADH ratio in supplemented embryos revealed that this ratio was no longer significantly different (not shown), suggesting that the defect in glycolysis had also been normalized. Prior to these results, we did not anticipate the effect the loss of MTHFD1L would have on glycolysis and the TCA cycle, and the role formate supplementation has in rescuing these pathways is still unclear. Within the last few years, folate-dependent 1C metabolism has emerged as an important source of energy production in certain types of cancer. Serine derived from the glycolytic intermediate 3-phosphoglycerate is broken down to generate ATP and NADPH (Tedeschi et al., 2013), though it is unclear if this process is relevant to embryogenesis. More work will be needed to elucidate the connection between 1C metabolism and energy metabolism in developing embryos.

Though we hypothesized formate would provide a source of 1C units for the synthesis of purines, thymidylate, and methionine, there were no clear indications from the steady state metabolite levels that this was the case. Growth curves with MEFs

derived from *Mthfd1l^{z/z}* embryos showed that formate supplementation rescued growth to a similar degree as hypoxanthine and thymidine, suggesting that formate and the nucleotide precursors may be affecting similar pathways, but this result is not conclusive. Experiments with cultured embryos have shown that formate supplementation decreases uptake of exogenous adenine and thymidine (Sudiwala et al., 2016), substantiating the idea that formate supports nucleotide synthesis. Future tracer experiments using ^{13}C formate will likely be needed to confirm specific metabolites that are being generated from the 1C units provided by formate.

The results reported here suggest some potential alternative supplements to prevent NTDs in *Mthfd1l^{z/z}* mice. A combination of hypoxanthine and thymidine was successful in rescuing the growth of *Mthfd1l^{z/z}* MEFs. This could be advantageous over formate supplementation, because a large amount of formate is necessary to rescue NTDs in *Mthfd1l^{z/z}* embryos (Figure 4.1), and formate can be toxic to embryos at high concentrations (Andrews et al., 1995). In the growth curve experiments however, a comparatively small amount of nucleotides was able to achieve the same result as a much larger amount of formate (30 μM nucleotides vs. 1 mM formate, Figure 4.4). If this result holds true for *Mthfd1l^{z/z}* embryos, nucleotide precursors may be able to prevent NTDs with a lower risk of adverse effects. Successful rescue of NTDs with nucleotides has been reported previously. Supplementation with a combination of thymidine and adenine has been shown to reduce spina bifida by 85% in *curly tail* mice (Leung et al., 2013). Supplementation with the TCA cycle intermediates succinate or fumarate, which were depleted in *Mthfd1l^{z/z}* embryos but rescued with formate supplementation, may also be

worth pursuing. More work will be needed to test these compounds and identify new supplements that are effective in preventing folic acid resistant NTDs.

Chapter 5: Summary and Future Directions

In the preceding chapters, studies centered on the mitochondrial folate-dependent enzymes MTHFD1L and MTHFD1L have been described. For decades the only known mitochondrial CH_2-THF dehydrogenase/CH^+-THF cyclohydrolase was MTHFD2 (Mejia and MacKenzie, 1985; Mejia et al., 1986). This protein could only be detected in immortalized mammalian cells, embryos, or nondifferentiated tissues, but not in adult differentiated tissues (Christensen and Mackenzie, 2008). MTHFD2L, which was first described by our laboratory (Bolusani et al., 2011), accounts for the CH_2-THF dehydrogenase/CH^+-THF cyclohydrolase activity that had previously been detected in adult liver mitochondria (Barlowe and Appling, 1988). Though it is still unknown why mammals possess two mitochondrial CH_2-THF dehydrogenases, we have identified differences in the expression of these isozymes and details of alternative splicing of MTHFD2L that may help shed some light on this question. We identified an apparent regulatory switch between E8.5 and E10.5 where expression of MTHFD2L increases and remains high throughout development. MTHFD2 expression was low at all time points examined, but higher expression has been reported at earlier embryonic days (Pike et al., 2010). In adults, MTHFD2L was widely expressed, with highest expression in brain and lung. Expression of MTHFD2 was low in most tissues, but modest expression was detected in the proliferative tissues testis and spleen. Future work identifying transcriptional regulators of MTHFD2L and MTHFD2 will help to better explain the temporal and spatial differences in their expression. The abundant splice variant of MTHFD2L lacking exon 8 was not found to be catalytically active, but future work could

118

identify a structural role for this splice variant similar to the structural role that has been reported for MTHFD2 in the nucleus (Gustafsson Sheppard et al., 2015).

In adult mice, we identified several behavioral anomalies associated with loss of MTHFD1L and folate deficiency, but more work will be needed to further investigate these findings. There were indications of a hyperactive phenotype in male mice associated with the mutant genotype. Female mice showed a diet-dependent aversion to the margin in open field and increased freezing during tone-shock training in a fear conditioning experiment, suggesting increased anxiety. This study was limited by inconsistent knockdown of MTHFD1L, particularly in the folate deficient mice. Several strategies may improve future studies. Tamoxifen treatment of mice by gavage rather than in the diet will give a more consistent Tamoxifen exposure. Using mice that are null for MTHFD1L in one allele and have the conditional cassette in the other allele may result in a more efficient knockdown. Aging the mice longer could give time for age-related deficits to become apparent. Finally, more stringent behavioral tests such as trace fear conditioning or the Morris water maze could reveal subtle defects that could not be detected in this study.

Finally we examined the metabolic consequences of deleting MTHFD1L in mouse embryos. We found that while deletion of MTHFD1L reduces mitochondrial production of formate from serine in isolated mitochondria, some formate synthesis capacity remains. This redundancy may be in part explained by an increase in the expression of ALDH1L2, which has been shown to have 10-CHO-THF hydrolase activity *in vitro* (Krupenko et al., 2010; Strickland et al., 2011). Work is currently underway to

generate mice that are nullizygous for both MTHFD1L and ALDH1L2. If ALDH1L2 alone is responsible for the redundant formate synthesis in *Mthfd1l*$^{z/z}$ embryos, mitochondria isolated from MTHFD1L/ALDH1L2 nullizygous embryos will completely unable to oxidize serine to formate.

Using several different methods we identified a range of metabolic defects in *Mthfd1l*$^{z/z}$ embryos that could contribute to the NTDs and growth restriction we have previously reported (Momb et al., 2013). We identified alterations in the TCA cycle, glycolysis, the metabolism of multiple amino acids, and the synthesis of methionine and purines. It is possible that supporting one or more of these affected pathways with supplementation of the appropriate nutrient may help to alleviate the defects observed in *Mthfd1l*$^{z/z}$ embryos. Future work testing the efficacy of different supplements could eventually lead to therapies in humans that are effective in preventing folate resistant NTDs.

Appendix I: List of Acronyms

10-CHO-THF	10-formyl-tetrahydrofolate
1C	one-carbon
2-DG	2-deoxyglucose
AD	Alzheimer's disease
AGT2	alanine:glyoxylate aminotransferase
ALDH	aldehyde dehydrogenase
AMT	aminomethyltransferase
CD	control diet
CH^+-THF	5,10-methenyl-tetrahydrofolate
CH_2-THF	5,10-methylene-tetrahydrofolate
CH_3-THF	5-methyl-tetrahydrofolate
CHO	Chinese hamster ovary
CS	conditioning stimulus
DHF	dihydrofolate
DHFR	dihydrofolate reductase
DMEM	Dulbecco's modified Eagle's medium
DMG	dimethylglycine
ECAR	extracellular acidification rate
eEF2	eukaryotic elongation factor 2
FBS	fetal bovine serum
FCCP	carbonyl cyanide-4 (trifluoromethoxy) phenylhydrazone
FD	folate-deficient diet
Folr	Folate receptor protein
FPGS	folylpolyglutamate synthetase
GCS	glycine cleavage system
GCSH	GCS H-protein
GCSL	GCS dihydrolipoyl dehydrogenase
GLDC	glycine decarboxylase
GRHL3	grainyhead-like 3
Hcy	homocysteine
HRP	horseradish peroxidase
IMP	inosine monophosphate
LOAD	late onset Alzheimer's disease
MEF	mouse embryonic fibroblast

MEM	modified Eagle's medium
MFT	mitochondrial folate transporter
MHP	median hinge point
MTFMT	methionyl-tRNA formyltransferase
MTHFD1	methylene-tetrahydrofolate 1
MTHFD1L	methylene-tetrahydrofolate 1-like
MTHFD2	methylene-tetrahydrofolate 2
MTHFD2L	methylene-tetrahydrofolate 2-like
MTHFR	methylenetetrahydrofolate reductase
NAD^+	nicotinamide adenine dinucleotide
$NADP^+$	nicotinamide adenine dinucleotide phosphate
NCC	neural crest cell
NTD	neural tube defect
OCR	oxygen consumption rate
PABA	para-aminobenzoic acid
PAGE	polyacrylamide gel electrophoresis
PCA	principal component analysis
PCFT	proton coupled folate transporter
PCR	polymerase chain reaction
RFC	reduced folate carrier
RT-PCR	real-time polymerase chain reaction
SAH	S-adenosylhomocysteine
SAM	S-adenosylmethionine
SD	standard deviation
SDS	sodium dodecyl sulfate
SEM	standard error of the mean
SHMT	serine hydroxymethyltransferase
TBP	TATA-box-binding protein
TCA	tricarboxylic acid cycle
THF	tetrahydrofolate
US	unconditioned stimulus
WT	wild-type

Appendix II: Metabolites in unsupplemented embryos

Metabolite	$Mthfd1l^{z/z}/$ $Mthfd1l^{+/+}$	q value	$Mthfd1l^{+/+}$ % var	$Mthfd1l^{z/z}$ % var
(3-Aminopropoxy)guanidine	1.07	0.57	15.2%	11.6%
1-Methyl-3-(2-thiazolyl)-1H-indole	0.71	0.08	19.9%	16.0%
2-Amino-3-phosphonopropionic acid	1.20	0.09	10.4%	11.1%
2-Hydroxy-4-(methylthio)butanoic acid	1.31	0.09	21.8%	11.3%
2-Hydroxyadipic acid/3-Hydroxyadipic acid	1.01	0.94	12.5%	8.0%
5-Hydroxyindoleacetic acid	0.79	0.16	23.4%	11.8%
5-Hydroxymethyl-2-furanoate	1.29	0.02	10.9%	8.3%
Acetate	0.90	0.03	3.8%	5.6%
ADP	1.26	0.01	8.0%	6.1%
Alanine	1.02	0.49	2.6%	3.7%
Allantoin	1.01	0.94	20.1%	15.4%
Aminoadipic acid	1.09	0.46	12.9%	15.5%
AMP	0.76	0.02	10.7%	9.2%
Arginine	0.86	0.01	4.0%	2.9%
Ascorbic acid	1.26	0.04	13.5%	8.1%
Asparagine	1.00	0.93	5.6%	3.7%
Aspartate	1.28	0.04	11.9%	11.7%
ATP	1.33	0.02	12.3%	7.4%
b-Alanine	1.02	0.88	16.2%	11.9%
Carnitine	1.07	0.61	16.6%	11.9%
Choline	0.88	0.12	8.6%	10.3%
cis-Aconitic acid/trans-Aconitic acid	1.12	0.35	16.1%	12.7%
Citrate	1.28	0.03	10.2%	10.0%
Citrulline	1.24	0.17	21.8%	14.2%
Creatine	1.09	0.02	3.2%	2.7%
Cytidine	0.84	0.23	18.5%	13.4%
D-Glucose	1.24	0.08	7.9%	14.7%
Diethyl fumarate	1.04	0.65	9.0%	11.9%
Dihydrothymine	0.81	0.25	25.6%	10.3%
Erythronic acid	1.14	0.40	8.9%	23.2%
Formate	0.93	0.03	3.2%	3.1%
Fucose 1-phosphate	1.27	0.02	7.3%	8.6%
Fumarate	0.84	0.01	3.7%	4.3%
Gamma-Glutamyl Glutamine	0.85	0.32	22.1%	12.8%

Gamma-glutamyl-L-putrescine/Alanyl-Lysine/Lysyl-Alanine/beta-Alanyl-L-lysine	1.08	0.58	11.0%	18.2%
gamma-L-Glutamyl-L-methionine sulfoxide	1.15	0.29	15.8%	15.7%
Glutamate	1.07	0.11	4.6%	5.0%
Glutamine	0.80	0.12	19.2%	6.5%
Glutarylglycine/N-Acetylglutamic acid	1.29	0.10	20.8%	13.4%
Glutathione	1.05	0.02	1.5%	1.8%
Glycerophosphocholine	1.11	0.12	7.7%	6.9%
Glycine	0.85	0.01	5.4%	2.9%
Glycyl-Phenylalanine/Phenylalanyl-Glycine	1.01	0.95	20.8%	7.4%
Glycylproline	1.01	0.64	4.3%	2.4%
Guanine	0.91	0.32	12.4%	9.0%
Histidine	0.90	0.12	5.3%	9.2%
Homocysteinesulfinic acid	1.10	0.31	14.4%	7.5%
Homo-L-arginine	1.02	0.90	10.6%	20.4%
Hydroxyglutaric acid	1.17	0.45	15.6%	28.6%
Hypotaurine	1.17	0.13	15.6%	6.7%
Inosine	1.08	0.61	20.0%	14.2%
Isocitric acid	1.13	0.27	13.1%	13.3%
Isoleucine	0.81	0.02	8.1%	7.0%
Kynurenine	0.92	0.62	21.3%	17.9%
Lactate	0.82	0.01	3.8%	7.9%
Leucine	0.87	0.02	4.9%	4.3%
L-Homocysteic acid	1.23	0.19	23.1%	14.3%
L-Threonine	1.47	0.08	18.5%	23.4%
Lysine	0.95	0.15	2.3%	5.0%
Maleic acid	1.11	0.34	13.6%	11.3%
Malic acid	1.11	0.25	11.4%	9.3%
Methionine	1.06	0.45	10.6%	6.4%
Mono-trans-p-coumaroylmesotartaric acid	1.03	0.88	22.7%	14.3%
Myo-Inositol	1.08	0.08	3.2%	5.7%
N-Acetylaspartylglutamic acid	1.25	0.11	15.6%	14.7%
N-Acetyl-L-aspartic acid	1.22	0.11	14.8%	12.4%
N-Acetyl-L-aspartic acid/N-Formyl-L-glutamic acid/D-N-(Carboxyacetyl)alanine/2-Amino-3-	1.24	0.09	17.2%	10.0%

oxoadipate

N-Acetyl-L-methionine	1.07	0.62	14.1%	15.3%
NAD	1.83	0.13	62.8%	34.1%
Niacinamide	0.90	0.30	8.5%	16.2%
Ornithine	0.91	0.11	6.4%	5.8%
Pantothenate	0.80	0.07	7.2%	16.4%
Phenylalanine	0.91	0.08	6.3%	4.6%
Phosphocholine	1.11	0.03	6.0%	3.2%
Phosphodimethylethanolamine	1.03	0.72	7.1%	12.0%
Phosphoethanolamine	1.15	0.04	8.1%	5.3%
Phosphoric acid	0.95	0.13	3.6%	3.5%
Proline	0.99	0.74	5.1%	1.7%
Pyroglutamic acid	0.99	0.85	5.8%	5.4%
Pyruvate	1.07	0.15	7.0%	3.4%
Ribitol	1.26	0.08	15.1%	12.5%
Sarcosine	1.04	0.78	10.6%	16.7%
S-Carboxymethyl-L-cysteine	1.10	0.44	13.3%	15.3%
Serine	1.16	0.01	4.3%	4.8%
Spermine	1.20	0.27	26.9%	10.1%
Succinic acid	0.76	0.08	18.2%	7.9%
Taurine	1.07	0.01	1.7%	1.1%
Theanine	1.02	0.92	6.3%	26.9%
Threonic acid	1.24	0.13	19.1%	13.0%
Tryptophan	1.03	0.71	7.6%	10.8%
Tyrosine	0.92	0.10	6.4%	3.3%
UDP-Acetylgalactosamine	1.01	0.94	16.9%	16.6%
UDP-Acetylglucosamine	1.09	0.06	3.8%	4.6%
UMP	0.85	0.09	11.5%	7.6%
Uracil	0.82	0.03	7.3%	9.8%
Urea	0.84	0.08	9.5%	10.4%
Uridine	0.71	0.08	22.1%	12.0%
Valine	0.88	0.03	5.9%	4.0%

Appendix III: Metabolites in supplemented embryos

Metabolite	$Mthfd1l^{z/z}/$ $Mthfd1l^{+/+}$	q value	$Mthfd1l^{+/+}$ % var	$Mthfd1l^{z/z}$ % var
(3-Aminopropoxy)guanidine	0.89	0.24	9.3%	13.6%
1-Pyrroline-5-carboxylic acid	0.91	0.55	18.5%	16.0%
2-Hydroxy-4-(methylthio)butanoic acid	1.86	0.21	50.9%	41.3%
2-Hydroxyadipic acid	0.90	0.34	6.8%	18.6%
2-Hydroxyglutaric acid	0.88	0.28	9.2%	17.3%
2-Keto-glutaramic acid	0.87	0.19	5.7%	13.2%
2-Oxoglutaric acid/3-Oxoglutaric acid	1.33	0.10	10.0%	16.9%
3-Methyladipic acid/Ethyl methyl_succinate	1.19	0.03	6.8%	4.8%
4-Hydroxy-2-oxoglutarate	0.92	0.61	19.9%	15.8%
4-Hydroxycitrulline	1.09	0.41	10.8%	13.1%
4-Hydroxyproline	1.74	0.19	42.3%	39.0%
4-Phosphopantothenoylcysteine	1.52	0.18	27.3%	34.3%
5-Aminoimidazole	1.03	0.87	25.2%	13.8%
Acetate	1.24	0.10	15.3%	6.3%
Acetylcarnitine	1.45	0.18	22.6%	32.6%
ADP	1.17	0.43	34.6%	7.3%
Alanine	1.06	0.18	5.0%	4.3%
Alanyl-Aspartate/Aspartyl-Alanine	1.14	0.19	8.8%	10.6%
Allantoin	1.01	0.90	12.1%	10.9%
Aminoadipic acid/Acetylhomoserine	0.89	0.26	8.2%	15.2%
AMP	0.57	0.04	22.0%	12.2%
Arginine	0.83	0.17	14.9%	6.6%
Ascorbic acid	0.84	0.19	13.3%	11.2%
Asparagine	1.32	0.01	9.0%	5.4%
Aspartate	0.85	0.18	17.1%	3.5%
Aspartyl-Cysteine/Cysteinyl-Aspartate	1.88	0.21	52.0%	41.6%
ATP	1.47	0.13	34.6%	12.9%
b-Alanine	1.19	0.14	8.8%	12.0%
Choline	0.94	0.39	9.0%	9.3%
Citrate	0.88	0.18	14.3%	3.2%
Citrulline	0.87	0.26	12.0%	16.0%
Creatine	0.89	0.18	9.9%	3.9%
Cytidine	1.46	0.07	27.0%	6.9%
Diethyl fumarate	1.89	0.01	18.7%	11.7%

126

Dimethyl succinate	1.25	0.11	11.7%	12.5%
Formate	1.10	0.19	6.0%	6.8%
Fucose 1-phosphate	1.79	0.20	46.2%	40.1%
Fumarate	1.04	0.78	17.9%	13.7%
Galactonic acid/Gulonic acid	1.09	0.24	7.5%	9.8%
gamma-L-Glutamyl-L-methionine sulfoxide	1.14	0.07	6.9%	5.0%
Glucose	0.96	0.75	8.2%	14.9%
Glutamate	1.01	0.87	6.6%	2.2%
Glutamine	1.02	0.80	9.7%	4.0%
Glutamylalanine	0.84	0.09	8.1%	8.9%
Glutarylglycine/N-Acetylglutamic acid	0.86	0.20	10.2%	15.8%
Glutathione	0.91	0.19	7.1%	7.3%
Glycerol 3-phosphate	0.91	0.47	20.0%	6.0%
Glycerophosphocholine	0.72	0.04	14.9%	4.4%
Glycerylphosphorylethanolamine	1.30	0.22	13.2%	28.7%
Glycine	0.59	0.00	11.1%	5.2%
Glycyl-Phenylalanine/Phenylalanyl-Glycine	1.05	0.70	16.1%	12.6%
Glycylproline	0.85	0.15	12.7%	6.5%
Histidine	1.35	0.05	17.7%	3.5%
Homocysteic acid	1.03	0.67	10.5%	5.9%
Homocysteinesulfinic acid	0.94	0.27	6.8%	5.3%
Homo-L-arginine	0.97	0.80	18.0%	16.2%
Hydantoin-5-propionic acid	1.14	0.19	11.1%	9.8%
Hydroxyglutaric acid	1.57	0.18	30.8%	35.5%
Hydroxyprolyl-Valine/Valyl-Hydroxyproline	1.66	0.19	37.3%	37.6%
Hypotaurine	0.95	0.56	9.8%	9.1%
Iminoaspartic acid/2-Oxosuccinamate	1.29	0.23	12.1%	28.2%
Isocitric acid	0.99	0.91	18.2%	17.4%
Isoleucine	0.94	0.66	18.7%	6.0%
Itaconic acid	0.86	0.20	13.1%	12.6%
Kynurenine	1.70	0.19	39.5%	38.2%
Lactate	1.03	0.73	13.1%	3.3%
L-beta-aspartyl-L-glycine/Carglumic acid/Aspartyl-Glycine/Glycyl-Aspartate	1.62	0.19	34.1%	36.6%
L-Carnitine	0.96	0.77	16.3%	15.8%
Leucine	0.98	0.82	13.5%	4.0%

Lysine	1.10	0.10	5.4%	4.5%
Maleic acid	0.81	0.20	16.3%	14.6%
Malic acid	0.91	0.44	15.3%	11.4%
Malonic acid/Hydroxypyruvic acid	1.05	0.52	10.7%	6.9%
Methionine	1.12	0.19	9.2%	6.0%
Methylmalonic acid	0.83	0.21	18.9%	13.0%
Monoethyl malonic acid	1.04	0.72	11.6%	11.7%
Myo-Inositol	0.82	0.29	26.2%	14.1%
N-Acetylaspartylglutamic acid	1.59	0.19	32.5%	36.1%
N-Acetyl-L-aspartic acid	0.85	0.24	17.4%	12.7%
N-Acetyl-L-methionine	0.87	0.24	17.4%	7.0%
NAD	0.76	0.37	39.9%	27.6%
Niacinamide	0.62	0.07	18.0%	25.7%
Nicotinamide N-oxide	1.05	0.75	23.3%	11.0%
Ornithine	0.87	0.49	30.8%	6.3%
Orotic acid	1.78	0.20	44.9%	39.8%
Pantothenate	1.11	0.09	7.7%	1.3%
Pantothenol	1.58	0.18	31.7%	35.8%
Phenylalanine	1.14	0.05	8.0%	0.9%
Phosphocholine	0.89	0.08	6.5%	3.0%
Phosphodimethylethanolamine	0.96	0.67	11.8%	4.5%
Phosphoethanolamine	0.89	0.12	8.6%	1.8%
Phosphoric acid	0.86	0.38	26.0%	6.1%
Proline	1.02	0.82	14.5%	2.1%
Propionic acid	0.97	0.86	17.8%	23.4%
Pyridine N-oxide glucuronide	1.37	0.20	17.5%	30.6%
Pyroglutamic acid	1.24	0.13	1.9%	16.6%
Pyruvaldehyde	0.80	0.17	14.7%	14.9%
Pyruvate	1.05	0.13	3.0%	2.7%
Sarcosine	1.07	0.64	21.7%	2.6%
S-Carboxymethyl-L-cysteine	1.19	0.37	32.0%	11.5%
Serine	3.06	0.00	16.0%	3.7%
Serinyl-Valine/Valyl-Serine	1.54	0.18	29.1%	34.9%
Spermine	1.81	0.21	47.4%	40.4%
Succinate	0.90	0.35	15.7%	6.8%
Succinylacetone	1.11	0.28	5.0%	14.4%
Taurine	0.84	0.01	5.6%	3.1%
Theanine	1.21	0.09	14.2%	4.9%
Threonic acid	0.96	0.73	10.3%	12.1%
Tryptophan	1.05	0.75	21.7%	15.7%

Tyrosine	1.24	0.06	14.3%	0.9%
UDP-Acetylgalactosamine	0.92	0.75	22.6%	32.2%
UDP-Acetylglucosamine	0.97	0.74	13.7%	9.0%
UMP	0.83	0.22	13.6%	13.9%
Uracil	1.56	0.18	30.0%	35.2%
Urea	1.14	0.26	19.0%	5.9%
Uridine	0.84	0.12	8.9%	10.6%
Valine	1.03	0.75	15.0%	6.1%

References

Akimova, D., Wlodarczyk, B.J., Lin, Y., Ross, M.E., Finnell, R.H., Chen, Q., and Gross, S.S. (2016). Metabolite profiling of whole murine embryos reveals metabolic perturbations associated with maternal valproate-induced neural tube closure defects. Birth Defects Res. Part A Clin. Mol. Teratol.

Alexiou, M., and Leese, H.J. (1992). Purine utilisation, de novo synthesis and degradation in mouse preimplantation embryos. Development *114*, 185–192.

Alluri, R.V., Mohan, V., Komandur, S., Chawda, K., Chaudhuri, J.R., and Hasan, Q. (2005). MTHFR C677T gene mutation as a risk factor for arterial stroke: a hospital based study. Eur. J. Neurol. *12*, 40–44.

Anderson, D.D., and Stover, P.J. (2009). SHMT1 and SHMT2 are functionally redundant in nuclear de novo thymidylate biosynthesis. PLoS ONE *4*, e5839.

Anderson, D.D., Woeller, C.F., and Stover, P.J. (2007). Small ubiquitin-like modifier-1 (SUMO-1) modification of thymidylate synthase and dihydrofolate reductase. Clin. Chem. Lab. Med. *45*, 1760–1763.

Andrews, J.E., Ebron-McCoy, M., Kavlock, R.J., and Rogers, J.M. (1995). Developmental toxicity of formate and formic acid in whole embryo culture: a comparative study with mouse and rat embryos. Teratology *51*, 243–251.

Appling, D.R., and West, M.G. (1997). Monofunctional NAD-dependent 5,10-methylenetetrahydrofolate dehydrogenase from Saccharomyces cerevisiae. Meth. Enzymol. *281*, 178–188.

Araújo, J.R., Martel, F., Borges, N., Araújo, J.M., and Keating, E. (2015). Folates and aging: Role in mild cognitive impairment, dementia and depression. Ageing Research Reviews *22*, 9–19.

Bao, X.R., Ong, S.-E., Goldberger, O., Peng, J., Sharma, R., Thompson, D.A., Vafai, S.B., Cox, A.G., Marutani, E., Ichinose, F., et al. (2016). Mitochondrial dysfunction remodels one-carbon metabolism in human cells. eLife *5*, e10575.

Barlowe, C.K., and Appling, D.R. (1988). In vitro evidence for the involvement of mitochondrial folate metabolism in the supply of cytoplasmic one-carbon units. Biofactors *1*, 171–176.

Beaudin, A.E., Abarinov, E.V., Noden, D.M., Perry, C.A., Chu, S., Stabler, S.P., Allen, R.H., and Stover, P.J. (2011). Shmt1 and de novo thymidylate biosynthesis underlie folate-responsive neural tube defects in mice. Am J Clin Nutr *93*, 789–798.

Beaudin, A.E., Abarinov, E.V., Malysheva, O., Perry, C.A., Caudill, M., and Stover, P.J. (2012). Dietary folate, but not choline, modifies neural tube defect risk in Shmt1 knockout mice. Am. J. Clin. Nutr. *95*, 109–114.

Benjamini, Y., and Hochberg, Y. (1995). Controlling the False Discovery Rate: A Practical and Powerful Approach to Multiple Testing. Journal of the Royal Statistical Society. Series B (Methodological) *57*, 289–300.

Bertrand, R., Beauchemin, M., Dayan, A., Ouimet, M., and Jolivet, J. (1995). Identification and characterization of human mitochondrial methenyltetrahydrofolate synthetase activity. Biochim. Biophys. Acta *1266*, 245–249.

Bjelland I, T.G. (2003). Folate, vitamin b12, homocysteine, and the mthfr 677c→t polymorphism in anxiety and depression: The hordaland homocysteine study. Arch Gen Psychiatry *60*, 618–626.

Blakley, R.L. (1957). The interconversion of serine and glycine; preparation and properties of catalytic derivatives of pteroylglutamic acid. Biochem. J. *65*, 331–342.

Bolusani, S., Young, B.A., Cole, N.A., Tibbetts, A.S., Momb, J., Bryant, J.D., Solmonson, A., and Appling, D.R. (2011). Mammalian MTHFD2L encodes a mitochondrial methylenetetrahydrofolate dehydrogenase isozyme expressed in adult tissues. J. Biol. Chem. *286*, 5166–5174.

Boulet, S.L., Yang, Q., Mai, C., Kirby, R.S., Collins, J.S., Robbins, J.M., Meyer, R., Canfield, M.A., Mulinare, J., and National Birth Defects Prevention Network (2008). Trends in the postfortification prevalence of spina bifida and anencephaly in the United States. Birth Defects Res. Part A Clin. Mol. Teratol. *82*, 527–532.

Bryan, K.J., Lee, H., Perry, G., Smith, M.A., and Casadesus, G. (2009). Transgenic Mouse Models of Alzheimer's Disease: Behavioral Testing and Considerations. In Methods of Behavior Analysis in Neuroscience, J.J. Buccafusco, ed. (Boca Raton (FL): CRC Press/Taylor & Francis), p.

Cantoni, G.L. (1951). Activation of methionine for transmethylation. J. Biol. Chem. *189*, 745–754.

Carl, G.F., Hudson, F.Z., and McGuire, B.S. (1995). Rat liver subcellular folate distribution shows association of formyltetrahydropteroylpentaglutamates with mitochondria and methyltetrahydropteroylhexaglutamates with cytoplasm. J. Nutr. *125*, 2096–2103.

Centers for Disease Control (1992). Recommendations for the use of folic acid to reduce the number of cases of spina bifida and other neural tube defects. MMWR Morb Mortal Wkly Rep *41*, 1–7.

Centers for Disease Control (1999). Knowledge and use of folic acid by women of
childbearing age. MMWR Morb Mortal Wkly Rep *48*, 325–327.

Chattopadhyay, S., Moran, R.G., and Goldman, I.D. (2007). Pemetrexed: biochemical
and cellular pharmacology, mechanisms, and clinical applications. Mol. Cancer
Ther. *6*, 404–417.

Chen, Z., Karaplis, A.C., Ackerman, S.L., Pogribny, I.P., Melnyk, S., Lussier-Cacan, S.,
Chen, M.F., Pai, A., John, S.W.M., Smith, R.S., et al. (2001). Mice deficient in
methylenetetrahydrofolate reductase exhibit hyperhomocysteinemia and
decreased methylation capacity, with neuropathology and aortic lipid deposition.
Hum Mol Genet *10*, 433–444.

Chiang, P.K., Gordon, R.K., Tal, J., Zeng, G.C., Doctor, B.P., Pardhasaradhi, K., and
McCann, P.P. (1996). S-Adenosylmethionine and methylation. FASEB J. *10*,
471–480.

Chow, N., Aarsland, D., Honarpisheh, H., Beyer, M.K., Somme, J.H., Elashoff, D.,
Rongve, A., Tysnes, O.B., Thompson, P.M., and Apostolova, L.G. (2012).
Comparing hippocampal atrophy in Alzheimer's dementia and dementia with
lewy bodies. Dement Geriatr Cogn Disord *34*, 44–50.

Christensen, K.E., and MacKenzie, R.E. (2006). Mitochondrial one-carbon metabolism is
adapted to the specific needs of yeast, plants and mammals. Bioessays *28*, 595–
605.

Christensen, K.E., and Mackenzie, R.E. (2008). Mitochondrial methylenetetrahydrofolate
dehydrogenase, methenyltetrahydrofolate cyclohydrolase, and
formyltetrahydrofolate synthetases. Vitam. Horm. *79*, 393–410.

Clark, R.E., and Squire, L.R. (1998). Classical Conditioning and Brain Systems: The
Role of Awareness. Science *280*, 77–81.

Cook, R.J., and Wagner, C. (1982). Purification and partial characterization of rat liver folate binding protein: cytosol I. Biochemistry *21*, 4427–4434.

Copp, A.J., Greene, N.D.E., and Murdoch, J.N. (2003). The genetic basis of mammalian neurulation. Nature Reviews Genetics *4*, 784–793.

Curthoys, N.P., and Rabinowitz, J.C. (1971). Formyltetrahydrofolate Synthetase BINDING OF ADENOSINE TRIPHOSPHATE AND RELATED LIGANDS DETERMINED BY PARTITION EQUILIBRIUM. J. Biol. Chem. *246*, 6942–6952.

Czeizel, A.E., and Dudás, I. (1992). Prevention of the first occurrence of neural-tube defects by periconceptional vitamin supplementation. N. Engl. J. Med. *327*, 1832–1835.

Davis, S.R., Stacpoole, P.W., Williamson, J., Kick, L.S., Quinlivan, E.P., Coats, B.S., Shane, B., Bailey, L.B., and Gregory, J.F. (2004). Tracer-derived total and folate-dependent homocysteine remethylation and synthesis rates in humans indicate that serine is the main one-carbon donor. American Journal of Physiology - Endocrinology and Metabolism *286*, E272–E279.

Denenberg, V.H. (1969). Open-Field Behavior in the Rat: What Does It Mean?*. Annals of the New York Academy of Sciences *159*, 852–859.

Detrait, E.R., George, T.M., Etchevers, H.C., Gilbert, J.R., Vekemans, M., and Speer, M.C. (2005). Human neural tube defects: developmental biology, epidemiology, and genetics. Neurotoxicol Teratol *27*, 515–524.

Di Pietro, E., Sirois, J., Tremblay, M.L., and MacKenzie, R.E. (2002). Mitochondrial NAD-Dependent Methylenetetrahydrofolate Dehydrogenase-Methenyltetrahydrofolate Cyclohydrolase Is Essential for Embryonic Development. Mol Cell Biol *22*, 4158–4166.

Di Pietro, E., Wang, X.-L., and MacKenzie, R.E. (2004). The expression of mitochondrial methylenetetrahydrofolate dehydrogenase-cyclohydrolase supports a role in rapid cell growth. Biochim. Biophys. Acta *1674*, 78–84.

Dorokhov, Y.L., Shindyapina, A.V., Sheshukova, E.V., and Komarova, T.V. (2015). Metabolic Methanol: Molecular Pathways and Physiological Roles. Physiological Reviews *95*, 603–644.

Ducker, G.S., Chen, L., Morscher, R.J., Ghergurovich, J.M., Esposito, M., Teng, X., Kang, Y., and Rabinowitz, J.D. (2016). Reversal of Cytosolic One-Carbon Flux Compensates for Loss of the Mitochondrial Folate Pathway. Cell Metabolism *23*, 1140–1153.

Dunlevy, L.P.E., Burren, K.A., Mills, K., Chitty, L.S., Copp, A.J., and Greene, N.D.E. (2006). Integrity of the methylation cycle is essential for mammalian neural tube closure. Birth Defects Res. Part A Clin. Mol. Teratol. *76*, 544–552.

E Michalska, A. (2007). Isolation and propagation of mouse embryonic fibroblasts and preparation of mouse embryonic feeder layer cells. Curr Protoc Stem Cell Biol *Chapter 1*, Unit1C.3.

Elwood, P.C. (1989). Molecular cloning and characterization of the human folate-binding protein cDNA from placenta and malignant tissue culture (KB) cells. J. Biol. Chem. *264*, 14893–14901.

Eszlari, N., Kovacs, D., Petschner, P., Pap, D., Gonda, X., Elliott, R., Anderson, I.M., Deakin, J.F.W., Bagdy, G., and Juhasz, G. (2016). Distinct effects of folate pathway genes MTHFR and MTHFD1L on ruminative response style: a potential risk mechanism for depression. Transl Psychiatry *6*, e745.

Feil, R., Wagner, J., Metzger, D., and Chambon, P. (1997). Regulation of Cre recombinase activity by mutated estrogen receptor ligand-binding domains. Biochem. Biophys. Res. Commun. *237*, 752–757.

Field, M.S., Kamynina, E., Agunloye, O.C., Liebenthal, R.P., Lamarre, S.G., Brosnan, M.E., Brosnan, J.T., and Stover, P.J. (2014). Nuclear enrichment of folate cofactors and methylenetetrahydrofolate dehydrogenase 1 (MTHFD1) protect de novo thymidylate biosynthesis during folate deficiency. J. Biol. Chem. *289*, 29642–29650.

Finer, L.B., and Henshaw, S.K. (2006). Disparities in rates of unintended pregnancy in the United States, 1994 and 2001. Perspect Sex Reprod Health *38*, 90–96.

Food and Drug Administration (1996). Food standards: Amendment of standards of identity for enriched grain products to require addition of folic acid. Federal Register *61*, 8781–8797.

Frosst, P., Blom, H.J., Milos, R., Goyette, P., Sheppard, C.A., Matthews, R.G., Boers, G.J.H., den Heijer, M., Kluijtmans, L. a. J., van den Heuve, L.P., et al. (1995). A candidate genetic risk factor for vascular disease: a common mutation in methylenetetrahydrofolate reductase. Nat Genet *10*, 111–113.

Fujioka, M. (1969). Purification and properties of serine hydroxymethylase from soluble and mitochondrial fractions of rabbit liver. Biochim. Biophys. Acta *185*, 338–349.

García-Martínez, L.F., and Appling, D.R. (1993). Characterization of the folate-dependent mitochondrial oxidation of carbon 3 of serine. Biochemistry *32*, 4671–4676.

Gietz, R.D., and Woods, R.A. (2002). Transformation of yeast by lithium acetate/single-stranded carrier DNA/polyethylene glycol method. Meth. Enzymol. *350*, 87–96.

Goldman, I.D. (1971). The characteristics of the membrane transport of amethopterin and the naturally occurring folates. Ann. N. Y. Acad. Sci. *186*, 400–422.

Grillo, M.A., and Colombatto, S. (2008). S-adenosylmethionine and its products. Amino Acids *34*, 187–193.

Gustafsson Sheppard, N., Jarl, L., Mahadessian, D., Strittmatter, L., Schmidt, A., Madhusudan, N., Tegnér, J., Lundberg, E.K., Asplund, A., Jain, M., et al. (2015). The folate-coupled enzyme MTHFD2 is a nuclear protein and promotes cell proliferation. Sci Rep *5*, 15029.

Gustavsson, P., Greene, N.D.E., Lad, D., Pauws, E., Castro, D., C.p, S., Stanier, P., and Copp, A.J. (2007). Increased expression of Grainyhead-like-3 rescues spina bifida in a folate-resistant mouse model. Hum Mol Genet *16*, 2640–2646.

Hamosh, A., and Johnston, M.V. (2001). Nonketotic Hyperglycinemia | The Online Metabolic and Molecular Bases of Inherited Disease (McGraw-Hill).

Han, C.J., O'Tuathaigh, C.M., Trigt, L. van, Quinn, J.J., Fanselow, M.S., Mongeau, R., Koch, C., and Anderson, D.J. (2003). Trace but not delay fear conditioning requires attention and the anterior cingulate cortex. PNAS *100*, 13087–13092.

Hansler, A., Chen, Q., Gray, J.D., Ross, M.E., Finnell, R.H., and Gross, S.S. (2014). Untargeted metabolite profiling of murine embryos to reveal metabolic perturbations associated with neural tube closure defects. Birth Defects Res. Part A Clin. Mol. Teratol.

Hardy, L.W., Finer-Moore, J.S., Montfort, W.R., Jones, M.O., Santi, D.V., and Stroud, R.M. (1987). Atomic structure of thymidylate synthase: target for rational drug design. Science *235*, 448–455.

Harris, M.J., and Juriloff, D.M. (2010). An update to the list of mouse mutants with neural tube closure defects and advances toward a complete genetic perspective of neural tube closure. Birth Defects Research Part A: Clinical and Molecular Teratology *88*, 653–669.

Henderson, G.B., and Zevely, E.M. (1983). Structural requirements for anion substrates of the methotrexate transport system in L1210 cells. Arch. Biochem. Biophys. *221*, 438–446.

Herbig, K., Chiang, E.-P., Lee, L.-R., Hills, J., Shane, B., and Stover, P.J. (2002). Cytoplasmic serine hydroxymethyltransferase mediates competition between folate-dependent deoxyribonucleotide and S-adenosylmethionine biosyntheses. J. Biol. Chem. *277*, 38381–38389.

Hibbard, B.M. (1964). THE ROLE OF FOLIC ACID IN PREGNANCY; WITH PARTICULAR REFERENCE TO ANAEMIA, ABRUPTION AND ABORTION. J Obstet Gynaecol Br Commonw *71*, 529–542.

Hibbard, B.M. (1967). Defective folate metabolism in pathological conditions of pregnancy. Acta Obstet Gynecol Scand *46*, Suppl 7:47-59.

Ho, S.N., Hunt, H.D., Horton, R.M., Pullen, J.K., and Pease, L.R. (1989). Site-directed mutagenesis by overlap extension using the polymerase chain reaction. Gene *77*, 51–59.

Hogg, S. (1996). A review of the validity and variability of the Elevated Plus-Maze as an animal model of anxiety. Pharmacology Biochemistry and Behavior *54*, 21–30.

Honein, M.A., Paulozzi, L.J., Mathews, T.J., Erickson, J.D., and Wong, L.-Y.C. (2001). Impact of Folic Acid Fortification of the US Food Supply on the Occurrence of Neural Tube Defects. JAMA *285*, 2981–2986.

Horne, D.W., Patterson, D., and Cook, R.J. (1989). Effect of nitrous oxide inactivation of vitamin B12-dependent methionine synthetase on the subcellular distribution of folate coenzymes in rat liver. Arch. Biochem. Biophys. *270*, 729–733.

Horne, D.W., Holloway, R.S., and Said, H.M. (1992). Uptake of 5-formyltetrahydrofolate in isolated rat liver mitochondria is carrier-mediated. J. Nutr. *122*, 2204–2209.

Huang, T., and Schirch, V. (1995). Mechanism for the coupling of ATP hydrolysis to the conversion of 5-formyltetrahydrofolate to 5,10-methenyltetrahydrofolate. J. Biol. Chem. *270*, 22296–22300.

Huang, X., and Saint-Jeannet, J.-P. (2004). Induction of the neural crest and the opportunities of life on the edge. Dev. Biol. *275*, 1–11.

Huang, W., Prasad, P.D., Kekuda, R., Leibach, F.H., and Ganapathy, V. (1997). Characterization of N5-methyltetrahydrofolate uptake in cultured human retinal pigment epithelial cells. Invest. Ophthalmol. Vis. Sci. *38*, 1578–1587.

Hunter, E.S., and Tugman, J.A. (1995). Inhibitors of glycolytic metabolism affect neurulation-staged mouse conceptuses in vitro. Teratology *52*, 317–323.

Jadavji, N.M., Deng, L., Leclerc, D., Malysheva, O., Bedell, B.J., Caudill, M.A., and Rozen, R. (2012). Severe methylenetetrahydrofolate reductase deficiency in mice results in behavioral anomalies with morphological and biochemical changes in hippocampus. Mol. Genet. Metab. *106*, 149–159.

Jadavji, N.M., Farr, T.D., Lips, J., Khalil, A.A., Boehm-Sturm, P., Foddis, M., Harms, C., Füchtemeier, M., and Dirnagl, U. (2015). Elevated levels of plasma homocysteine, deficiencies in dietary folic acid and uracil-DNA glycosylase impair learning in a mouse model of vascular cognitive impairment. Behav. Brain Res. *283*, 215–226.

James, G.O., Hardiman, M.J., and Yeo, C.H. (1987). Hippocampal lesions and trace conditioning in the rabbit. Behavioural Brain Research *23*, 109–116.

Kallen, R.G., and Jencks, W.P. (1966). The Mechanism of the Condensation of Formaldehyde with Tetrahydrofolic Acid. J. Biol. Chem. *241*, 5851–5863.

Kawai, J., Shinagawa, A., Shibata, K., Yoshino, M., Itoh, M., Ishii, Y., Arakawa, T., Hara, A., Fukunishi, Y., Konno, H., et al. (2001). Functional annotation of a full-length mouse cDNA collection. Nature *409*, 685–690.

Kawasaki, H., Okuyama, M., and Kikuchi, G. (1966). α-Ketoglutarate-dependent Oxidation of Glyoxylic Acid in Rat-liver Mitochondria. The Journal of Biochemistry *59*, 419–421.

Kennedy, M.D., Jallad, K.N., Lu, J., Low, P.S., and Ben-Amotz, D. (2003). Evaluation of folate conjugate uptake and transport by the choroid plexus of mice. Pharm. Res. *20*, 714–719.

Kenten, R.H., and Mann, P.J.G. (1952). Hydrogen peroxide formation in oxidations catalysed by plant α-hydroxyacid oxidase. Biochemical Journal *52*, 130–134.

Kikuchi, G. (1973). The glycine cleavage system: composition, reaction mechanism, and physiological significance. Mol. Cell. Biochem. *1*, 169–187.

Kim, J.-M., Stewart, R., Kim, S.-W., Shin, I.-S., Yang, S.-J., Shin, H.-Y., and Yoon, J.-S. (2008). Changes in folate, vitamin B12 and homocysteine associated with incident dementia. J. Neurol. Neurosurg. Psychiatr. *79*, 864–868.

Kouadjo, K.E., Nishida, Y., Cadrin-Girard, J.F., Yoshioka, M., and St-Amand, J. (2007). Housekeeping and tissue-specific genes in mouse tissues. BMC Genomics *8*, 127.

Kozak, M. (1983). Comparison of initiation of protein synthesis in procaryotes, eucaryotes, and organelles. Microbiol. Rev. *47*, 1–45.

Kruman, I.I., Culmsee, C., Chan, S.L., Kruman, Y., Guo, Z., Penix, L., and Mattson, M.P. (2000). Homocysteine elicits a DNA damage response in neurons that promotes apoptosis and hypersensitivity to excitotoxicity. J. Neurosci. *20*, 6920–6926.

Kruman, I.I., Kumaravel, T.S., Lohani, A., Pedersen, W.A., Cutler, R.G., Kruman, Y., Haughey, N., Lee, J., Evans, M., and Mattson, M.P. (2002). Folic Acid Deficiency and Homocysteine Impair DNA Repair in Hippocampal Neurons and Sensitize Them to Amyloid Toxicity in Experimental Models of Alzheimer's Disease. J. Neurosci. *22*, 1752–1762.

Krupenko, S.A. (2009). FDH: an aldehyde dehydrogenase fusion enzyme in folate metabolism. Chem. Biol. Interact. *178*, 84–93.

Krupenko, S.A., and Oleinik, N.V. (2002). 10-Formyltetrahydrofolate Dehydrogenase, One of the Major Folate Enzymes, Is Down-Regulated in Tumor Tissues and Possesses Suppressor Effects on Cancer Cells. Cell Growth Differ *13*, 227–236.

Krupenko, N.I., Dubard, M.E., Strickland, K.C., Moxley, K.M., Oleinik, N.V., and Krupenko, S.A. (2010). ALDH1L2 is the mitochondrial homolog of 10-formyltetrahydrofolate dehydrogenase. J. Biol. Chem. *285*, 23056–23063.

Lalonde, R., Barraud, H., Ravey, J., Guéant, J.-L., Bronowicki, J.-P., and Strazielle, C. (2008). Effects of a B-vitamin-deficient diet on exploratory activity, motor coordination, and spatial learning in young adult Balb/c mice. Brain Research *1188*, 122–131.

Lehtinen, L., Ketola, K., Mäkelä, R., Mpindi, J.-P., Viitala, M., Kallioniemi, O., and Iljin, K. (2012). High-throughput RNAi screening for novel modulators of vimentin expression identifies MTHFD2 as a regulator of breast cancer cell migration and invasion. Oncotarget *4*, 48–63.

Leung, K.-Y., De Castro, S.C.P., Savery, D., Copp, A.J., and Greene, N.D.E. (2013). Nucleotide precursors prevent folic acid-resistant neural tube defects in the mouse. Brain *136*, 2836–2841.

Levav-Rabkin, T., Blumkin, E., Galron, D., and Golan, H.M. (2011). Sex-dependent behavioral effects of Mthfr deficiency and neonatal GABA potentiation in mice. Behavioural Brain Research *216*, 505–513.

Li, D., Ahmed, M., Li, Y., Jiao, L., Chou, T.-H., Wolff, R.A., Lenzi, R., Evans, D.B., Bondy, M.L., Pisters, P.W., et al. (2005). 5,10-Methylenetetrahydrofolate reductase polymorphisms and the risk of pancreatic cancer. Cancer Epidemiol. Biomarkers Prev. *14*, 1470–1476.

Li, Y., Holmes, W.B., Appling, D.R., and RajBhandary, U.L. (2000). Initiation of protein synthesis in Saccharomyces cerevisiae mitochondria without formylation of the initiator tRNA. J. Bacteriol. *182*, 2886–2892.

Liew, S.-C., and Gupta, E.D. (2015). Methylenetetrahydrofolate reductase (MTHFR) C677T polymorphism: epidemiology, metabolism and the associated diseases. Eur J Med Genet *58*, 1–10.

Lim, J.-H., Lee, Y.-M., Chun, Y.-S., Chen, J., Kim, J.-E., and Park, J.-W. (2010). Sirtuin 1 Modulates Cellular Responses to Hypoxia by Deacetylating Hypoxia-Inducible Factor 1α. Molecular Cell *38*, 864–878.

Lin, B.F., Huang, R.F., and Shane, B. (1993). Regulation of folate and one-carbon metabolism in mammalian cells. III. Role of mitochondrial folylpoly-gamma-glutamate synthetase. J. Biol. Chem. *268*, 21674–21679.

Liu, F., Liu, Y., He, C., Tao, L., He, X., Song, H., and Zhang, G. (2014). Increased MTHFD2 expression is associated with poor prognosis in breast cancer. Tumour Biol. *35*, 8685–8690.

Liu, M., Ge, Y., Cabelof, D.C., Aboukameel, A., Heydari, A.R., Mohammad, R., and Matherly, L.H. (2005). Structure and Regulation of the Murine Reduced Folate Carrier Gene IDENTIFICATION OF FOUR NONCODING EXONS AND PROMOTERS AND REGULATION BY DIETARY FOLATES. J. Biol. Chem. *280*, 5588–5597.

Loughlin, R.E., Elford, H.L., and Buchanan, J.M. (1964). ENZYMATIC SYNTHESIS OF THE METHYL GROUP OF METHIONINE. VII. ISOLATION OF A COBALAMIN-CONTAINING TRANSMETHYLASE (5-METHYLTETRAHYDRO-FOLATE-HOMOCYSTEINE) FROM MAMMALIAN LIVER. J. Biol. Chem. *239*, 2888–2895.

Luchsinger, J.A., Tang, M.-X., Shea, S., Miller, J., Green, R., and Mayeux, R. (2004). Plasma homocysteine levels and risk of Alzheimer disease. Neurology *62*, 1972–1976.

Ludwig, C., Easton, J., Lodi, A., Tiziani, S., Manzoor, S.E., Southam, A.D., Byrne, J.J., Bishop, L.M., He, S., Arvanitis, T.N., et al. Birmingham Metabolite Library: A publicly accessible database of 1-D 1H and 2-D 1H J-resolved NMR spectra of authentic metabolite standards (BML-NMR). Metabolomics *8*, 8–18.

Ma, X.-Y., Yu, J.-T., Wu, Z.-C., Zhang, Q., Liu, Q.-Y., Wang, H.-F., Wang, W., and Tan, L. (2012). Replication of the MTHFD1L gene association with late-onset Alzheimer's disease in a Northern Han Chinese population. J. Alzheimers Dis. *29*, 521–525.

MacFarlane, A.J., Anderson, D.D., Flodby, P., Perry, C.A., Allen, R.H., Stabler, S.P., and Stover, P.J. (2011). Nuclear localization of de novo thymidylate biosynthesis pathway is required to prevent uracil accumulation in DNA. J. Biol. Chem. *286*, 44015–44022.

de Marchi, W.J., and Johnston, G. a. R. (1969). THE OXIDATION OF GLYCINE BY d-AMINO ACID OXIDASE IN EXTRACTS OF MAMMALIAN CENTRAL NERVOUS TISSUE. Journal of Neurochemistry *16*, 355–361.

Maren, S. (2001). Neurobiology of Pavlovian fear conditioning. Annu. Rev. Neurosci. *24*, 897–931.

Martínez-Vega, R., Murillo-Cuesta, S., Partearroyo, T., Varela-Moreiras, G., Varela-Nieto, I., and Pajares, M.A. (2016). Long-Term Dietary Folate Deficiency Accelerates Progressive Hearing Loss on CBA/Ca Mice. Front Aging Neurosci *8*, 209.

Matsuda, M. (1990). Comparison of the incidence of 5-azacytidine-induced exencephaly between MT/HokIdr and Slc:ICR mice. Teratology *41*, 147–154.

Mattson, M.P., Pedersen, W.A., Duan, W., Culmsee, C., and Camandola, S. (1999). Cellular and Molecular Mechanisms Underlying Perturbed Energy Metabolism and Neuronal Degeneration in Alzheimer's and Parkinson's Diseases. Annals of the New York Academy of Sciences *893*, 154–175.

McBurney, M.W., and Whitmore, G.F. (1974). Characterization of a chinese hamster cell with a temperature-sensitive mutation in folate metabolism. Cell *2*, 183–188.

McCarthy, E.A., Titus, S.A., Taylor, S.M., Jackson-Cook, C., and Moran, R.G. (2004). A mutation inactivating the mitochondrial inner membrane folate transporter creates a glycine requirement for survival of chinese hamster cells. J. Biol. Chem. *279*, 33829–33836.

McEchron, M.D., Bouwmeester, H., Tseng, W., Weiss, C., and Disterhoft, J.F. (1998). Hippocampectomy disrupts auditory trace fear conditioning and contextual fear conditioning in the rat. Hippocampus *8*, 638–646.

McEchron, M.D., Tseng, W., and Disterhoft, J.F. (2000). Neurotoxic lesions of the dorsal hippocampus disrupt auditory-cued trace heart rate (fear) conditioning in rabbits. Hippocampus *10*, 739–751.

Mejia, N.R., and MacKenzie, R.E. (1985). NAD-dependent methylenetetrahydrofolate dehydrogenase is expressed by immortal cells. J. Biol. Chem. *260*, 14616–14620.

Mejia, N.R., and MacKenzie, R.E. (1988). NAD-dependent methylenetetrahydrofolate dehydrogenase-methenyltetrahydrofolate cyclohydrolase in transformed cells is a mitochondrial enzyme. Biochemical and Biophysical Research Communications *155*, 1–6.

Mejia, N.R., Rios-Orlandi, E.M., and MacKenzie, R.E. (1986). NAD-dependent methylenetetrahydrofolate dehydrogenase-methenyltetrahydrofolate cyclohydrolase from ascites tumor cells. Purification and properties. J. Biol. Chem. *261*, 9509–9513.

Melamed, E., Reches, A., and Hershko, C. (1975). Reversible central nervous system dysfunction in folate deficiency. J. Neurol. Sci. *25*, 93–98.

Middaugh, L.D., Grover, T.A., Blackwell, L.A., and Zemp, J.W. (1976). Neurochemical and behavioral effects of diet related perinatal folic acid restriction. Pharmacol. Biochem. Behav. *5*, 129–134.

Minguzzi, S., Selcuklu, S.D., Spillane, C., and Parle-McDermott, A. (2014). An NTD-associated polymorphism in the 3' UTR of MTHFD1L can affect disease risk by altering miRNA binding. Hum. Mutat. *35*, 96–104.

Momb, J., Lewandowski, J.P., Bryant, J.D., Fitch, R., Surman, D.R., Vokes, S.A., and Appling, D.R. (2013). Deletion of Mthfd1l causes embryonic lethality and neural tube and craniofacial defects in mice. Proc. Natl. Acad. Sci. U.S.A. *110*, 549–554.

Morris, R. (1984). Developments of a water-maze procedure for studying spatial learning in the rat. J. Neurosci. Methods *11*, 47–60.

Morrow, G.P., MacMillan, L., Lamarre, S.G., Young, S.K., MacFarlane, A.J., Brosnan, M.E., and Brosnan, J.T. (2015). In Vivo Kinetics of Formate Metabolism in Folate-deficient and Folate-replete Rats. J. Biol. Chem. *290*, 2244–2250.

Motokawa, Y., and Kikuchi, G. (1971). Glycine metabolism in rat liver mitochondria. V. Intramitochondrial localization of the reversible glycine cleavage system and serine hydroxymethyltransferase. Arch. Biochem. Biophys. *146*, 461–464.

MRC Vitamin Study Research Group (1991). Prevention of neural tube defects: Results of the Medical Research Council Vitamin Study. The Lancet *338*, 131–137.

Mudd, S.H., Finkelstein, J.D., Irreverre, F., and Laster, L. (1965). Transsulfuration in mammals. Microassays and tissue distributions of three enzymes of the pathway. J. Biol. Chem. *240*, 4382–4392.

Naj, A.C., Beecham, G.W., Martin, E.R., Gallins, P.J., Powell, E.H., Konidari, I., Whitehead, P.L., Cai, G., Haroutunian, V., Scott, W.K., et al. (2010). Dementia revealed: novel chromosome 6 locus for late-onset Alzheimer disease provides genetic evidence for folate-pathway abnormalities. PLoS Genet. *6*.

Nakada, H.I., and Sund, L.P. (1958). Glyoxylic Acid Oxidation by Rat Liver. J. Biol. Chem. *233*, 8–13.

Nakada, H.I., and Weinhouse, S. (1953). Non-enzymatic transamination with glyoxylic acid and various amino acids. J. Biol. Chem. *204*, 831–836.

Nakada, H.I., Friedmann, B., and Weinhouse, S. (1955). Pathways of Glycine Catabolism in Rat Liver. J. Biol. Chem. *216*, 583–592.

Narisawa, A., Komatsuzaki, S., Kikuchi, A., Niihori, T., Aoki, Y., Fujiwara, K., Tanemura, M., Hata, A., Suzuki, Y., Relton, C.L., et al. (2012). Mutations in genes encoding the glycine cleavage system predispose to neural tube defects in mice and humans. Hum. Mol. Genet. *21*, 1496–1503.

Neymeyer, V.R., and Tephly, T.R. (1994). Detection and quantification of 10-formyltetrahydrofolate dehydrogenase (10-FTHFDH) in rat retina, optic nerve, and brain. Life Sci. *54*, PL395-399.

Nijhout, H.F., Reed, M.C., Lam, S.-L., Shane, B., Gregory, J.F., 3rd, and Ulrich, C.M. (2006). In silico experimentation with a model of hepatic mitochondrial folate metabolism. Theor Biol Med Model *3*, 40.

Nilsson, R., Jain, M., Madhusudhan, N., Sheppard, N.G., Strittmatter, L., Kampf, C., Huang, J., Asplund, A., and Mootha, V.K. (2014). Metabolic enzyme expression highlights a key role for MTHFD2 and the mitochondrial folate pathway in cancer. Nat Commun *5*, 3128.

Noguchi, T., Okuno, E., Takada, Y., Minatogawa, Y., Okai, K., and Kido, R. (1978). Characteristics of hepatic alanine-glyoxylate aminotransferase in different mammalian species. Biochem. J. *169*, 113–122.

Pai, Y.J., Leung, K.-Y., Savery, D., Hutchin, T., Prunty, H., Heales, S., Brosnan, M.E., Brosnan, J.T., Copp, A.J., and Greene, N.D.E. (2015). Glycine decarboxylase deficiency causes neural tube defects and features of non-ketotic hyperglycinemia in mice. Nat Commun *6*, 6388.

Palmer, K.F., and Williams, D. (1974). Optical properties of water in the near infrared. Journal of the Optical Society of America *64*, 1107.

Parle-McDermott, A., Pangilinan, F., O'Brien, K.K., Mills, J.L., Magee, A.M., Troendle, J., Sutton, M., Scott, J.M., Kirke, P.N., Molloy, A.M., et al. (2009). A common

variant in MTHFD1L is associated with neural tube defects and mRNA splicing efficiency. Hum. Mutat. *30*, 1650–1656.

Pasternack, L.B., Laude, D.A., and Appling, D.R. (1994). Carbon-13 NMR analysis of intercompartmental flow of one-carbon units into choline and purines in Saccharomyces cerevisiae. Biochemistry *33*, 74–82.

Pellow, S., Chopin, P., File, S.E., and Briley, M. (1985). Validation of open : closed arm entries in an elevated plus-maze as a measure of anxiety in the rat. Journal of Neuroscience Methods *14*, 149–167.

Peters, G.J., Backus, H.H.J., Freemantle, S., van Triest, B., Codacci-Pisanelli, G., van der Wilt, C.L., Smid, K., Lunec, J., Calvert, A.H., Marsh, S., et al. (2002). Induction of thymidylate synthase as a 5-fluorouracil resistance mechanism. Biochim. Biophys. Acta *1587*, 194–205.

Piedrahita, J.A., Oetama, B., Bennett, G.D., van Waes, J., Kamen, B.A., Richardson, J., Lacey, S.W., Anderson, R.G., and Finnell, R.H. (1999). Mice lacking the folic acid-binding protein Folbp1 are defective in early embryonic development. Nat. Genet. *23*, 228–232.

Pike, S.T., Rajendra, R., Artzt, K., and Appling, D.R. (2010). Mitochondrial C1-Tetrahydrofolate Synthase (MTHFD1L) Supports the Flow of Mitochondrial One-carbon Units into the Methyl Cycle in Embryos. Journal of Biological Chemistry *285*, 4612–4620.

Pinson, K.I., Brennan, J., Monkley, S., Avery, B.J., and Skarnes, W.C. (2000). An LDL-receptor-related protein mediates Wnt signalling in mice. Nature *407*, 535–538.

Porter, D.H., Cook, R.J., and Wagner, C. (1985). Enzymatic properties of dimethylglycine dehydrogenase and sarcosine dehydrogenase from rat liver. Archives of Biochemistry and Biophysics *243*, 396–407.

Poulin, S.P., Dautoff, R., Morris, J.C., Barrett, L.F., and Dickerson, B.C. (2011). Amygdala atrophy is prominent in early Alzheimer's disease and relates to symptom severity. Psychiatry Res *194*, 7–13.

Prasannan, P., and Appling, D.R. (2009). Human mitochondrial C1-tetrahydrofolate synthase: Submitochondrial localization of the full-length enzyme and characterization of a short isoform. Archives of Biochemistry and Biophysics *481*, 86–93.

Prasannan, P., Pike, S., Peng, K., Shane, B., and Appling, D.R. (2003). Human Mitochondrial C1-Tetrahydrofolate Synthase: GENE STRUCTURE, TISSUE DISTRIBUTION OF THE MRNA, AND IMMUNOLOCALIZATION IN CHINESE HAMSTER OVARY CELLS. J. Biol. Chem. *278*, 43178–43187.

Qiu, A., Jansen, M., Sakaris, A., Min, S.H., Chattopadhyay, S., Tsai, E., Sandoval, C., Zhao, R., Akabas, M.H., and Goldman, I.D. (2006). Identification of an intestinal folate transporter and the molecular basis for hereditary folate malabsorption. Cell *127*, 917–928.

Qiu, A., Min, S.H., Jansen, M., Malhotra, U., Tsai, E., Cabelof, D.C., Matherly, L.H., Zhao, R., Akabas, M.H., and Goldman, I.D. (2007). Rodent intestinal folate transporters (SLC46A1): secondary structure, functional properties, and response to dietary folate restriction. Am. J. Physiol., Cell Physiol. *293*, C1669-1678.

Quinn, J.J., Oommen, S.S., Morrison, G.E., and Fanselow, M.S. (2002). Post-training excitotoxic lesions of the dorsal hippocampus attenuate forward trace, backward trace, and delay fear conditioning in a temporally specific manner. Hippocampus *12*, 495–504.

Rai, V. (2016a). Association of methylenetetrahydrofolate reductase (MTHFR) gene C677T polymorphism with autism: evidence of genetic susceptibility. Metab Brain Dis *31*, 727–735.

Rai, V. (2016b). Folate Pathway Gene Methylenetetrahydrofolate Reductase C677T Polymorphism and Alzheimer Disease Risk in Asian Population. Indian J Clin Biochem *31*, 245–252.

Ramírez-Lorca, R., Boada, M., Antúnez, C., López-Arrieta, J., Moreno-Rey, C., Hernández, I., Marín, J., Gayán, J., González-Pérez, A., Alegret, M., et al. (2011). The MTHFD1L gene rs11754661 marker is not associated with Alzheimer's disease in a sample of the Spanish population. J. Alzheimers Dis. *25*, 47–50.

Rassin, D.K., and Gaull, G.E. (1975). Subcellular distribution of enzymes of transmethylation and transsulphuration in rat brain. J. Neurochem. *24*, 969–978.

Refsum, H., Ueland, P.M., Nygård, O., and Vollset, S.E. (1998). Homocysteine and cardiovascular disease. Annu. Rev. Med. *49*, 31–62.

Ren, R.-J., Wang, L.-L., Fang, R., Liu, L.-H., Wang, Y., Tang, H.-D., Deng, Y.-L., Xu, W., Wang, G., and Chen, S.-D. (2011). The MTHFD1L gene rs11754661 marker is associated with susceptibility to Alzheimer's disease in the Chinese Han population. J. Neurol. Sci. *308*, 32–34.

Román, G.C. (2015). MTHFR Gene Mutations: A Potential Marker of Late-Onset Alzheimer's Disease? J. Alzheimers Dis. *47*, 323–327.

Ross, J.F., Wang, H., Behm, F.G., Mathew, P., Wu, M., Booth, R., and Ratnam, M. (1999). Folate receptor type beta is a neutrophilic lineage marker and is differentially expressed in myeloid leukemia. Cancer *85*, 348–357.

Ruzankina, Y., Pinzon-Guzman, C., Asare, A., Ong, T., Pontano, L., Cotsarelis, G., Zediak, V.P., Velez, M., Bhandoola, A., and Brown, E.J. (2007). Deletion of the Developmentally Essential Gene ATR in Adult Mice Leads to Age-Related Phenotypes and Stem Cell Loss. Cell Stem Cell *1*, 113–126.

Sabharanjak, S., and Mayor, S. (2004). Folate receptor endocytosis and trafficking. Adv. Drug Deliv. Rev. *56*, 1099–1109.

Sacchi, S., Cappelletti, P., Giovannardi, S., and Pollegioni, L. (2011). Evidence for the interaction of D-amino acid oxidase with pLG72 in a glial cell line. Mol. Cell. Neurosci. *48*, 20–28.

Salojin, K.V., Cabrera, R.M., Sun, W., Chang, W.C., Lin, C., Duncan, L., Platt, K.A., Read, R., Vogel, P., Liu, Q., et al. (2011). A mouse model of hereditary folate malabsorption: deletion of the PCFT gene leads to systemic folate deficiency. Blood *117*, 4895–4904.

Selcuklu, S.D., Donoghue, M.T.A., Rehmet, K., de Souza Gomes, M., Fort, A., Kovvuru, P., Muniyappa, M.K., Kerin, M.J., Enright, A.J., and Spillane, C. (2012). MicroRNA-9 inhibition of cell proliferation and identification of novel miR-9 targets by transcriptome profiling in breast cancer cells. The Journal of Biological Chemistry.

Seller, M.J. (1994). Vitamins, folic acid and the cause and prevention of neural tube defects. Ciba Found. Symp. *181*, 161-173; discussion 173-179.

Sener, E.F., Oztop, D.B., and Ozkul, Y. (2014). MTHFR Gene C677T Polymorphism in Autism Spectrum Disorders. Genet Res Int *2014*, 698574.

Seshadri, S., Beiser, A., Selhub, J., Jacques, P.F., Rosenberg, I.H., D'Agostino, R.B., Wilson, P.W.F., and Wolf, P.A. (2002). Plasma Homocysteine as a Risk Factor

151

for Dementia and Alzheimer's Disease. New England Journal of Medicine *346*, 476–483.

Shane, B. (1989). Folylpolyglutamate synthesis and role in the regulation of one-carbon metabolism. Vitam. Horm. *45*, 263–335.

Shen, F., Ross, J.F., Wang, X., and Ratnam, M. (1994). Identification of a novel folate receptor, a truncated receptor, and receptor type beta in hematopoietic cells: cDNA cloning, expression, immunoreactivity, and tissue specificity. Biochemistry *33*, 1209–1215.

Shin, M., Bryant, J.D., Momb, J., and Appling, D.R. (2014). Mitochondrial MTHFD2L Is a Dual Redox Cofactor-specific Methylenetetrahydrofolate Dehydrogenase/Methenyltetrahydrofolate Cyclohydrolase Expressed in Both Adult and Embryonic Tissues. J. Biol. Chem. *289*, 15507–15517.

Smithells, R.W., Sheppard, S., and Schorah, C.J. (1976). Vitamin deficiencies and neural tube defects. Arch. Dis. Child. *51*, 944–950.

Snell, K. (1986). The duality of pathways for serine biosynthesis is a fallacy. Trends in Biochemical Sciences *11*, 241–243.

Spiegelstein, O., Mitchell, L.E., Merriweather, M.Y., Wicker, N.J., Zhang, Q., Lammer, E.J., and Finnell, R.H. (2004). Embryonic development of folate binding protein-1 (Folbp1) knockout mice: Effects of the chemical form, dose, and timing of maternal folate supplementation. Dev. Dyn. *231*, 221–231.

Stanisławska-Sachadyn, A., Woodside, J.V., Brown, K.S., Young, I.S., Murray, L., McNulty, H., Strain, J.J., Boreham, C.A., Scott, J.M., Whitehead, A.S., et al. (2008). Evidence for sex differences in the determinants of homocysteine concentrations. Mol. Genet. Metab. *93*, 355–362.

Strachan, R.W., and Henderson, J.G. (1967). Dementia and folate deficiency. Q. J. Med. *36*, 189–204.

Stratman, J.L., Barnes, W.M., and Simon, T.C. (2003). Universal PCR Genotyping Assay that Achieves Single copy Sensitivity with Any Primer Pair. Transgenic Res *12*, 521–522.

Strickland, K.C., Krupenko, N.I., Dubard, M.E., Hu, C.J., Tsybovsky, Y., and Krupenko, S.A. (2011). Enzymatic properties of ALDH1L2, a mitochondrial 10-formyltetrahydrofolate dehydrogenase. Chem. Biol. Interact. *191*, 129–136.

Su, X., Wellen, K.E., and Rabinowitz, J.D. (2016). Metabolic control of methylation and acetylation. Current Opinion in Chemical Biology *30*, 52–60.

Sudiwala, S., De Castro, S.C.P., Leung, K.-Y., Brosnan, J.T., Brosnan, M.E., Mills, K., Copp, A.J., and Greene, N.D.E. (2016). Formate supplementation enhances folate-dependent nucleotide biosynthesis and prevents spina bifida in a mouse model of folic acid-resistant neural tube defects. Biochimie *126*, 63–70.

Suliman, H.S., Sawyer, G.M., Appling, D.R., and Robertus, J.D. (2005). Purification and properties of cobalamin-independent methionine synthase from Candida albicans and Saccharomyces cerevisiae. Arch. Biochem. Biophys. *441*, 56–63.

Taylor, R.T., and Hanna, M.L. (1977). Folate-dependent enzymes in cultured Chinese hamster cells: folypolyglutamate synthetase and its absence in mutants auxotrophic for glycine + adenosine + thymidine. Arch. Biochem. Biophys. *181*, 331–334.

Tedeschi, P.M., Markert, E.K., Gounder, M., Lin, H., Dvorzhinski, D., Dolfi, S.C., Chan, L.L.-Y., Qiu, J., DiPaola, R.S., Hirshfield, K.M., et al. (2013). Contribution of serine, folate and glycine metabolism to the ATP, NADPH and purine requirements of cancer cells. Cell Death Dis *4*, e877.

Tedeschi, P.M., Vazquez, A., Kerrigan, J.E., and Bertino, J.R. (2015). Mitochondrial Methylenetetrahydrofolate Dehydrogenase (MTHFD2) Overexpression Is Associated with Tumor Cell Proliferation and Is a Novel Target for Drug Development. Mol. Cancer Res. *13*, 1361–1366.

Thigpen, A.E., West, M.G., and Appling, D.R. (1990). Rat C1-tetrahydrofolate synthase. cDNA isolation, tissue-specific levels of the mRNA, and expression of the protein in yeast. J. Biol. Chem. *265*, 7907–7913.

Thompson, J.S., and Richardson, K.E. (1967). Isolation and characterization of an L-alanine: glyoxylate aminotransferase from human liver. J. Biol. Chem. *242*, 3614–3619.

Thompson, H.R., Jones, G.M., and Narkewicz, M.R. (2001). Ontogeny of hepatic enzymes involved in serine- and folate-dependent one-carbon metabolism in rabbits. Am. J. Physiol. Gastrointest. Liver Physiol. *280*, G873-878.

Tibbetts, A.S., and Appling, D.R. (1997). Saccharomyces cerevisiae expresses two genes encoding isozymes of 5-aminoimidazole-4-carboxamide ribonucleotide transformylase. Arch. Biochem. Biophys. *340*, 195–200.

Tibbetts, A.S., and Appling, D.R. (2000). Characterization of two 5-aminoimidazole-4-carboxamide ribonucleotide transformylase/inosine monophosphate cyclohydrolase isozymes from Saccharomyces cerevisiae. J. Biol. Chem. *275*, 20920–20927.

Tibbetts, A.S., and Appling, D.R. (2010). Compartmentalization of Mammalian folate-mediated one-carbon metabolism. Annu. Rev. Nutr. *30*, 57–81.

Titus, S.A., and Moran, R.G. (2000). Retrovirally mediated complementation of the glyB phenotype. Cloning of a human gene encoding the carrier for entry of folates into mitochondria. J. Biol. Chem. *275*, 36811–36817.

154

Troen, A.M., Chao, W.-H., Crivello, N.A., D'Anci, K.E., Shukitt-Hale, B., Smith, D.E., Selhub, J., and Rosenberg, I.H. (2008). Cognitive Impairment in Folate-Deficient Rats Corresponds to Depleted Brain Phosphatidylcholine and Is Prevented by Dietary Methionine without Lowering Plasma Homocysteine. J. Nutr. *138*, 2502–2509.

Tucker, E.J., Hershman, S.G., Köhrer, C., Belcher-Timme, C.A., Patel, J., Goldberger, O.A., Christodoulou, J., Silberstein, J.M., McKenzie, M., Ryan, M.T., et al. (2011). Mutations in MTFMT underlie a human disorder of formylation causing impaired mitochondrial translation. Cell Metab *14*, 428–434.

Turner, M.A., Yang, X., Yin, D., Kuczera, K., Borchardt, R.T., and Howell, P.L. (2000). Structure and function of S-adenosylhomocysteine hydrolase. Cell Biochem. Biophys. *33*, 101–125.

Van Dam, F., and Van Gool, W.A. (2009). Hyperhomocysteinemia and Alzheimer's disease: A systematic review. Arch Gerontol Geriatr *48*, 425–430.

Vorhees, C.V., and Williams, M.T. (2014). Assessing spatial learning and memory in rodents. ILAR J *55*, 310–332.

Wagner, W., Breksa, A.P., Monzingo, A.F., Appling, D.R., and Robertus, J.D. (2005). Kinetic and structural analysis of active site mutants of monofunctional NAD-dependent 5,10-methylenetetrahydrofolate dehydrogenase from Saccharomyces cerevisiae. Biochemistry *44*, 13163–13171.

Walkup, A.S., and Appling, D.R. (2005). Enzymatic characterization of human mitochondrial C1-tetrahydrofolate synthase. Arch. Biochem. Biophys *442*, 196–205.

Wang, L.-D., Guo, R.-F., Fan, Z.-M., He, X., Gao, S.-S., Guo, H.-Q., Matsuo, K., Yin, L.-M., and Li, J.-L. (2005). Association of methylenetetrahydrofolate reductase

and thymidylate synthase promoter polymorphisms with genetic susceptibility to esophageal and cardia cancer in a Chinese high-risk population. Dis. Esophagus *18*, 177–184.

Weike, A.I., Schupp, H.T., and Hamm, A.O. (2007). Fear acquisition requires awareness in trace but not delay conditioning. Psychophysiology *44*, 170–180.

West, M.G., Barlowe, C.K., and Appling, D.R. (1993). Cloning and characterization of the Saccharomyces cerevisiae gene encoding NAD-dependent 5,10-methylenetetrahydrofolate dehydrogenase. J. Biol. Chem. *268*, 153–160.

West, M.G., Horne, D.W., and Appling, D.R. (1996). Metabolic Role of Cytoplasmic Isozymes of 5,10-Methylenetetrahydrofolate Dehydrogenase in Saccharomyces cerevisiae†. Biochemistry *35*, 3122–3132.

Whetstine, J.R., Flatley, R.M., and Matherly, L.H. (2002). The human reduced folate carrier gene is ubiquitously and differentially expressed in normal human tissues: identification of seven non-coding exons and characterization of a novel promoter. Biochem. J. *367*, 629–640.

Whiting, J., Marshall, H., Cook, M., Krumlauf, R., Rigby, P.W., Stott, D., and Allemann, R.K. (1991). Multiple spatially specific enhancers are required to reconstruct the pattern of Hox-2.6 gene expression. Genes Dev. *5*, 2048–2059.

Willems, E., Mateizel, I., Kemp, C., Cauffman, G., Sermon, K., and Leyns, L. (2006). Selection of reference genes in mouse embryos and in differentiating human and mouse ES cells. Int. J. Dev. Biol *50*, 627–635.

Williams, L.J., Mai, C.T., Edmonds, L.D., Shaw, G.M., Kirby, R.S., Hobbs, C.A., Sever, L.E., Miller, L.A., Meaney, F.J., and Levitt, M. (2002). Prevalence of spina bifida and anencephaly during the transition to mandatory folic acid fortification in the United States. Teratology *66*, 33–39.

Williamson, D.H., Lund, P., and Krebs, H.A. (1967). The redox state of free nicotinamide-adenine dinucleotide in the cytoplasm and mitochondria of rat liver. Biochem J *103*, 514–527.

Wishart, D.S., Tzur, D., Knox, C., Eisner, R., Guo, A.C., Young, N., Cheng, D., Jewell, K., Arndt, D., Sawhney, S., et al. (2007). HMDB: the Human Metabolome Database. Nucleic Acids Res. *35*, D521-526.

Wittwer, A.J., and Wagner, C. (1980). Identification of folate binding protein of mitochondria as dimethylglycine dehydrogenase. Proc. Natl. Acad. Sci. U.S.A. *77*, 4484–4488.

Woeller, C.F., Anderson, D.D., Szebenyi, D.M.E., and Stover, P.J. (2007). Evidence for small ubiquitin-like modifier-dependent nuclear import of the thymidylate biosynthesis pathway. J. Biol. Chem. *282*, 17623–17631.

Xia, J., and Wishart, D.S. (2011). Metabolomic data processing, analysis, and interpretation using MetaboAnalyst. Curr Protoc Bioinformatics *Chapter 14*, Unit 14.10.

Xia, J., Psychogios, N., Young, N., and Wishart, D.S. (2009). MetaboAnalyst: a web server for metabolomic data analysis and interpretation. Nucleic Acids Res *37*, W652–W660.

Xu, L., Wang, L., Wang, J., Zhu, Z., Chang, G., Guo, Y., Tian, X., and Niu, B. (2016). The effect of inhibiting glycinamide ribonucleotide formyl transferase on the development of neural tube in mice. Nutr Metab (Lond) *13*, 56.

Yang, C.H., Sirotnak, F.M., and Dembo, M. (1984). Interaction between anions and the reduced folate/methotrexate transport system in L1210 cell plasma membrane vesicles: directional symmetry and anion specificity for differential mobility of loaded and unloaded carrier. J. Membr. Biol. *79*, 285–292.

Yang, Y., Chen, J., Wang, B., Ding, C., and Liu, H. (2015). Association between MTHFR C677T polymorphism and neural tube defect risks: A comprehensive evaluation in three groups of NTD patients, mothers, and fathers. Birth Defects Res. Part A Clin. Mol. Teratol. *103*, 488–500.

Ye, J., Coulouris, G., Zaretskaya, I., Cutcutache, I., Rozen, S., and Madden, T.L. (2012). Primer-BLAST: A tool to design target-specific primers for polymerase chain reaction. BMC Bioinformatics *13*, 134.

Yi, P., Melnyk, S., Pogribna, M., Pogribny, I.P., Hine, R.J., and James, S.J. (2000). Increase in Plasma Homocysteine Associated with Parallel Increases in Plasma S-Adenosylhomocysteine and Lymphocyte DNA Hypomethylation. J. Biol. Chem. *275*, 29318–29323.

Zhao, R., Russell, R.G., Wang, Y., Liu, L., Gao, F., Kneitz, B., Edelmann, W., and Goldman, I.D. (2001). Rescue of embryonic lethality in reduced folate carrier-deficient mice by maternal folic acid supplementation reveals early neonatal failure of hematopoietic organs. J. Biol. Chem. *276*, 10224–10228.

Zhao, R., Gao, F., Hanscom, M., and Goldman, I.D. (2004). A prominent low-pH methotrexate transport activity in human solid tumors: contribution to the preservation of methotrexate pharmacologic activity in HeLa cells lacking the reduced folate carrier. Clin. Cancer Res. *10*, 718–727.

Zhao, R., Diop-Bove, N., Visentin, M., and Goldman, I.D. (2011). Mechanisms of Membrane Transport of Folates into Cells and Across Epithelia. Annual Review of Nutrition *31*, 177–201.

Vita

Joshua Dale Bryant was born on February 19, 1987 in Amarillo, Texas. He was raised in Amarillo, then moved to Abilene, Texas to attend Hardin-Simmons University. In May of 2009, he graduated *summa cum laude* with a Bachelor's of Science degree in chemistry. In June of 2009, he moved to Austin, Texas to begin his doctoral studies in the Biochemistry Graduate Program at the University of Texas.

Permanent email address: jbryant@utexas.edu

This dissertation was typed by the author.